# TEXTILE RESEARCH JOURNAL

*VOLUME XXI* June, 1951 *NUMBER 6*

PUBLICATION OF

TEXTILE RESEARCH INSTITUTE, INC.

*Editorial Office:* 10 East 40th Street, New York 16, N. Y.

# E. F. DREW & CO., INC.

**Producers of Basic Raw Materials and Finished Products For Specific End Uses in the Textile Industry**

Nature has proved that *fatty materials* are the best lubricant for fibrous materials. The wool on sheep is protected by a fatty coating . . . as are all fur bearing animals. Cotton and bast fibres are protected by natural waxes.

For over 40 years, Drew has specialized in the production of fatty products from nature's abundant store of vegetable, marine and animal oils. Applying modern chemistry to years of processing experience, Drew has produced a wide variety of superior textile finishing oils, finishing materials, detergents, wetting agents and other surface active chemicals. These products are truly "kind to all fibres."

*For Information, Write*

*TEXTILE CHEMICALS DEPARTMENT*

**E. F. DREW & CO., Inc.**

**15 EAST 26th STREET, NEW YORK 10, N.Y.**

**DREW PRODUCTS**

# TEXTILE RESEARCH JOURNAL

VOL. XXI, No. 6 June, 1951


## In This Issue


**Interfiber Stress and Its Transmission**
Rogers B. Finch
Part I: Measurement of the Contact Area Between Fibers Under Pressure 375
Part II: Theory of the Pressure Distribution and Contact Area Between Fibers 383

**The Measurement of Dynamic Modulus and Energy Losses in Single Textile Filaments Subjected to Forced Longitudinal Vibrations**
Basil A. Dunell and J. H. Dillon 393

**Stress Relaxation and Dynamic Properties of Polymers**
A. V. Tobolsky, B. A. Dunell, and R. D. Andrews 404

**Contradictory Data on Spiral Structures in the Secondary Cell Wall of Fibers of Flax, Hemp, and Ramie**
P. A. Roelofsen 412

**Pore-Size Distribution in a Selected Series of Closely Woven Fabrics**
Edith Honold and Evald L. Skau 419

**The Sorption of Synthetic Surface-Active Compounds by Carbon Black**
G. R. F. Rose, A. S. Weatherburn, and C. H. Bayley 427

**Letters to the Editor**
A Cold-Solvent Extractor 433

INDUSTRIAL SECTION

**The Measurement of Stiffness in Textile Fabrics**
N. J. Abbott
Part I: A Comparison of Five Methods of Laboratory Evaluation 435
Part II: A Study of the Peirce Cantilever Test for Stiffness of Textile Fabrics 441

**An Experimental, Gas-Fired, Infrared Textile Slasher**
Ralph A. Rusca and George J. Kyame 445

**Book Reviews** 450



*Editor:* Julian S. Jacobs *Production Editor:* Lois E. Emma

*Associate Editors*

H. J. Ball
Earl E. Berkley
Henry Eyring
Gustavus J. Esselen
Earl K. Fischer
Milton Harris
K. L. Hertel
H. Mark
E. R. Schwarz
Kyle Ward, Jr.



TEXTILE RESEARCH JOURNAL, published monthly at Prince and Lemon Streets, Lancaster, Pa., is devoted to the interest of research in textile and allied industries. It is the official publication of Textile Research Institute, Inc.

Manuscripts and communications should be sent to the editorial office, 10 East 40th Street, New York 16, N. Y.

Subscription rates (including, monthly, bound copy of the Abstracts from the *Journal of the Textile Institute*): General—$15.00 per year; additional for postage, 50 cents to Canada, $1.00 to all other countries. Special—$10.00 per year for United States and Canadian students, teachers, educational institutions, public libraries, governmental libraries and departments, plus 50 cents for postage to Canada. Single copies, $1.50 each.

Entered as second-class matter, April 27, 1945, at the postoffice at Lancaster, Pa., under the Act of August 24, 1912. Accepted for mailing at special rate of postage provided for in paragraph (d-2), Section 34.40, P. L. & R. of 1948, authorized May 9, 1950.



Contents copyrighted 1951 by Textile Research Institute, Inc.

Advertising rates supplied on request.

# 400% RETURN
## on your investment the first year

**COLOR-EYE improves die batches . . . eliminates rejects . . . provides ultra-precise color matching**

Plant after plant reports the same amazing story: Color-Eye pays for itself in weeks by taking the guesswork out of dyeing operations. Unbelievable results because variance in human vision, operator fatigue and lighting difficulties are eliminated in color-matching problems. You slash number of stock pigments or dyes required . . . simplify formulas . . . reduce inventory . . . *savings which add up to 400% return on your investment the first year.*

Use coupon below for more details or request for demonstration in your own plant. Clip and mail today!

**COLOR-EYE**
TRADE MARK

**5 times more accurate than human eye**

The super-human accuracy of Color-Eye can bring real precision to your dye-matching operations.

- Cuts dye and pigment requirements . . . improves starting formulas
- Controls incoming dyes and pigments to close tolerances
- Reduces adds in production runs
- Predetermines color shift due to sanforizing, tentering, etc.
- Permits quantitative lab study of pigment fading

You can't afford to be without COLOR-EYE send coupon for proof

"If color is important to your product COLOR-EYE is important to you."

**INSTRUMENT DEVELOPMENT LABORATORIES, Inc.**
163 Highland Ave. Needham Heights, Mass.

☐ Please send detailed information on Color-Eye.
☐ I would like a demonstration arranged in my own plant.

Name _____ Title _____
Company _____
Address _____
City _____ Zone _____ State _____

*Over 20,000,000 "joint-use" poles, spaced about 125 feet apart, carry both electric and telephone lines throughout the United States.*

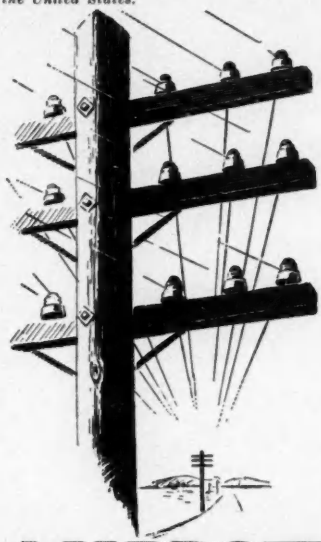

# AMPROZYME
## DOES TWO JOBS AT ONE TIME

### New De-Sizing Powder Converts Both Starches and Proteins in One Operation!

Amprozyme does two jobs better, faster and cheaper. It eliminates the guess work from de-sizing by digesting either starches or proteins, or both, at the same time and in the same operation. If the size is starch, Amprozyme's amylolytic enzymes go right to work. If a protein size is present, its proteolytic enzymes start attacking. Amprozyme insures rapid and complete de-sizing of cottons, rayons, and mixed goods, resulting in a good hand and uniform ground for perfect dyeing, without streaks or shading. Amprozyme eliminates the necessity for two different agents or two separate operations, thus reducing storage, handling, and shipping costs. It can be utilized at normal or elevated dyebox temperatures, in a wide pH range. Amprozyme also remains stable longer. Detailed information and a sample for a test run are available upon request.

Plants: Passaic, N. J.
Carlstadt, N. J.
Los Angeles, California

**JACQUES WOLF & CO.**
*Chemicals* PASSAIC, N. J.

TEXTILE RESEARCH JOURNAL

VOL. XXI, No. 6 June, 1951

# Interfiber Stress and Its Transmission*

## Part I: Measurement of the Contact Area Between Fibers Under Pressure

**Rogers B. Finch†**

*Slater Memorial Research Laboratory, Massachusetts Institute of Technology, Cambridge, Massachusetts*

**Abstract**

A method is described for revealing the contact area between a plane and a fiber under the action of a transverse pressure distribution. It involves pressing the fiber against a plane-glass surface which has been lightly smoked with a gas flame and measuring the resultant impression microscopically.

THE PROCESSING AND USE of textile fibers depend upon the ability of each fiber to transmit stresses to another fiber. Such stress transfer can only take place at the surface of contact between the fibers. The nature of the stress transfer is, then, dependent upon the nature of the surfaces in contact, their mutual area of contact, the history of the stress application, the visco-elastic properties of the fibers in contact, and their relative motion.

The transmission of tangential stress between fibers is described as friction, whether static or kinetic, and is a phenomenon which represents a particular combination of the above variables. Whereas a comparatively adequate unified physical theory exists for elastic materials [1], no such theory exists, even in elementary form, for visco-elastic materials. At the present time, the frictional phenomenon in these materials is described in purely empirical terms, a situation which is not conducive to the development of the desired physical theory.

The objective of the present investigation is to select one element of the unified theory and pursue it to

* This report constitutes a portion of a thesis with the same general title written in partial fulfillment of the requirements for the degree of Doctor of Science, June 1950.

† Professor of Textile Technology.

a conclusive end. One such basic element is that of the area of the surface of contact between fibers under the action of normal stresses. The ability to measure such areas permits experimental verification of a mathematical theory of large deformations of anisotropic visco-elastic materials to be obtained. It would appear, then, that the measurement of contact areas is basic to the development of the desired unified physical theory of interfiber stress transmission.

## Experimental Procedure and Results

In the transmission of stress between fibers under the application of a normal load, the nature of the stress distribution depends upon the area over which the stress is distributed, the shapes of the bodies in contact, and their relative mechanical properties. Hertz [2] has shown that in the case of small strains in isotropic Hookean materials, the distribution of stress and the nature of the area of contact may be expressed quantitatively from the theory of contact of such bodies. No such theory exists for anisotropic visco-elastic materials. It is important, then, that before quantitative study may be made of the transmission of the stress within fibrous structures such as yarns and fabrics, the means by which fibers transfer stress to one another and the nature of the contact area be established.

In the absence of an adequate theory for the transmission of such stress, it would appear to be necessary to develop means for measuring the contact area under the application of a wide range of normal loads. It is then obvious that if the relationship between the area of contact and the applied load conforms to the Hertzian relationships for Hookean materials, as a first approximation, it may be assumed that the distribution of stress likewise conforms. At the present stage, also, no adequate means exists for the direct measurement of this stress distribution. Thus, it is necessary to use indirect means of this nature.

The primary problem, then, consists of placing fibers in contact under measurable normal loads and determining the nature of their contact areas.

### *A. Apparatus*

*1. The Contact Area.*—The principal experimental problem is that of revealing the contact area in such a manner that its shape and dimensions may be determined for a given set of contact conditions. One important qualification which must be placed on such a method is that it must be rapid. This is important inasmuch as the size and shape of the area may be expected to change with time. A rapid method would also permit the measurement of the change in area as a function of time, a property which should be related to the stress-relaxation behavior of the material.

In the investigation of Hookean materials, Hertz [2] stated that he had revealed the contact area between metals and glass plates by placing the thinnest possible layer of lampblack over the glass surface and then placing the bodies in contact. The area of contact could then be clearly delineated from the surrounding area when viewed with obliquely reflected light. No mention was made of the method by which he produced such a layer, but he did state that if transmitted light could be seen through the film at the area of contact, the contact was imperfect. The measurement of the area should only be made if the film in the area of contact is unbroken. Evidently, he employed an opaque layer.

This suggestion hinted at a possible method for application to the problem at hand. However, the thickness of the layer to be obtained depends upon the size of the carbon particles, their density on the glass surface, and the number of layers of such particles. Hertz mentioned that this layer was only satisfactory when applied to a glass surface, a fact which will have greater significance later in this discussion. The various methods of producing layers of controllable particle size, density, and thickness were then considered.

In a quest for simplicity of method, recourse was taken to a Bunsen burner as a source of a flame which could be used for producing a thin smoke film on a glass surface. Such a flame was produced by burning commercial gas and closing the air ports on the burner so as to produce a completely yellow flame. The coarseness of particles produced from such a flame decreases toward the tip of the flame. It has also been reported that the finest particles are produced by flames of commercial gas. Flames of such pure gases as benzene produce much coarser particles.

In the author's early investigations with the flame, opaque layers were produced on microscope cover glasses by passing the cover glass through the flame a number of times. Such layers would transmit no light at all until a fiber had been pressed against the slide. The thickness of such layers, however, approximated the diameter of the fiber itself so that the impression obtained was merely that of the fiber

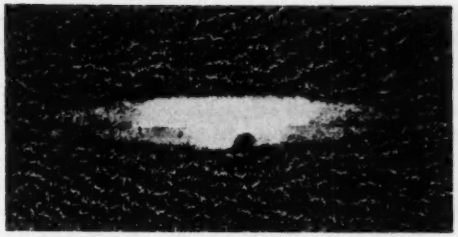

FIG. 1. *Impression of a fiber that had been pressed into a thick layer of carbon deposited by a flame on a glass slide.*

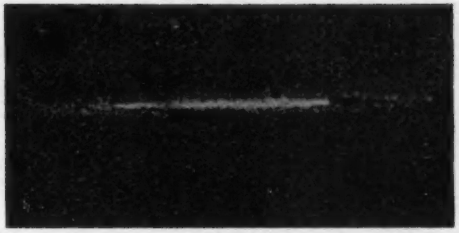

FIG. 2. *Impression of the same fiber as in Figure 1 under the same load, but obtained by using a thin film.*

in the layer. This is evidently the type of layer employed by Hertz.

Figure 1 shows the nature of such impressions in transmitted light. The area surrounding the fiber impression is composed of a thick layer of carbon particles. Within the impression itself may be seen the clear portion in the center where the fiber has removed or pushed aside the carbon particles of the layer. Between that area and the undisturbed film may be seen an area which consists of chains which have been crushed down and partially removed but where no contact has taken place between the fiber and the glass slide. A double impression may also be seen, which is due to the comparatively great distance which the fiber must travel in the experimental apparatus from the time it first touches the outer particles of the carbon layer until it is removed from the slide. This distance allows the lateral motions, which are possible in the platform of the experimental apparatus, to have an effect which is virtually eliminated when the layer is thin.

Removal of particles from the middle portion of the impression was verified by subsequent examination of the fiber. Particles of carbon could be seen clinging to the fiber.

When the impression shown in Figure 1 was examined by obliquely reflected light (produced by causing the light to impinge upon the slide from a small angle above the plane of the layer),* the width of the impression shadow was found to be 17.0 $\mu$. This may be compared with the diameter of the fiber, 29.2 $\mu$. Clearly, then, this must be a profile of the deformed fiber and not just the contact area between the glass and the fiber.

With the knowledge that this layer was far too thick to be used for the purpose desired, thinner layers were produced by placing the cover glass in the flame for shorter and shorter times. Eventually, it was a matter merely of drawing the cover glass rather rapidly through the tip of the flame. To the eye, the glass appeared slightly smoked and slightly reduced the intensity of light transmitted through it. However, in the microscope, no evidence of the layer could be detected other than the reduction of the intensity of transmitted light. This indicated that a layer of a very thin nature had been produced. Comparison with the thick layer, using the same fiber and the same normal load (Figure 2), indicated that the dimensions of the impressed area decreased to 5.1 $\mu$. Variations in the thickness of the layer, due to the difficulty in drawing the slide through the same point in the flame at the same velocity each time, did not produce significant changes in the dimensions of the impressed area at this level of thickness. This indicated that the thickness of the layer must be well below the diameter of the fiber and must be capable of indicating only the area of contact. Thus, any variation in the thickness of the layer must be well within the precision of the measurement of such parameters as the width of the contact area, the diameter of the fiber, and the applied normal load. It was decided that this condition was satisfactory for making the desired measurements.

The full significance of the nature of a carbon film produced in this manner was revealed in a discussion with the Cabot Laboratories, considered to be an authority in the field of carbon black. They have developed a method for producing layers of con-

* All photomicrographs have been taken with transmitted light, which requires the use of relatively thick layers of carbon film in order for them to be photographed. Measurements were made with reflected light, as described, but the intensity of illumination was insufficient for them to be photographed.

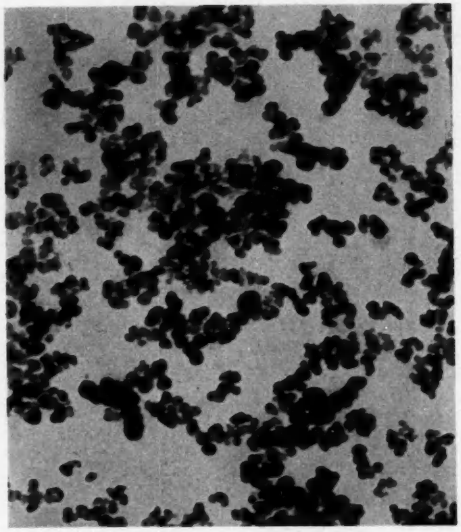

FIG. 3. *Electron photomicrograph of carbon-black layer produced by evaporation of an aqueous dispersion. Magnification, 50,000 ×. Particle size, 260 Å.* (Courtesy, Godfrey L. Cabot, Inc.)

trollable thickness on Formvar films supported by screens for use in the electron microscope. This consists of allowing a drop of an aqueous dispersion of carbon-black particles of known concentration to evaporate, leaving a thin film of carbon black for electron microscopic examination. Figure 3 shows the nature of the distribution and size of particles obtained in a layer of this kind. Such particles are relatively evenly dispersed and have a high density as compared with the thickness of the layer. On the other hand, layers produced by a flame are of an entirely different structure. Figure 4 shows quite clearly the exact nature of such layers and provides an explanation for the performance of these layers under the action of an impressed fiber. The film produced by the aqueous-dispersion method is virtually two-dimensional in nature, since its compressibility normal to the slide is of such a small order of magnitude that when a fiber is impressed upon it, it does not respond by providing a distinguishable contact area. On the other hand, a film produced by a flame, as shown by the stereo-micrographs of Figure 4, shows a remarkable three-dimensional structure.* It can be clearly seen that the carbon particles are arranged in long, branched chains extending out from the surface of the slide. However, these chains are thinly dispersed over the surface of the slide. It is not too difficult to imagine what occurs when a fiber is pressed against this structure. It may be presumed that these chains are crushed down against

* There are three ways in which the stereo effect may be obtained without removing Figure 4 from the JOURNAL: (1) holding one hand in front of the nose with the plane of the hand at a right angle to the face; (2) using a viewer which rests on a tripod; (3) using an ordinary viewer, which requires a mounted card, by holding up the page and bringing the viewer up to it.—*Editor.*

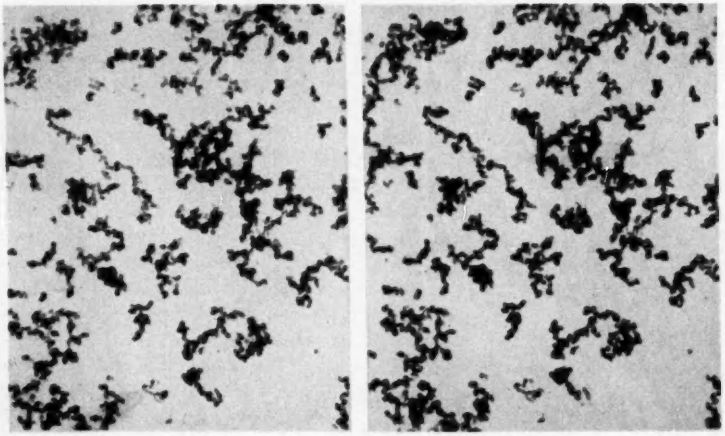

FIG. 4. *Electron stereomicrographs of carbon-black layer produced by passage through a benzene flame. Magnification, 10,000 ×. Particle size, 400–500 Å.* (Courtesy, Godfrey L. Cabot, Inc.)

the slide into a dense and chainless structure and, thus, produce a contact area which is clearly distinguishable in obliquely reflected light.

The thickness of such a layer may also be readily determined from a slide especially prepared for the electron microscope. In this instance, it was stated that the particle size was about 200 Å., and, with about 15 particles in the chain extending out from the slide, produced a chain length of about 3,000 Å. If, then, the layer is crushed down to a thickness of 4 or 5 particles, which is difficult to verify without considerable electron-microscope examination, it is not difficult to see that the crushed areas and noncrushed areas become sufficiently different to give measureable delineation. This thickness of layer is well within the dimensions necessary to eliminate the influence of its own thickness on the true width of the contact area. A thicker layer would tend to provide a measured area larger than the true area because of its contact with the fiber outside of the true plane or surface of contact.

An explanation for the chaining phenomenon has been suggested. When a glass surface is drawn through the flame, there is a large temperature differential between the glass surface and the particles in the flame. Thus, when the first particles come into contact with the surface, they are cooled rapidly. Subsequent particles, being of higher temperature, come into contact with these particles before they have a chance to reach the glass surface and, therefore, attach themselves to the cooler particles. This procedure continues for the length of time that the glass is in the flame. If, however, the slide is left in the flame for a longer period of time, the slide heats up and a large number of particles are interspersed with those already existing in chains. This produces the thick and opaque layer which was observed at the outset.

It is to be noted that the above observations were obtained with the use of Formvar films rather than with glass slides, as were used in the method described here. It has been stated that chains formed on a hydrocarbon base would tend, theoretically, to be much longer than those formed on a glass surface. Those films obtained on glass, then, might be expected not to exceed the thickness of those described above but, rather, to be somewhat thinner and, therefore, well within the required thickness limit.

It is to be appreciated that the character of layer produced is highly dependent upon the judgment of the operator. It is unfortunate that the procedure is not more quantitative and precise. However, with experimentation of the type indicated above, there is no reason why an operator cannot become proficient in producing sufficiently thin and reproducible layers which give results well within the precision of measurements of the other parameters.

*2. The Normal Load.*—This investigation has been limited to the effect of the load normal to the surfaces in contact. The problem in connection with the normal load is to be able to ensure that the load is normal to the surfaces and that the mechanism for producing and measuring the load level does not influence the area of contact. Obviously, much mechanical motion or vibration in the mechanical system would have great influence upon the contact area.

Again, simplicity of mechanism was sought. Figure 5 is a picture of the apparatus used to produce the normal load. It consists of an inverted projection microscope that is securely fastened to the table. This mechanical arrangement minimizes bending the entire system due to the application of load. It is apparent that apparatus could be designed which would have exceedingly higher rigidity factors, but this apparatus appeared to be adequate for the present

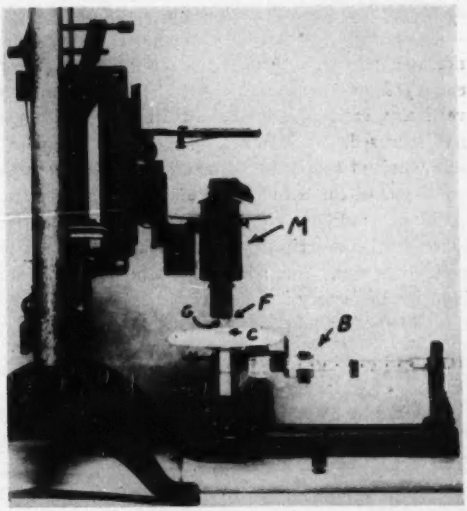


FIG. 5. *Load-producing and -measuring apparatus. F—Fiber. M—Microscope. G—Solid glass rod. B—Beam balance. C—Cover glass on slide cemented to platform.*

investigation. Across the bottom end of the body tube was cemented a glass slide on which was mounted a length of solid glass rod 2.485 mm. in radius.

Beneath this tube is a triple-beam balance with a scale range from 0 to 2,000 g., sensitive to 0.1 g. A stop was arranged to prevent the beam from dropping more than two divisions below the balance point, thus minimizing any lateral motion of the platform. It is obvious that this balance is not necessarily uniquely adapted for this investigation. Its principal merits are that it allows a wide range of loads in the region desired and it is sufficiently rugged to give mechanical rigidity of the type encountered in the projection-microscope system. It is likewise true that a more universal and mechanically rigid load-measuring system could be designed to do a more adequate job, but the system described gave reproducible results except in the low-capacity range of the instrument and was considered to be adequate for the present investigation.

*3. The Microscope.*—The contact areas obtained were of exceedingly small dimensions and, thus, it was necessary to employ a calibrated microscope in order to measure the dimensions of these areas.

A filar micrometer was employed in combination with 4-, 8-, and 16-mm. objectives. A stage micrometer was used to calibrate the filar-micrometer scale.

The arrangement of the source of light was of particular importance. A focusable microscope light was employed for this work. It could be readily adjusted vertically, easily rotated, adjusted for vertical angle, and focussed. A satisfactory lighting arrangement was obtained simply by adjusting the glancing angle and focus of the light source until the contact areas could be readily distinguished and measured. No more precise description of the arrangement can be given than this. The criterion of whether or not the light is satisfactory is a matter of the personal judgment of the individual observer.

### *B. Method of Measurement*

*1. Fibers.*—The problem at hand required that the fibers employed have diameters lying in the range occupied by textile fibers and that they be perfectly circular. It was also considered desirable to use a fiber which had no secondary creep and which had a relatively high modulus of elasticity to permit the use of relatively high loads in the measurement of contact areas. These requirements were met quite adequately through the use of nylon which was fully drawn. This had the additional feature of being a continuous-filament fiber and, as such, had a relatively uniform diameter over the lengths employed in this investigation.

The fibers actually used were dissected from a continuous-filament yarn composed of many filaments. It was not expected that these filaments would be identical in diameter. A study was made, therefore, to determine if the mean diameter of a group of measurements was representative of all the filaments or if it would be necessary to measure the diameter of each filament in the region of applied normal load. A statistical comparison of the differences between the diameters of different filaments and between those measured along the same filament indicated that the variation along a filament is insignificant in comparison with the differences between filaments. Thus, it was necessary to measure the diameter of each filament used.

*2. Contact Areas.*—Inasmuch as the carbon film described above cannot be obtained on a fiber but only on a glass surface, the type of glass solid against which to press the fiber was investigated. In order to provide a rigid plane surface, a microscope slide was cemented to the surface of the triple-beam-balance scale platform. The smoke film could then be placed on cover glasses and these placed on the glass-slide base. This formed an almost ideally plane surface against which to press the fiber.

The glass rod mounted on the lower end of the inverted projection microscope was employed as a means for overcoming the problem of getting the lower end of the load unit absolutely parallel with the surface of the balance. This was done by making the length of the glass rod about equal to the rod's diameter or considerably smaller than the width of the cover glass. Slight nonparallelism in any direction, then, would not be expected to affect the results so long as the rod did not at any time contact the cover glass.

The fiber was then placed across this rod at right angles to its axis. This angle could be made any one desired, but the simplest theoretical case is when the angle is 90 degrees. The two principal radii involved are the radius of the straightened fiber, as predetermined in the microscope, and that of the glass rod. When this arangement was pressed against the smoked cover glass, elliptical patterns were produced over a considerable range of loads.

In use, the value of the load to be applied to the fiber was set on the beam of the balance and the tube was run down until the fiber touched the smoked slide. The tube was run down further until the balance was level and was then reversed until the fiber was withdrawn from the surface. The slide was then removed and placed in the microscope for examination. The filar micrometer could then be used to measure the principal axes of the elliptical impression or camera-lucida drawings could be made.

### *C. Contact Areas of Various Textile Materials*

The development of the carbon-film method of revealing the contact area between fully drawn nylon filaments and glass surfaces has made it possible to investigate the contact areas of other forms of textile materials. At this stage, however, it is not possible to obtain simple mathematical relationships between the contact area, applied normal load, geometry of the material, and the stress distribution over the area of contact. However, the method is capable of providing the concentrated area of contact as a function of the load applied to a given material. In order to explore the application of the method to other forms of textile materials, a number of varied examples of such materials were subjected to the method described.

Continuous-filament viscose rayon is equivalent, in many respects, to the fully drawn nylon used in this investigation in that it is relatively uniform in cross section axially and does not have a complex microscopic structure. As a fiber, however, it represents a degree of complexity which is above that of the fully drawn nylon. It has considerable secondary creep and a highly irregular cross section as a result of the longitudinal striations which are characteristic of this fiber. It may be expected, then, that the area of contact would not be of the regular character of that obtained for the fully drawn nylon filament. Figure 6 shows an impression of such a viscose filament under a normal load of 5 g. The appearance of two separate areas of contact is not an accident of the experiment but could be repeated many times. The only explanation for the appearance of two such areas is that two striations are in contact with the cover glass and that a distinct region separates them.

Another type of fiber structure is that represented by the wool fiber. It is a natural staple fiber and, consequently, has a variable structure along its length. Internally, the wool fiber consists of cells and a central channel, departing materially from the simple structure of the nylon and the viscose filaments. It is naturally highly crimped and cannot be completely straightened without stretching. Its surface is highly irregular, consisting of visible scales. A specimen of 62's domestic wool was subjected to a normal load of 5 g. and the contact area obtained as in Figure 7. The area of contact is not as clearly defined as that obtained with the nylon and viscose filaments. This may be accounted for, in part, by the irregularity of the surface of the fiber itself; but the waviness of the pattern may be accounted for in the crimp of the fiber.

A 40/1 combed cotton yarn was selected to show the effect of combining a number of fibers and inserting twist into the strand. Figure 8 shows the result of the application of a 5-g. load to such a yarn. It is

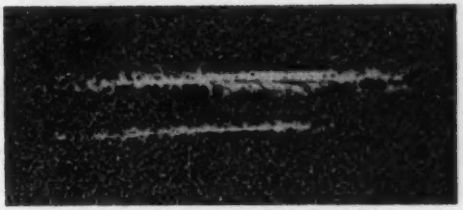

FIG. 6. *Carbon-film imprint of a filament of viscose rayon.*

FIG. 7. *Carbon-film imprint of a wool fiber.*

FIG. 8. *Carbon-film imprint of a 40/1 combed cotton yarn.*

FIG. 9. *Carbon-film imprint of a cotton tire cord.*

FIG. 10. *Carbon-film imprint of an 8.5-oz.-per-sq.-yd., high-sley tent duck, two ends woven as one. Dashed areas indicate contacts of double ends.*

quite evident that the individual fibers of which the yarn is composed are at a uniform angle with the axis of the yarn, and the area of contact of each is clearly definable. Nothing can be said, however, about the distribution of stress among such a group of fibers.

The diagrams produced with cotton tire cord under a 500-g. load exhibit a similar type of contact area of individual fibers but, in addition, give a clear picture of the ply and cord twist structure. This can be seen in Figure 9. It is to be noted in particular that the individual fibers lie parallel with the axis of the cord, an indication of balanced twist.

The final material investigated was an 8.5-oz.-per-sq.-yd., high-sley cotton duck. This construction is composed of single warp and filling yarns, but is woven in an Oxford weave, two ends woven as one. Figure 10 clearly shows both the general contact areas produced by the warp yarns and the concentrated areas of the fibers of which they are composed. In this respect, the areas produced by the exposed warp yarns are similar to those of the individual yarn shown in Figure 8. However, a load of 500 g. was used on the fabric against 5 g. on the individual yarn.

## Summary and Conclusions

The above results show that the method of revealing concentrated contact areas is applicable to a wide variety of textile materials. In this respect, it may prove valuable in such studies as the transmission of stress within textile materials, transmission of stress through friction to other materials, and the abrasive wear of textile materials.

## Acknowledgment

Gratitude is expressed for the assistance of Miss Mary Martin and Mr. Henry Avery of the Godfrey L. Cabot Laboratories, Inc., in furnishing various samples of carbon black, for preparing aqueous dispersions and electron photomicrographs of the structure of their films on glass, and advising on the structure of films produced by flames on glass.

The advice of Dr. Kurt Lion of the M. I. T. Department of Biology relative to experimental techniques and the structure of carbon films on various bases is gratefully mentioned. The remainder of the photographs and photomicrographs were prepared by Mr. Henry H. Broadfoot of the M. I. T. Textile Division.

## Literature Cited

1. Germant, A., "Frictional Phenomena," Brooklyn, N. Y., Chemical Publishing Co., 1950.
2. Hertz, H. R., "On the Contact of Rigid Elastic Solids and on Hardness," Miscellaneous Papers, London, Macmillan Co., 1896, pp. 163–83.

(*Manuscript received November 16, 1950.*)

# Part II: Theory of the Pressure Distribution and Contact Area Between Fibers

**Abstract**

A study of the assumptions underlying the development of the Hertzian equations for the distribution of pressure and the shape of the contact areas of curved isotropic elastic solids has been made. The applicability of these equations to certain anisotropic visco-elastic fibers has been experimentally investigated and verified.

IN PART I it was shown that the development of a method for determining the contact area between fibers under the action of a pressure distribution is fundamental to the development of a unified physical theory of interfiber stress transmission. A method which employed a thin layer of smoke on a glass surface as the means for revealing the shape of the contact area of a fiber was described.

In the transmission of stress between fibers, it is necessary to recognize those factors which play a dominant part in determining the nature of the stress transfer. The first of these is the geometry of the surfaces in contact. Obviously, rough surfaces in contact would manifest completely different stress distributions from those which are smooth at the molecular level. A complete definition and description of the surface geometry is, then, necessary if the frictional phenomenon is to be understood other than empirically. Surfaces which in the larger geometrical sense are curved or plane would reflect stress distributions and contact areas that are dependent upon the degree of curvature. Finally, the physical behavior of the solid continuum underlying the surface would determine the extent to which areas under stress would deform and the manner in which the stress would be transferred into the continuum. A rather complete study of these factors has been made in the field of isotropic elastic solids [2] and rather adequate theories developed for these materials. However, little such information in the field of anisotropic visco-elastic materials is available for the development of similar theories.

The principal barrier in the development of such a complete and fundamental theory is the lack of an adequate theory of large deformations of solid continua of the visco-elastic type. Many investigators are now concerning themselves with this problem in basic research. However, until a completely adequate theory is found, a rather serious limitation will continue to be imposed upon those seeking to explain physical phenomena in this class of materials in terms of fundamental scientific laws.

Even with the lack of such a complete theory, it is necessary to proceed within the imposed limitations to select a simple theory already in existence, even though the basic assumptions might not be adequate, and determine experimentally whether or not the theory is adequate. Such a starting point is provided in the form of the development for isotropic elastic solids based upon the derivations of Hertz [3]. It was reasoned that if the relationship between the applied normal load, the contact area between two isotropic elastic solids, their physical properties, and their geometry were verified experimentally, both the area of contact and the stress distribution over the area could then be quantitatively defined. Obviously, both of these parameters must be known before the addition of tangential stresses may be investigated as in the frictional phenomenon.

Recognizing the drastic limitations placed upon the materials being investigated, it was decided to determine whether or not the Hertzian derivations were even a first approximation to the performance of anisotropic visco-elastic materials in the form of fibers or filaments. It was reasoned that if this were a close approximation, the assumptions relative to the stress distribution might likewise be applied. For this purpose, fully drawn nylon filaments approximately 15 $\mu$ in radius were selected for the reason that they are exceedingly uniform along their lengths in radius and circularity. This eliminated the necessity for having to investigate this relationship with a large number of specimens in order to treat the results statistically. Another

factor was that the fully drawn nylon is almost completely devoid of secondary creep, and, thus, it could be expected that cyclic evaluations would be comparable.

Although nylon might not be representative of the bulk of the natural and synthetic textile fibers, nevertheless it might be considered to be a model anisotropic visco-elastic material and, in this respect, to be admirably suited to a basic investigation. The apparatus was limited in accuracy to readings of 0.5 g. in so far as the calibration of the platform scale was concerned. However, investigation of the contact areas between filaments and smoked cover glasses indicated that the practical limit for the entire assembly was slightly above 1.5 g. No readings below 2 g., therefore, were taken. The reason for this limitation appeared to be the rigidity of the entire system, and primarily that of the platform scale; at very low loads, the slightest vibration from any source caused the fiber to slip over the surface of the cover glass and produce multiple patterns which could not be analyzed. Thus, investigation was limited to moderately high and high normal loads.

This limitation made even more questionable the possibility that the Hertzian derivations would be applicable even as a first approximation. It might be expected that for very low loads and very low deformations there might be good agreement. Agreement at large deformations, however, would certainly be less certain. In this respect, there is a definite need for an instrument which would provide sensitivities and rigidities far greater than those of the instrument used in this investigation; this would make possible an extension of the experimental and theoretical approach employed here to the region of small strains.

## Theory of the Area of Contact of Curved Elastic Solids

Hertz [3, 4] was the first to provide a quantitative basis for the theoretical area of contact of curved elastic solids. The following is based upon his original conception and represents an extension to special cases which are of interest in connection with the basic problem.

When two curved elastic isotropic bodies are pressed together, they contact each other over a finite area. The common pressure is distributed over this area. Such a contact area may be expressed mathematically since the bodies are assumed to be perfectly smooth. Furthermore, the force which presses the bodies together acts along the common normal. In a rectangular rectilinear system of coordinates the common tangent plane is designated as the $xy$-plane, with the common normal as the $z$-axis. The origin of the axis system is at the point of contact. Only the region in the vicinity of this origin will be considered, as the stresses acting between the surfaces are confined to this area and are dependent to a minor extent upon the state of stress elsewhere in the bodies.

### *A. General Case*

The distance between points on the surface of the bodies and the tangent plane in the area close to the origin (Figure 1) can be represented by a homogeneous quadratic function of $x$ and $y$ as a close approximation. The equations for the two surfaces may then be given by

$$z_1 = A_1x^2 + C_1xy + B_1y^2$$

and (1)

$$z_2 = A_2x^2 + C_2xy + B_2y^2,$$

and the distance between the two surfaces by

$$z_1 - z_2 = Ax^2 + By^2, \qquad (2)$$

where $A = A_1 - A_2$ and $B = B_1 - B_2$. The term involving $xy$ is eliminated by suitably orienting the

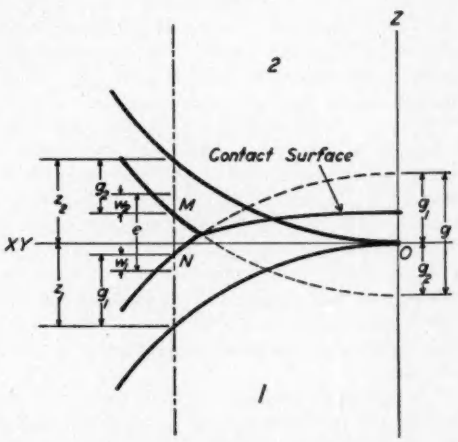


FIG. 1. *Contact surface of pressure formed when two curved bodies (1 and 2) are pressed together.*

$x$- and $y$-axes. By selecting the positive $z$-axis in the body designated by the index $I$, $A$ and $B$ become positive quantities. The locus of corresponding points on the two surfaces having the same value of $z_1 - z_2$ is an ellipse the center of which is the origin. Thus, for different values of $z_1 - z_2$ a system of similar ellipses is formed.

Next, consider that in each body there exists a rectangular rectilinear system of axes rigidly connected with each body at infinity and coinciding with the $xyz$ system of axes defined above. Upon application of pressure between the two bodies, the coordinate systems will be shifted along the $z$-axis relative to one another. The motion of each set of axes from the origin along $z$ will be equal to the distance which a point at an infinite distance from the point of contact approaches the origin under the action of the pressure. This will also correspond with the motion of all points in the body if the solids could penetrate each other without change in shape. Such motion is shown in Figure 1 by the dashed lines. The relative motions of the bodies are $g_1$ and $g_2$, respectively. As points such as $M$ and $N$ enter the surface of pressure, however, they are respectively compressed $w_2$ and $w_1$. If $e$ is the distance between two corresponding points after deformation, then

$$e = (z_1 - z_2) - (g_1 - g_2) + (w_1 - w_2), \quad (3)$$

or, from before,

$$e = Ax^2 + By^2 - g + (w_1 - w_2). \quad (4)$$

The problem now is to obtain a mathematical shape for the surface of pressure, a system of displacements, and a system of stresses which will conform with the following conditions:

1. The bodies in contact are Hookean in their elastic behavior and may be described in terms of a Young's modulus, $E$, and a Poisson's ratio, $\nu$.

2. Internal distribution of stress, $\sigma$, and strain, $\epsilon$, must be such that the equations of compatibility are conformed with:

$$(1 + \nu)\nabla^2\sigma_x + \frac{\partial^2\theta}{\partial x^2} = 0; \quad (5a)$$

$$(1 + \nu)\nabla^2\sigma_y + \frac{\partial^2\theta}{\partial y^2} = 0; \quad (5b)$$

$$(1 + \nu)\nabla^2\sigma_z + \frac{\partial^2\theta}{\partial z^2} = 0; \quad (5c)$$

where $\theta = \sigma_x + \sigma_y + \sigma_z$, and

$$\nabla\sigma = \frac{\partial\sigma}{\partial x} + \frac{\partial\sigma}{\partial y} + \frac{\partial\sigma}{\partial z}.$$

3. The following boundary conditions must be met:

   (*a*) At infinity, $\epsilon_x$, $\epsilon_y$, $\epsilon_z$ vanish because the coordinate system is rigidly connected to the body at this point.

   (*b*) Outside the surface of pressure, the normal stress vanishes.

   (*c*) Inside the surface of pressure: (1) tangential stresses normal to the $z$-axis are zero; (2) at a point, the normal stress in one body equals that in the other; (3) integral of pressure equals total load, $N$, applied; (4) $\sigma_z$ is positive; (5) $e$ reduces to zero and

$$w_1 - w_2 = g - Ax^2 - By^2. \quad (6)$$

   Outside the surface of pressure:

$$w_1 - w_2 > g - Ax^2 - By^2; \quad (7)$$

   otherwise, one body would flow into the other.

Hertz [4] has shown by analogy with the distribution of static charges that such a surface is given by

$$Q = \frac{3N}{16\pi}\int_u^\infty \left(1 - \frac{x^2}{a^2 + \lambda} - \frac{y^2}{b^2 + \lambda} - \frac{z^2}{\lambda}\right) \times \frac{d\lambda}{\sqrt{(a^2 + \lambda)(b^2 + \lambda)\lambda}}, \quad (8)$$

where $u$ is the positive root of the cubic equation

$$0 = 1 - \frac{x^2}{a^2 + u} - \frac{y^2}{b^2 + u} - \frac{z^2}{u}. \quad (9)$$

Such a surface is bounded by an ellipse the semi-axes of which ($a$ and $b$) lie along the axes $x$ and $y$, respectively. The equations for the axes of the ellipse of pressure are then given by

$$\int_0^\infty \frac{du}{\sqrt{(a^2 + u)^3(b^2 + u)u}} = \frac{4}{3N}\frac{A}{k_1 + k_2} \quad (10)$$

and

$$\int_0^\infty \frac{du}{\sqrt{(a^2 + u)(b^2 + u)^3u}} = \frac{4}{3N}\frac{B}{k_1 + k_2}, \quad (11)$$

where

$$k = \frac{1 - \nu^2}{\pi E}. \quad (12)$$

If the ratio $f = \frac{b}{a}$ is introduced, then, by the transformation $u = b^2z^2$:

$$\frac{1}{a^3}\int_0^\infty \frac{dz}{\sqrt{(1+f^2z^2)^3(1+z^2)}} = \frac{2}{3N}\frac{A}{k_1+k_2}; \quad (13)$$

and $u = a^2z^2$:

$$\frac{1}{b^3}\int_0^\infty \frac{dz}{\sqrt{\left(1+\frac{z^2}{f^2}\right)^3(1+z^2)}} = \frac{2}{3N}\frac{B}{k_1+k_2}. \quad (14)$$

The constants $A$ and $B$ which appear in equation (2) are related to the principal radii of curvature of the two bodies as well as the angle between the planes containing these radii. Let these radii for the first body be $R_{11}$ and $R_{12}$, and for the second body $R_{21}$ and $R_{22}$. Let $\omega$ be the angle between the planes of $R_{11}$ and $R_{21}$. Radii are considered as being positive if their centers lie within the body. The axes $xy$ are so placed that the $xz$-plane forms an angle $\omega'$ with the plane of $R_{11}$.

The equations of the surfaces then become

$$2z_1 = \frac{(x\cos\omega' + y\sin\omega')^2}{R_{11}} + \frac{(y\cos\omega' - x\sin\omega')^2}{R_{12}} \quad (15)$$

and

$$2z_2 = -\frac{[x\cos(\omega'-\omega) + y\sin(\omega'-\omega)]^2}{R_{21}} - \frac{[y\cos(\omega'-\omega) - x\sin(\omega'-\omega)]^2}{R_{22}}. \quad (16)$$

From equation (2) the distance between the two surfaces, $z_1 - z_2$, is equal to $Ax^2 + By^2$. Subtracting equation (16) from equation (15) and substituting $Ax^2 + By^2$ gives three equations in $A$, $B$, and $\omega'$, where

$$\tan 2\omega' = \frac{\left(\frac{1}{R_{21}} - \frac{1}{R_{22}}\right)\sin 2\omega}{\left(\frac{1}{R_{11}} - \frac{1}{R_{12}}\right) + \left(\frac{1}{R_{21}} - \frac{1}{R_{22}}\right)\cos 2\omega}, \quad (17)$$

$$2(A+B) = \frac{1}{R_{11}} + \frac{1}{R_{12}} + \frac{1}{R_{21}} + \frac{1}{R_{22}}, \quad (18a)$$

$$2(A-B) = -\left[\left(\frac{1}{R_{11}} - \frac{1}{R_{12}}\right)^2 + 2\left(\frac{1}{R_{11}} - \frac{1}{R_{12}}\right)\times\left(\frac{1}{R_{21}} - \frac{1}{R_{22}}\right)\cos 2\omega + \left(\frac{1}{R_{21}} - \frac{1}{R_{22}}\right)^2\right]^{\frac{1}{2}}. \quad (18b)$$

Introducing an auxiliary angle, $\tau$, where

$$\cos\tau = -\frac{A-B}{A+B}, \quad (19)$$

gives

$$2A = \left(\frac{1}{R_{11}} + \frac{1}{R_{12}} + \frac{1}{R_{21}} + \frac{1}{R_{22}}\right)\sin^2\frac{\tau}{2} \quad (20)$$

and

$$2B = \left(\frac{1}{R_{11}} + \frac{1}{R_{12}} + \frac{1}{R_{21}} + \frac{1}{R_{22}}\right)\cos^2\frac{\tau}{2}. \quad (21)$$

Equations (13) and (14) may now be expressed in the form

$$\frac{1}{a^3}\int_0^\infty \frac{dz}{\sqrt{(1+f^2z^2)^3(1+z^2)}} = \frac{1}{3N}\frac{\left(\frac{1}{R_{11}} + \frac{1}{R_{12}} + \frac{1}{R_{21}} + \frac{1}{R_{22}}\right)}{k_1+k_2}\sin^2\frac{\tau}{2} \quad (22)$$

and

$$\frac{1}{b^3}\int_0^\infty \frac{dz}{\sqrt{\left(1+\frac{z^2}{f^2}\right)^3(1+z^2)}} = \frac{1}{3N}\frac{\left(\frac{1}{R_{11}} + \frac{1}{R_{12}} + \frac{1}{R_{21}} + \frac{1}{R_{22}}\right)}{k_1+k_2}\cos^2\frac{\tau}{2}. \quad (23)$$

By dividing equation (22) by equation (23), we obtain

$$f^3\frac{\int_0^\infty \frac{dz}{\sqrt{(1+f^2z^2)^3(1+z^2)}}}{\int_0^\infty \frac{dz}{\sqrt{\left(1+\frac{z^2}{f^2}\right)^3(1+z^2)}}} = \tan^2\frac{\tau}{2}, \quad (24)$$

a transcendental equation in the ratio $f$ and in $\tau$. Legendre's tables may then be used to evaluate this integral so that $a$ and $b$ may be expressed as

$$a = m\sqrt[3]{\frac{3\pi N(k_1+k_2)}{2\left(\frac{1}{R_{11}} + \frac{1}{R_{12}} + \frac{1}{R_{21}} + \frac{1}{R_{22}}\right)}} \quad (25)$$

and

$$b = n\sqrt[3]{\frac{3\pi N(k_1+k_2)}{2\left(\frac{1}{R_{11}} + \frac{1}{R_{12}} + \frac{1}{R_{21}} + \frac{1}{R_{22}}\right)}}. \quad (26)$$

The coefficients $m$ and $n$ are then transcendental functions of the auxiliary angle, $\tau$. These values

TABLE I. HERTZ COEFFICIENTS AS A FUNCTION OF AUXILIARY ANGLE, $\tau$ [4, 6]

| $\tau$ | $m$ | $n$ |
|---|---|---|
| 0 | $\infty$ | 0.000 |
| 10 | 6.612 | 0.319 |
| 20 | 3.778 | 0.408 |
| 30 | 2.731 | 0.493 |
| 35 | 2.397 | 0.530 |
| 40 | 2.136 | 0.567 |
| 45 | 1.926 | 0.604 |
| 50 | 1.754 | 0.641 |
| 55 | 1.611 | 0.678 |
| 60 | 1.486 | 0.717 |
| 65 | 1.378 | 0.759 |
| 70 | 1.284 | 0.802 |
| 75 | 1.202 | 0.846 |
| 80 | 1.128 | 0.893 |
| 85 | 1.061 | 0.944 |
| 90 | 1.000 | 1.000 |

are given in Table I, having been calculated by Hertz [4] and by Whittemore and Petrenko [6].

The above expressions indicate that the semi-axes of the ellipse of pressure vary as the cube root of the normal pressure, inversely as the cube root of the sum of the reciprocals of the radii of curvature, and inversely as the cube root of the moduli of elasticity.

The surface of pressure so described is not a plane, but, rather, is part of a quadric surface formed by the contact of the two bodies. It takes a shape most like that of the body having the larger modulus of elasticity. Thus, the bodies essentially indent each other and approach each other an amount $g$, previously described. Hertz [3] has shown that it may be expressed as

$$g = \frac{3N}{2}\frac{k_1 + k_2}{a}\int_0^\infty \frac{dz}{\sqrt{(1 + f^2z^2)(1 + z^2)}}. \quad (27)$$

If $g$ is separated into its two parts, composed of $k_1$ and $k_2$, it is found that these are the respective indentations or amounts that the origin has approached the infinitely distant portions of the bodies. If the value $a$ is substituted, $g$ may be seen to vary as the $\frac{2}{3}$ power of the applied normal load, $N$.

The distribution of the pressure, $\sigma_z$, over the surface of pressure is given by Hertz [3]:

$$\sigma_z = -\frac{3N}{2\pi ab}\sqrt{1 - \frac{x^2}{a^2} - \frac{y^2}{b^2}}, \quad (28)$$

the equation of a semi-ellipsoid constructed on the

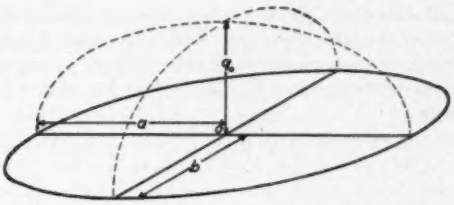


FIG. 2. *Semi-ellipsoid of stress over the ellipse of contact between two curved bodies under pressure. (Timoshenko* [5].)

surface (Figure 2). $\sigma_z$ has its maximum value at the origin;

$$q_0 = -\frac{3N}{2\pi ab}, \quad (29)$$

or a value which is $1\frac{1}{2}$ times the average pressure, $\frac{N}{\pi ab}$, over the surface.

*B. Special Case—Cylinders in Contact*

*1. At an Angle $\omega$ Between the Planes of Their Principal Radii.*—Two cylinders in contact at an angle $\omega$ between the planes of their principal radii introduce a simplification in that $R_{12} = \infty$ and $R_{22} = \infty$.

Thus, equation (18) becomes

$$2(A + B) = \left(\frac{1}{R_1} + \frac{1}{R_2}\right) \quad (30)$$

and

$$2(A - B) = -\sqrt{\left(\frac{1}{R_1}\right)^2 + \left(\frac{2}{R_1R_2}\right)\cos 2\omega + \left(\frac{1}{R_2}\right)^2}, \quad (31)$$

while equation (19) becomes

$$\cos\tau = \sqrt{\frac{\left(\frac{1}{R_1}\right)^2 + \left(\frac{2}{R_1R_2}\right)\cos 2\omega + \left(\frac{1}{R_2}\right)^2}{\left(\frac{1}{R_1}\right)^2 + \left(\frac{2}{R_1R_2}\right) + \left(\frac{1}{R_2}\right)^2}}; \quad (32)$$

$a$ and $b$ reduce to

$$a = m\sqrt[3]{\frac{3\pi N(k_1 + k_2)}{2\left(\frac{1}{R_1} + \frac{1}{R_2}\right)}} \quad (33)$$

$$b = n\sqrt[3]{\frac{3\pi N(k_1 + k_2)}{2\left(\frac{1}{R_1} + \frac{1}{R_2}\right)}}, \quad (34)$$

while $g$ is given by equation (27).

*2. Identical Cylinders at an Angle $\omega$ Between the Planes of Their Principal Radii.*—A case of particular interest arises when two identical cylinders are in contact. Here $R_1 = R_2 = R$ and $k_1 = k_2 = k$. Then

$$2(A + B) = \frac{2}{R} \tag{35}$$

and

$$2(A-B) = -\sqrt{\frac{2}{R^2}(1 + \cos 2\omega)} = -\frac{2}{R}\cos\omega. \tag{36}$$

Hence,

$$\cos\tau = \cos\omega, \tag{37}$$

or

$$\tau = \omega; \tag{38}$$

then

$$a = m\sqrt[3]{\frac{3\pi NkR}{2}} = m\sqrt[3]{\frac{3NR(1-\nu^2)}{2E}} \tag{39}$$

and

$$b = n\sqrt[3]{\frac{3\pi NkR}{2}} = n\sqrt[3]{\frac{3NR(1-\nu^2)}{2E}}, \tag{40}$$

while $g$ becomes

$$g = \frac{3N(1-\nu^2)}{\pi aE}\int_0^\infty \frac{dz}{\sqrt{(1+f^2z^2)(1+z^2)}}. \tag{41}$$

*3. Along a Generator.*—This case is not as easily derived as the above. As $\omega = 0$, $\tau = 0$, the semi-major axis $a$ approaches infinity, and the normal load, $N$, also must approach infinity if the normal load per unit length of contact is to be finite.

Thus, in equation (21):

$$B = \frac{1}{2}\left(\frac{1}{R_1} + \frac{1}{R_2}\right). \tag{42}$$

In equation (11), $u$ is small compared with $a^2$. $a$ may then be taken outside the sign of integration and an arbitrary constant, $\frac{4}{3}p$, substituted for $\frac{N}{a} = \frac{\infty}{\infty}$. Thus,

$$\int_0^\infty \frac{du}{\sqrt{(b^2+u)^3u}} = \frac{\left(\frac{1}{R_1} + \frac{1}{R_2}\right)}{2p(k_1 + k_2)}. \tag{43}$$

Integration then gives

$$b = \sqrt{\frac{4p(k_1 + k_2)}{\left(\frac{1}{R_1} + \frac{1}{R_2}\right)}}. \tag{44}$$

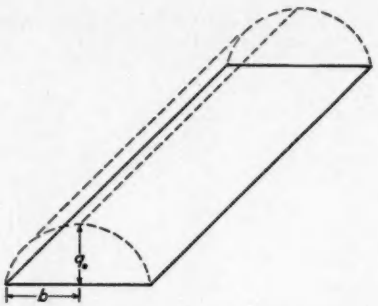


FIG. 3. *Semi-elliptical band of stress between two cylinders under pressure.* (*Timoshenko* [5].)

The distribution of pressure over the surface now becomes a semi-ellipse (Figure 3) and equation (28) reduces to

$$\sigma_z = -\frac{2p}{\pi b^2}\sqrt{b^2 - y^2}. \tag{45}$$

The maximum value, $q_o$, is again at the origin and becomes

$$q_o = -\frac{2p}{\pi b} = -\sqrt{\frac{p\left(\frac{1}{R_1} + \frac{1}{R_2}\right)}{\pi^2(k_1 + k_2)}}. \tag{46}$$

Thus, it may be seen that $p$ is the normal load per unit length of contact. The distance of approach, $g$, becomes logarithmically infinite in the general equation (27). Thus, it depends upon the shape of the body as a whole and not just upon the place of contact. As such, it cannot be determined from the above relationships.

*4. Identical Cylinders in Contact Along a Generator.*—This is again a case of particular interest in which $R_1 = R_2 = R$ and $k_1 = k_2 = k$. Then

$$b = \sqrt{4pkR} = 2\sqrt{\frac{pR(1-\nu^2)}{\pi E}} \tag{47}$$

and

$$q_o = -\sqrt{\frac{p}{\pi^2 kR}} = -\sqrt{\frac{pE}{\pi R(1-\nu^2)}}. \tag{48}$$

*5. Cylinder in Contact with an Incompressible Plane.*—If a cylinder is in contact with a plane composed of material such that $k_1$ of the cylinder is very much larger than $k_2$ of the plane ($k_1 \gg k_2$), the relationships reduce to

$$b = 2\sqrt{\frac{pR(1-\nu^2)}{\pi E}} \tag{49}$$

and

$$q_o = -\sqrt{\frac{pE}{\pi R(1-\nu^2)}}, \qquad (50)$$

or expressions which are identical with those obtained for two identical cylinders in contact along a generator, as given in equations (47) and (48). Inasmuch as the cylinders deform by like amounts, all points of contact must lie in the plane $z = 0$, as simulated by the contact of a single cylinder and an incompressible plane.

### Experimental Procedure and Results

With the use of the apparatus that is described in Part, I, a filament of fully drawn nylon with a radius of 12.6 $\mu$ was placed over the lower end of the microscope tube and bent over the glass rod at that point. The glass rod has a radius of 2,485 $\mu$ and is shown diagrammatically in Figure 4. Under standard testing conditions of 70°F and 65% R.H., the specimen was subjected to a succession of normal loads in the apparatus described. A slow rate of load was used, although it was not possible to define it quantitatively because it was done by hand. Each impression at each different load was obtained in approximately 30 sec.—from the time the fiber first touched the smoked coverglass, through the point at which the triple-beam balance point reached the balance, to the time the fiber was removed from contact with the cover glass. An interval of approximately 5 min. elapsed between readings made with successive values of load.

Care was taken to ensure that the fiber was not subjected to any handling prior to its being placed in the apparatus and that it was fastened to the microscope tube with a very light tension. No mechanical preconditioning was attempted because it was felt that the secondary creep in the fully drawn nylon was of a magnitude which was well below the relatively large deformations to which the fiber would be subjected. The 30-sec. time interval was arbitrary and was certainly not sufficient to allow the primary creep to become relatively stabilized. This was considered to be desirable because of the vibrations present in the vicinity of the test equipment. Longer intervals produced fuzzy patterns because of these vibrations. However, the 5-min. rest between impressions gave the fiber a sufficiently long time to allow a major proportion of the primary creep to recover.

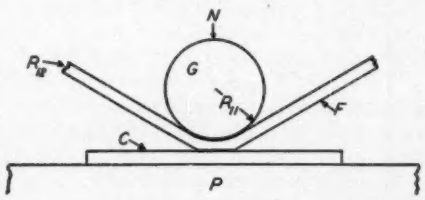


FIG. 4. *Experimental apparatus arranged with fiber,* F, *of radius* $R_{12}$ *bent across glass rod,* G, *of radius* $R_{11}$; *the fiber acts with normal force,* N, *on the smoked coverglass,* C, *resting on platform scale,* P.

The geometrical conditions chosen for test—that of a curved cylinder in contact with an incompressible plane—is identical with the condition which would be met if two such identical cylinders of the same curvature were in contact at an angle of zero between their axes ($\omega = 0$). This has been shown in the above cases and can easily be proved for this special case of identically curved cylinders. For this reason, it is not necessary to actually bring two fibers into contact in the investigation of contact area.

Figure 4 shows the relationships of the various components during the course of obtaining an impression. In the general case of contact of curved solids, as given in equation (18), $R_{21}$ and $R_{22}$ are infinite and $\omega = 0$:

$$2(A + B) = \frac{1}{R_{11}} + \frac{1}{R_{12}} \qquad (51)$$

$$2(A - B) = -\left(\frac{1}{R_{11}} - \frac{1}{R_{12}}\right). \qquad (52)$$

Thus, from equation (19),

$$\cos\tau = \frac{\left(\frac{1}{R_{11}} - \frac{1}{R_{12}}\right)}{\left(\frac{1}{R_{11}} + \frac{1}{R_{12}}\right)} = \frac{R_{12} - R_{11}}{R_{12} + R_{11}}. \qquad (53)$$

Since $R_{11} = 2485\,\mu$ and $R_{12} = 12.6\,\mu$, $\cos\tau = 0.9896$ and $\tau = 8.26°$. By curvilinear interpolation in Table I, $m = 7.69$ and $n = 0.293$.

Alfrey [1] has stated that deformation processes in visco-elastic materials may be considered to occur at constant volume, and, thus, have a Poisson ratio of 0.5. However, as has been stated, there is no single value of Young's modulus, $E$, which applies over the range of large deformations which may be expected in this class of materials.

Then, for the filament,

$$k_1 = \frac{1 - 0.25}{\pi E_1} = \frac{3}{4\pi E_1}, \tag{54}$$

where $E_1$ represents a variable Young's modulus, dependent upon $N$.

The glass surface may be considered to be infinitely rigid relative to the filament because of its high Young's modulus. Thus, $E_2 \gg E_1$ and $k_2 \ll k_1$, so that from equations (25) and (26):

$$a = m\sqrt[3]{\frac{9}{8}\left(\frac{R_{11}R_{12}}{R_{11} + R_{12}}\right)\left(\frac{N}{E_1}\right)} \tag{55}$$

and

$$b = n\sqrt[3]{\frac{9}{8}\left(\frac{R_{11}R_{12}}{R_{11} + R_{12}}\right)\left(\frac{N}{E_1}\right)}. \tag{56}$$

On the assumption that the value of $E_1$ is substantially constant for a given range of values of $N$, measurements of $a$ and $b$ experimentally should conform with equations (55) and (56). For the specific filament investigated, the equations would then reduce to

$$\log a = (1.269 - \tfrac{1}{3}\log E_1) + \tfrac{1}{3}\log N; \tag{57}$$

$$\log b = -(0.150 + \tfrac{1}{3}\log E_1) + \tfrac{1}{3}\log N, \tag{58}$$

or linear log-log relationships between $a$, $b$, and $N$. Under this assumption, also, it would be expected that the stress distribution over the area of contact would be given by the semi-ellipsoid

$$\sigma = -\frac{3N}{\pi ab}\sqrt{1 - \frac{x^2}{a^2} - \frac{y^2}{b^2}}. \tag{59}$$

If the material is to meet the above conditions, it must show a linear relationship between $a$, $b$, and $N$ expressed logarithmically, with a slope of $\frac{1}{3}$. It must further be capable of giving independent but identical estimates of the quantity $E_1$.

Experiments with the material described produced the relationships given in Figure 5, indicating that the condition of log-log linearity is apparently met in the region from 2- to 100-g. applied normal load, $N$. Fitting these data with a least-square, linear log-log equation gives the relationships

$$\log a = 1.591 + 0.405 \log N; \tag{60}$$

$$\log b = 0.259 + 0.491 \log N. \tag{61}$$

Eliminating $\log a$ from equations (57) and (60), combining, and solving for $E_1$ gives

$$E_1 = \frac{N^{-0.215}}{9.25}. \tag{62}$$

Performing the same operations for $\log b$ in equations (58) and (61) gives

$$E_1 = \frac{N^{-0.473}}{16.86}. \tag{63}$$

Neither of the above estimates are constants, nor are they identical.

Consider now the fact that $R_{11} \gg R_{12}$ and that in the region of the origin of axes the load per unit length along the $a$-axis may be considered to be a constant. Thus, the condition approaches that of a cylinder in contact with a plane and

$$b = \sqrt{\frac{4pR_{12}(1 - \nu^2)}{\pi E_1}}, \tag{64}$$

where $p$ is the load per unit length along the $a$-axis and may be approximated from the expression for the maximum pressure at the origin of axes:

$$q_0 = \frac{3N}{2\pi ab}; \tag{65}$$

then

$$p = q_0 b = \frac{3N}{2\pi a} \tag{66}$$

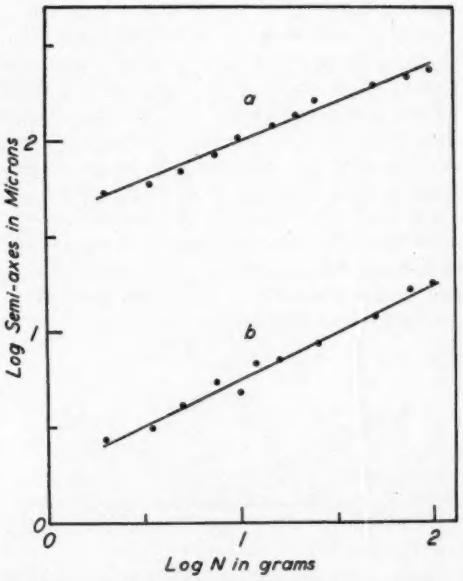


FIG. 5. *Log-log linear relationship between the normal load,* N, *and the semi-axes of the area of contact,* a *and* b.

and

$$b = \sqrt{\frac{6R(1-\nu^2)}{\pi^2}\left(\frac{N}{aE_1}\right)} = \sqrt{5.75\left(\frac{N}{aE_1}\right)}. \quad (67)$$

Taking the log of both sides of equation (67), substituting the value of $\log a$ from equation (60) and the value of $\log b$ from equation (61), and solving for $E_1$ gives

$$E_1 = \frac{N^{-0.386}}{22.40}. \quad (68)$$

A comparison of the values of $E_1$ for each of the above derivations obtained with the experimental values of $N$ is given in Table II. As the value of $E_1$, as calculated from the above, is in units of grams per square micron when the value of the normal load is in grams, this may be converted to the more conventional grams per denier by multiplying by 72. This assumes the value 1.54 as the density of nylon.

TABLE II. RELATIONSHIP BETWEEN YOUNG'S MODULUS, $E_1$, AND THE NORMAL LOAD, $N$, AS DETERMINED FROM THEORY AND EXPERIMENT

| | $E_1$ (g./den.) | | |
|---|---|---|---|
| | Semi-major axis | Semi-minor axis | |
| $N$ (g.) | Equation (62) | Equation (63) | Equation (68) |
| 2 | 6.7 | 3.1 | 2.4 |
| 5 | 5.5 | 2.0 | 1.7 |
| 10 | 4.6 | 1.4 | 1.3 |
| 20 | 4.1 | 1.0 | 1.0 |
| 50 | 3.3 | 0.7 | 0.7 |
| 100 | 2.9 | 0.5 | 0.5 |

## Discussion

The above results indicate that there is a log-log linear relationship between the applied normal load and the semi-axes of the elliptical area of contact. This is in qualitative agreement with the Hertzian theory, despite the fact that the assumptions made in its derivation could not be considered to be rigorously correct for this class of materials. This indicates, then, that the relationships between the semi-axes and the normal load are comparatively simple functions of the materials in contact, as a first assumption.

Quantitatively, if the modulus of elasticity of the materials is Hookean, the results should agree closely with the theory. It was found that the slopes of the log-log relationships for the semi-major and semi-minor axes were, respectively, 0.405 and 0.491. These may be compared with the value 0.333 expected from the theory. The value obtained for the semi-major axis agrees with the theoretical value to a much greater extent than that for the semi-minor axis.

On closer examination of the Hertzian derivation, it may be seen that the assumption of a Hookean modulus of elasticity was not necessary since throughout the expressions the modulus of elasticity appears as a ratio with the applied normal load. Therefore, if there is a functional relationship between the modulus of elasticity and the applied normal load, or, better, the compression of a differential volume, the slope of the log-log relationship will be altered, but not its linearity.

Assuming, then, that the experimentally derived relationships and the theoretical ones are in agreement, they may be combined in order to evaluate the relationship between the modulus of elasticity and the applied normal load for the given geometrical situation. The modulus of elasticity so determined is, then, an over-all one, representative only of the particular set of mechanical parameters employed. For this reason, it is not surprising that the independent relationships obtained from the semi-minor and semi-major axes are significantly different from each other.

This difference may be ascribed to several factors. The first of these has to do with the method of obtaining the transcendental factors, $m$ and $n$, from Table I. The geometrical relationships between the fiber and the glass rod over which it was bent result in an auxiliary angle, $\tau$, which is less than 10 degrees, thus requiring interpolation in the region between 0 and 10 degrees. This region is one of rapidly changing slope, and, therefore, is subject to possible errors in interpolation. In the case of the semi-major axis, the error is small in comparison with that for the semi-minor axis. Thus, the results obtained for the semi-major axis may be considered, based on this one factor, to be more reliable.

The second, and probably more important, factor is based on the relationships among the mechanical parameters employed in the experimental equipment. The solid glass rod over which the filaments were bent has a radius which is very large relative to the radius of the filaments. As a result, the patterns obtained give values of semi-major axis which are many times greater than the semi-minor axis. In this respect, the semi-minor axis begins

to approach the condition represented by a straight cylinder in contact with a plane under the action of a constant load per unit length of the fiber over the length of contact. A comparison between this condition and that given by the more exact relationship which requires an interpolation of the transcendental factor, as shown in Table I, indicates that there is close agreement between the two relationships. This shows that the interpolation error referred to above is evidently small and that the relationships between the modulus of elasticity and the applied normal load obtained in each case are equally valid.

These relationships, obtained independently from the semi-major and semi-minor axes, may be expected to be different on physical grounds. The semi-major axis is many times greater than the semi-minor axis, and its value depends upon deformations occurring axially along the filament. There is, then, a very gradual change in these deformations from the axis of stress symmetry to the point where the filament first touches the plane surface. In the case of the semi-minor axis, this deformation changes rapidly from the symmetry center to the edge of the pattern. These deformations, then, contain a higher proportion of large deformations. It would be expected that this would be reflected in the modulus of elasticity-normal load relationship. Table II shows how the modulus of elasticity changes over the range of normal loads employed.

The values of modulus of elasticity obtained by use of the semi-minor axis are considerably smaller than those for the semi-major axis because they represent a larger proportion of contribution by points of large deformation. Since there is a decrease of modulus as the normal load is increased, such a difference between the axes might, then, be expected. It was also observed in the course of the experimental work that above 50 g., the semi-minor axis was not recoverable, whereas the semi-major axis was partially recoverable. This explains not only why the values of modulus are lower for the same load than are those for the semi-major axis but also why they decrease at a greater rate. The permanent deformations in the semi-minor-axis direction represent a condition of compressive failure with a modulus of elasticity approaching zero.

This departure from the Hertzian assumptions means that the expression for the distribution of stress over the area of contact cannot be considered to be exactly semi-ellipsoidal. The area of contact, however, was observed to be nearly elliptical. Thus, the distribution of pressure, as a first approximation, may be considered to be given by the Hertzian relationships. These relationships may now be used in the development of a unified physical theory of interfiber stress transmission.

## Summary

1. A method has been described for measuring the contact area between a filament and a curved surface under the action of an applied normal load.

2. For a given set of geometrical conditions, the Hertz relationships for the contact area of curved isotropic elastic solids may be employed to obtain the relationship between the over-all modulus of elasticity and the applied normal load for viscoelastic filaments in contact with curved surfaces.

3. As the dimensional nature of the contact area between a filament and a curved surface is in accordance with the Hertz relationships, it may be concluded that the distribution of stress over the contact area is semi-ellipsoidal, as a first approximation.

## Literature Cited

1. Alfrey, T., "Mechanical Behavior of High Polymers," Vol. VI, New York, Interscience Publishers, Inc., 1948.
2. Gemant, A., "Frictional Phenomena," Brooklyn, N. Y., Chemical Publishing Co., 1950.
3. Hertz, H. R., "On the Contact of Rigid Elastic Solids and on Hardness," Miscellaneous Papers, London, Macmillan Co., 1896, pp. 146–62.
4. Hertz, H. R., "On the Contact of Rigid Elastic Solids and on Hardness," Miscellaneous Papers, London, Macmillan Co., 1896, pp. 163–83.
5. Timoshenko, S., "Theory Of Elasticity," New York and London, McGraw-Hill Book Co., Inc., 1934.
6. Whittemore, H. L., and Petrenko, S. N., *U. S. Bur. Standards, Tech. Paper* 201 (1921).

(*Manuscript received December 18, 1950.*)

# The Measurement of Dynamic Modulus and Energy Losses in Single Textile Filaments Subjected to Forced Longitudinal Vibrations*

**Basil A. Dunell† and J. H. Dillon‡**

*Contribution from Textile Research Institute Laboratories and Frick Chemical Laboratory, Princeton University, Princeton, New Jersey*

**Abstract**

Apparatus and techniques for measuring the dynamic properties of single fibers in the frequency range 1–100 cycles/sec. at 70° F and 65% R.H. are described. For the viscose rayon, acetate rayon, nylon, feather keratin, silk, and polyethylene fibers studied, it was found that the quantities $\eta\omega$ and $E$ were approximately independent of frequency in this range, where $\eta$ is the internal friction, $\omega$ the radian frequency, and $E$ the dynamic modulus. Measured values of the energy dissipated per cycle were found to be proportional to the square of the amplitude, in accordance with the prediction of the simple differential equation of vibration assumed (viscous damping and Hookean elastic reaction). Stress relaxation data were obtained with the same fibers and the results are given. Theoretical interpretation of the results is given in another paper [19].

INCREASING ATTENTION is being given to investigation of the mechanical properties of high polymers, reflecting a growing realization of the scientific and industrial importance of this field. Among the large number of contributions in this zone of study must be included the work on creep by Leaderman [12], on the stress-strain properties of wool and other fibers by Harris and coworkers [11] and by Speakman [17] and Meredith [14], on the application of absolute reaction rate theory by Eyring and by later workers of Textile Research Institute Laboratories [4, 7], on the elucidation of structure by stress relaxation by Tobolsky and coworkers [1, 18], on high-frequency vibrational properties by Nolle [15], Ferry [2, 16], and Guth [20], on low-frequency vibrational properties by Dillon *et al.* [5, 6], Gehman *et al.* [9], and Lyons [13], and over a wide range of frequencies by Ballou and Smith [3]. Hamburger [10] and his associates have employed sonic techniques in conjunction with stress-strain tests at normal speed to study the mechanical properties of filaments and yarns. The present paper deals with the measurement of the dynamic modulus of single textile filaments in forced longitudinal vibration of low frequency, and with the energy losses which accompany these vibrations. Tobolsky, Dunell, and Andrews have given an interpretation of these measurements [19].

Such measurements of dynamic modulus and of energy losses involve a diversity of techniques the applicability of which depends upon the sample size and nature of the material to be investigated and upon the frequency region in which the investigation is to be made. Ferry, Sawyer, and Ashworth [8] have published an excellent review on this subject in which they point out that experimental methods may be divided into two major divisions: (1) those methods applicable to samples in which the inertial

* This article is based on a thesis submitted by Basil A. Dunell in partial fulfillment of the requirements for the degree of Doctor of Philosophy at Princeton University.

† Research Fellow of Textile Research Institute. Present address: Department of Chemistry, University of British Columbia, Vancouver, Canada.

‡ Director of Research, Textile Research Institute, Princeton, New Jersey.

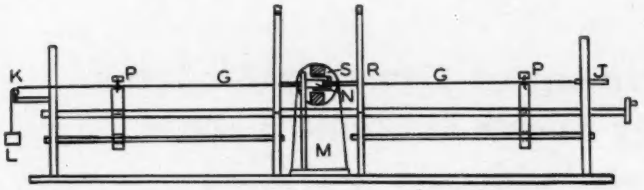


FIG. 1. *Schematic diagram of the filament vibrator.*

forces acting on the material itself can be neglected; and (2) those methods applicable to samples in which the inertial forces acting on the material itself must be taken into account. The technique used in the investigations described in this paper belongs to the first category, and involves making measurements on the material at a condition of mechanical resonance. Methods of this general type are discussed in a review by Dillon and Gehman [5].

## Apparatus

The apparatus which has been used in this investigation is similar to that of Lyons and Prettyman [13], both pieces of apparatus being patterned after the Firestone resonance vibrator for rubber samples in shear constructed by Dillon, Prettyman, and Hall [6]. It is a forced vibrator for oscillating single high-polymer filaments longitudinally. A schematic diagram of the oscillator is shown in Figure 1 and a more detailed diagram of two of its components in Figure 2. Referring to Figure 2, the driving mechanism consists of a solenoid of fine (No. 39 B & S gage) Formex magnet wire, *A*, wound on a paper core, *B*, which is cemented to a disc, *C*, and spindle, *D*, machined from a piece of magnesium alloy, the solenoid coil lying in a radial magnetic field which traverses the annular space, *E*. The coil has effectively three windings with about 200, 15, and 2 turns per winding. This allows a wide variation in the energy input to the vibrating system. The unit is suspended by fine nylon filaments, *F*, which permit free motion in an axial direction and which can be adjusted to center and orient the coil in the magnetic field. The whole vibrator unit weighs some 2.5 g. The coil is supplied with alternating current from a variable-frequency Hewlett-Packard low-range oscillator through leads of the same fine wire that forms the winding, coiled into small helical springs to allow free motion of the vibrator unit. The permanent magnetic field is maintained by the two magnets, *M*, of Figure 2, two similar poles, *S*, facing one another on one side of the radial gap, *E*, and the steel cylinder, *N*, forming the opposite pole on the other side of the gap. The filaments, *G*, which are to be tested are fixed to the vibrator unit and are kept in tension by the load, *L* (see Figure 1). They may be clamped at any point along their length by means of the movable clamps, *P*.

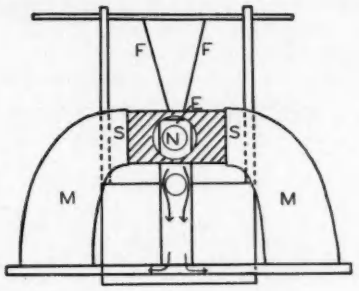


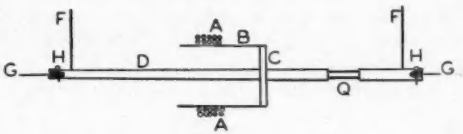


FIG. 2. *Detail of magnet and vibrator unit.*

The amplitude of vibration of the vibrator unit is determined by means of a cathetometer which reads to 0.0001 cm. the apparent increase during vibration in the length of the recessed portion, *Q* (Figure 2), on the shaft of the vibrator unit. The current which the Hewlett-Packard oscillator supplies to the solenoid is indicated by a Weston thermo-milliammeter. The mass of the vibrating system may be increased by loading the shaft of the vibrator unit with small brass weights made for the purpose. As much as 90 g. can be added to the mass of the system in this manner.

This ocillator differs from others chiefly in that the vibrating part is very light so that the machine

can be used for very fine single filaments up to resonant frequencies considerably higher than those attainable with other similar devices. It is also possible to obtain very low frequencies for fine filaments with this apparatus.

### Theory of Forced Vibration in Relation to the Experimental Method

The behavior of a material in forced vibration may be described *at any one frequency* by a single Voigt unit (spring and dashpot in parallel) the parameters of which are $E$ and $\eta$, and whose equation of motion for forced vibration under a harmonic applied force $F = F_{max} \cos \omega t$ is

$$M\frac{d^2x}{dt^2} + \frac{2A}{l}\eta\frac{dx}{dt} + \frac{2A}{l}Ex = F_{max}\cos\omega t, \quad (1)$$

where $x$ is the displacement of the vibrator unit, $t$ is the time, $M$ the mass vibrating, $\omega$ the radian frequency, $A$ the cross-sectional area of the fiber, and $l$ the length of each of the two fibers.

Now, this equation holds only if no frictional resistance or elastic reaction is offered by the mechanical parts of the vibrator itself. But since the leads and supports and air friction offer some dissipative resistance, $R_1 dx/dt$, and since the spring part of the leads and the pendulum action of the oscillator unit (its path of motion is not exactly in a straight line along the axis of the filaments, but, rather, it rises above the original plane of the filaments at either end of its oscillation) provide an elastic reaction, $P_1 x$, equation (1) may be rewritten in more realistic form as

$$M\frac{d^2x}{dt^2} + R\frac{dx}{dt} + Px = F_{max}\cos\omega t, \quad (2)$$

where

$$R = \frac{2A}{l}\eta + R_1 \quad (3)$$

and

$$P = \frac{2A}{l}E + P_1. \quad (4)$$

The assumption made here that the dissipative resistance due to the machine is proportional to the velocity of the moving member is very difficult to verify. Further, $M$ is the effective mass of the oscillating system, and $l$ is the vibrating length, or clamped length, of each of the two filaments in the oscillator. The factor 2 in the second and third terms of equation (1) takes into account the fact that there are two filaments of length $l$, one on each side of the vibrator unit. The use of the term "effective mass" indicates that since all vibrating parts do not have the same acceleration, $d^2x/dt^2$, the mass $M$ is not equal to the sum of the masses of the vibrator unit, the coil leads, supporting threads, and specimen. The chief contribution to $M$ is the mass of the vibrator unit, and the method of determining $M$ is described later (p. 397). If equation (2) is to be valid for any material over a range of frequencies, $E$ and $\eta$ must be considered as parameters which are functions of $\omega$. Since, however, the variables of equation (2) are $t$ and $x$, the solution of equation (2) does not depend upon whether the parameters $E$ and $\eta$ are frequency-dependent, and the steady-state solution is given by

$$x = \alpha' \cos\omega t + \beta' \sin\omega t, \quad (5)$$

where

$$\alpha' = \frac{F_{max}(M\omega^2 - P)}{(M\omega^2 - P)^2 + R^2\omega^2} \quad (6)$$

and

$$\beta' = \frac{F_{max}R\omega}{(M\omega^2 - P)^2 + R^2\omega^2}. \quad (7)$$

That the displacement is known to be simple harmonic from observations made with a cathode-ray oscilloscope* serves as a verification of the validity of the formulation of equations (1) and (2).

Differentiation of equation (5) with respect to time and use of equations (6) and (7) show that the displacement amplitude is

$$x_{max} = F_{max}[(M\omega^2 - P)^2 + R^2\omega^2]^{-\frac{1}{2}}. \quad (8)$$

Now, in most of these investigations the condition of mechanical resonance—that is, the condition in which $(x_{max}/F_{max})$ is a maximum—was found by adjusting the frequency at given sample length and mass of the system until the condition $(x_{max}/F_{max})$ = maximum was satisfied. The amplitude to impressed force ratio at resonance is determined analytically for such a case by differentiating equation (8) with respect to $\omega$. Such an operation requires that one consider the dependence of $P$ and $R$ upon frequency. The work of Dillon *et al.* [6] suggested at the outset that $\eta\omega$ be put equal to a constant, and, hence, $R_1$ being negligible, that $R\omega$ be put equal to a constant. Similarly, $P$ is set equal to a constant since previous work [6] indicates that $E$ is largely independent of $\omega$. With

* T. F. Evans, unpublished results.

these assumptions, one finds that the resonance condition

$$\frac{\partial}{\partial \omega}\left[\frac{x_{max}}{F_{max}}\right] = 0$$

is satisfied if

$$M\omega^2 = P;$$

and this, in turn, gives, from equation (8),

$$x_{max} = \frac{F_{max}}{R\omega}.$$

That is, the parameters $E$ and $\eta$ are given by

$$P = \frac{2A}{l}E + P_1 = M\omega_r^2 \qquad (9)$$

and

$$R = \frac{2A}{l}\eta + R_1 = (F_{max}/x_{max}\omega)_r, \qquad (10)$$

assuming that $\eta\omega$ = constant and $E \neq E(\omega)$, the subscript $r$ indicating the resonance condition. Determination of $E$ and $\eta$ for all the fibers studied, using equations (9) and (10), showed $\eta\omega$ = constant and $E$ = constant and supported the validity of the assumptions.

Resonance may also be achieved by variation of the mass of the system. If mass-tuning is used, the resonance condition

$$\frac{\partial}{\partial M}\left[\frac{x_{max}}{F_{max}}\right] = 0$$

is satisfied unequivocally by the condition

$$M_r\omega^2 = P;$$

from which

$$R = (F_{max}/x_{max}\omega)_r.$$

Some mass-tuning experiments which were performed indicate that the values of the parameters $E$ and $\eta$ so obtained are the same as those obtained by the frequency-tuning method.

The immediate interpretation of the experiments may be approached in a somewhat different fashion by considering the energy dissipated during vibration. The energy dissipated per cycle of vibration is

$$W_c = \int_{\omega t=0}^{2\pi} F_{max} \cos \omega t \, dx. \qquad (11)$$

Substituting from equation (2) gives

$$W_c = M\int_{\omega t=0}^{2\pi} \frac{d^2x}{dt^2}dx + R\int_{\omega t=0}^{2\pi} \frac{dx}{dt}dx + P\int_{\omega t=0}^{2\pi} x dx,$$

and in these integrals $d^2x/dt^2$, $dx/dt$, $x$, and $dx$ are replaced by functions of $\omega t$, using equations (5), (6), and (7). As should be expected, the first and third integrals vanish since inertial and purely elastic forces are conservative and make no contribution to work done over a closed cycle. Hence

$$W_c = \pi R\omega x_{max}^2, \qquad (12)$$

which indicates that the energy dissipated per cycle is independent of frequency if $R\omega$ is constant. This proposition can be directly verified experimentally; thus, consider equation (11) again. The force $F = F_{max} \cos \omega t$ exerted by the solenoid is directly proportional to the current supplied to the coil:

$$F = 0.1\,BIL,$$

where $B$ is the magnetic flux density in the air gap, $I$ is the current in amperes, and $L$ is the length of wire in the coil. Since the oscillator supplies a sinusoidal output, $I = I_{max} \cos \omega t$ and

$$F = 0.1\,BLI_{max} \cos \omega t;$$

and since the displacement is known to be simple harmonic and out of phase with the current, $I$, the work done per cycle is

$$W_c = 0.1\,BLI_{max}\,x_{max} \sin \delta.$$

Cathode-ray-oscilloscope studies by Evans* show that $\delta$ approaches a value $\pi/2$ very closely at resonance. Hence, since all measurements are made at resonance, $W_c \propto (I_{max}\,x_{max})_r$—that is, work done per cycle is independent of frequency since, for given amplitude of vibration, $I_{max}$ is found experimentally to be independent of frequency. A plot of $(I_{max}\,x_{max})_r$ against $x_{max}$ further shows that $W_c \propto x_{max}^2$, which was predicted by equation (12).

### Calibration and Determination of Mass of the Vibrator Unit

The solenoid, or vibrator unit, that was constructed was calibrated so that the force it exerts can be determined from the current supplied to it. The whole apparatus was set up with its axis vertical, and the vibrator unit was suspended in the magnetic field from a linear spring of accurately known modulus. The vibrator and spring were then loaded with a succession of analytical balance weights, and after each weight was added the

* T. F. Evans, unpublished results. See also Robertson and Yorgiadis, *J. Applied Mechanics* **13**, A173 (1946).

vibrator unit was brought back to approximately its original unloaded position by passing a direct current through the solenoid coil in the appropriate direction.

The effective mass of the system may be determined from vibrational data if the solenoid has been calibrated. In equation (8), $R\omega$ is negligible compared to $M\omega^2 - P$ for values of $\omega$ which are not too close to $\omega_r$. Hence, a plot of $\pm (F_{max}/x_{max})$ against $\omega^2$ for any material being tested yields a curve which deviates from a straight line only near resonance, the slope of the straight-line portion being $M$, the effective mass of the oscillating system. This method of calculating $M$ was used throughout the work.

### Evaluation of Correction Terms

The elastic reaction of the coiled leads is negligible compared to the effect of the pendulum action of the vibrator unit. Let $h$ be the vertical length of the suspension which holds the vibrator unit. Then a small displacement $x$ of the unit is accompanied by a rise $x^2/h$ in the height of the unit and a restoring force $Mgx/h$ acting in the same direction as the elastic reaction of the sample filaments. Then $P_1 = Mg/h$ (see equations (2) and (4)).

$R_1$ has been evaluated for the vibrator unit alone and for the vibrator loaded with extra masses, but with no filaments attached to it; and both forced-vibration and free-vibration methods have been used. In the case of the forced-vibration method, the resonant frequency was found and the values of the current to the solenoid and the resonant amplitude observed in just the same manner as though a specimen had been in the machine. For the case of free vibrations, the period of free vibration and the decrease in amplitude of vibration during any $n$ successive complete vibrations were determined and the damping factor calculated by use of the equation

$$R_1 = \frac{M\omega}{n\pi} \ln \left[ \frac{(x_{max})m}{(x_{max})m + n} \right],$$

which is obtained by examining the solution of the equation of motion of the freely vibrating system (equation (2) with $F_{max} = O$). Rather poor precision was attainable in the evaluation of $R_1$, and several determinations of $R_1$ were made during the course of the work. An attempt was made to determine whether $R_1$ is frequency-dependent. esults were inconclusive, h owever, and the assumption has been made, for purposes of calculating $\eta$, that $R_1$ is independent of frequency. The approximate magnitude of $R_1$ used as a correction factor is 3 dyne-sec.-cm.$^{-1}$.

### Experimental Conditions and Results

Preliminary experimental determinations of the dynamic properties of single textile filaments showed a marked increase in dynamic modulus with time and a decrease in the energy loss for a filament as it creeps under a dead load. For example, the modulus, $E$, increased by about 5% and the energy-loss factor $\eta\omega$ decreased by about 5% of its initially obtained value during one cycle of logarithmic time. In order to compare rigorously the dynamic properties of one type of fiber with another, the dynamic properties should be measured at a time after the application of tension to the filament such that comparable points on the creep curves for the fibers concerned are reached. Points for comparison on the creep curves of fibers were not found, however, and the experimental procedure adopted was to allow the filament to creep in position in the vibrator for 16 hrs. before dynamic measurements were made. After 16 hrs., the change in dynamic parameters with time was found to be sufficiently small so as to be insignificant during the time required to complete the experiments to be done on the fiber.

The tensioning load used was in all cases except that of feather keratin 0.5 g. per $10^{-6}$ cm.$^2$ cross-sectional area. For feather keratin, a tensioning load of 0.25 g. per $10^{-6}$ cm.$^2$ was used. All experiments were performed in a conditioned room maintained at 70° F and 65% R.H. In all experiments investigating the variation of parameters with frequency, the strain amplitude at resonance was approximately 0.002.

The dynamic parameters of single filaments of the following materials were obtained: nylon, viscose and acetate rayons, raw and degummed silk, chicken-feather keratin, and polyethylene. To obtain dynamic parameters over the frequency range of approximately 1.5 to 100 cycles per sec., 2.5-den. and 30-den. viscose rayon, 3.75- and 25-den. acetate rayon, and 3.0- and 30-den. nylon filaments were used.

The experimentally obtained values of dynamic modulus are plotted against frequency, $\nu$ $(= \omega/2\pi)$, in Figures 3 to 6; and the experimental values of the parameter $\eta$ are plotted against frequency in

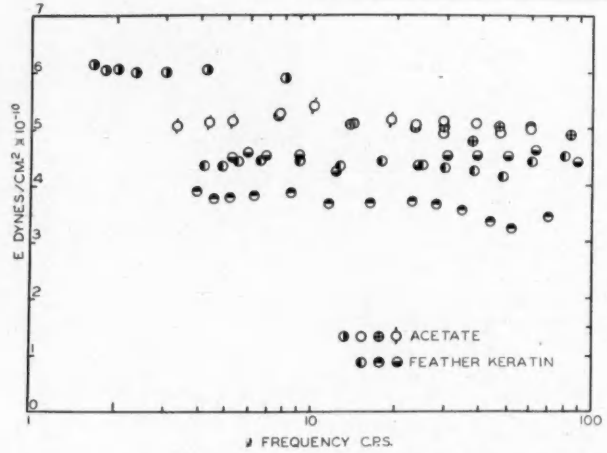


FIG. 3. *Dynamic modulus* vs. *log frequency for acetate rayon and feather keratin.*

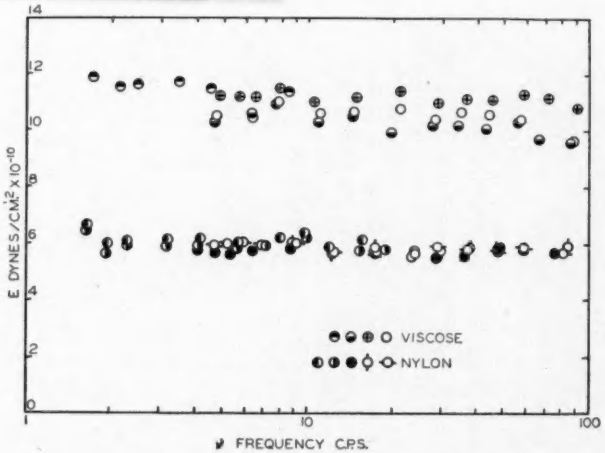


FIG. 4. *Dynamic modulus* vs. *log frequency for viscose rayon and nylon.*

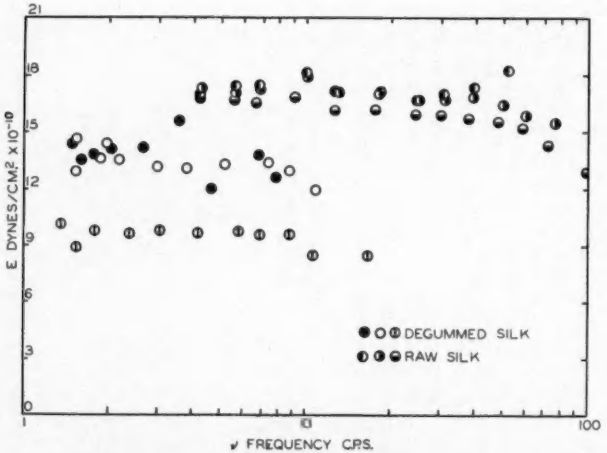


FIG. 5. *Dynamic modulus* vs. *log frequency for raw and degummed silk.*

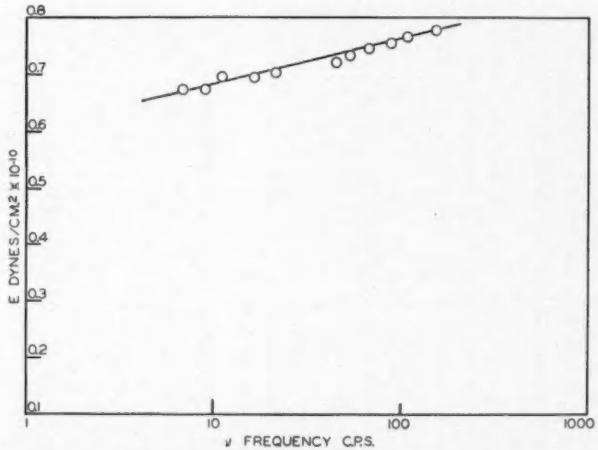


FIG. 6. *Dynamic modulus* vs. *log frequency for polyethylene.*

logarithmic coordinates in Figures 7 to 11. Duplicate experiments for any one kind of fiber are indicated each by its own symbol. Significant differences between duplicate experiments may be attributed in part to differences in cross-sectional area of the various samples, and in part to the general fiber-to-fiber variation which is always encountered in both physical and chemical work with textile materials, especially with natural fibers.

For all the materials except polyethylene, the dynamic modulus was observed to be essentially constant with frequency. The modulus of polyethylene increased linearly with logarithmic frequency, in the frequency range observed, with a slope of $8.2 \times 10^8$ dynes/cm.$^2$. In the plots of $\log \eta$ against $\log \nu$, the relationship $\eta\omega$ = constant is plotted as a line of slope $-1$ passing among the experimental points. In general, the points for any

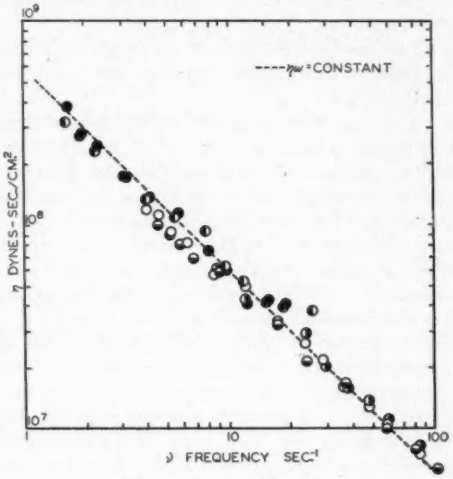


FIG. 7. $\eta$ vs. $\nu$ *for nylon.*

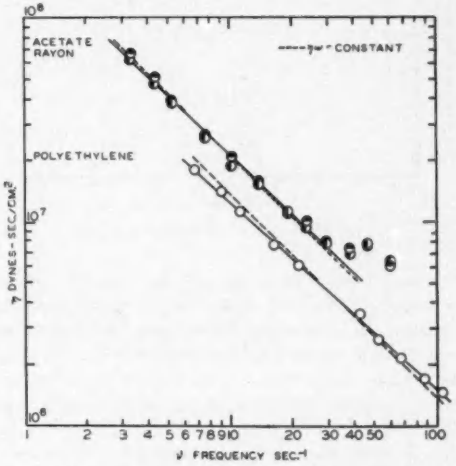


FIG. 8. $\eta$ vs. $\nu$ *for acetate rayon and polyethylene.*

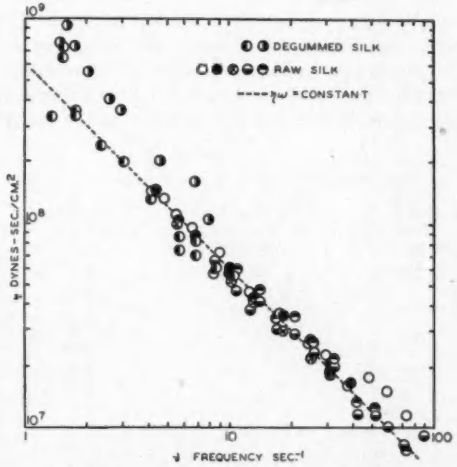


FIG. 9. $\eta$ vs. $\nu$ *for raw and degummed silk.*

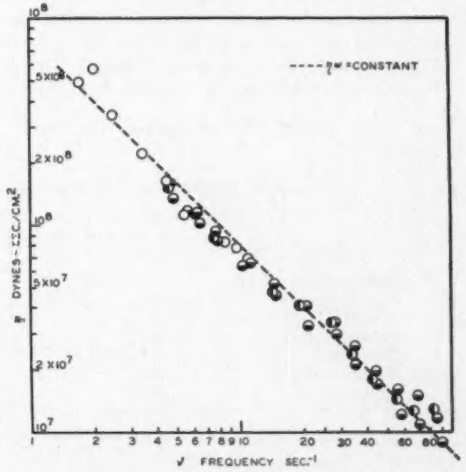


FIG. 10. $\eta$ vs. $\nu$ *for viscose rayon.*

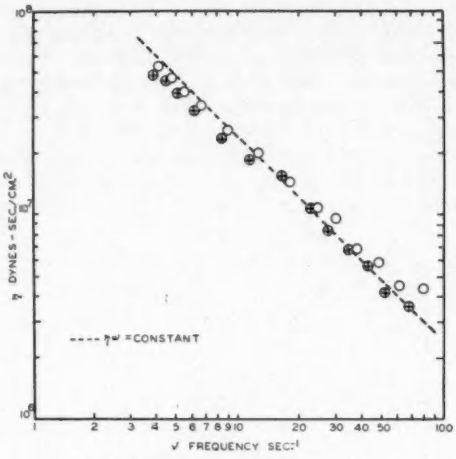


FIG. 11. $\eta$ vs. $\nu$ *for feather keratin.*

one sample of a material are best fitted by a line of slope a little less than that for $\eta\omega$ = constant. That is, the product $\eta\omega$ increases slightly with frequency in most cases for any one filament. Radical departures from linearity of two or three experimental points obtained at short sample lengths, and hence at the higher frequencies obtainable with the sample concerned, are not considered to be very significant since this behavior has been observed for very small diameter fibers at frequencies which are low compared with those attainable with heavier filaments of the same material. The data plotted in Figures 3 to 11 are summarized briefly in Table I.

It has been shown that at resonance

$$W_c = 0.1\,BLI_{\max}\,x_{\max}.$$

Although $B$ and $L$ are not known, they are constants, and hence the product $Ix_{\max}$ is proportional to the work dissipated per cycle, $W_c$, or is equal to the work dissipated expressed in arbitrary units. $W_c$ has been calculated directly from experimental data in this manner; and the results, plotted in Figures 12 to 14, show that at constant frequency

$$W_c \propto x^2_{\max}.$$

This result supports the validity of the linear differential equation of motion (equation (1)) which was assumed for the system since the result $W_c \propto x^2_{\max}$ at constant $\nu$ (equation (12)) was predicted from equation (1).

These results are discussed in terms of a spectrum of relaxation times corresponding to an infinite parallel array of Maxwell units and are correlated with stress relaxation data in a paper by Tobolsky, Dunell, and Andrews [19]. Stress relaxation data were obtained during this investigation for the types of fiber whose dynamic properties were measured. It was supposed that the stress relaxation curve would depend upon the elongation at which the stress relaxation took place and upon the rate at which this elongation was attained. Hence, three experiments were done on each type of fiber. In the first experiment the filament was stretched to 5% elongation in 15 sec. and the stress relaxation recorded and plotted from that point as zero time. In the second experiment the filament was stretched to 0.5% elongation in 15 sec. and the stress relaxation recorded and plotted from that origin. In the third experiment the filament was stretched to a 5% elongation in 25 min. and the stress relaxation started from that time origin. This experiment was intended to simulate, as closely as the Instron

TABLE I. SUMMARY OF EXPERIMENTAL DYNAMIC DATA OBTAINED FOR CERTAIN FIBERS

| Material | Dynamic modulus, $E$ (dynes/cm.²) | Energy-loss factor, $\eta\nu$ (dynes/cm.²) | Energy-loss/ cycle/unit vol.* (ergs/cm.³) | Slope of log $\eta$ *vs.* log $\nu$ curve |
|---|---|---|---|---|
| Viscose rayon | $10.6 \times 10^{10}$ | $7.6 \times 10^{8}$ | $12 \times 10^{4}$ | −0.9 |
| Acetate rayon | 5.1 | 2.4 | 3.8 | −0.87 |
| Nylon | 5.8 | 6.1 | 9.6 | −0.9 |
| Feather keratin | 4.4 | 2.4 | 3.8 | −0.9 |
| Raw silk | 16.8 | 6.1 | 9.6 | −0.97 |
| Degummed silk | 13.5 | 6.9 | 11 | −1.1 |
| Polyethylene | 0.68† | 1.3 | 2.1 | −0.9 |

* Energy loss per cycle per unit volume is calculated for a strain amplitude $\epsilon_{\max} = 0.002$ from the relation

$$\frac{W_c}{V} = 4\pi^2\epsilon^2_{\max}\,\eta\nu.$$

† At a frequency of 10 cycles/sec.

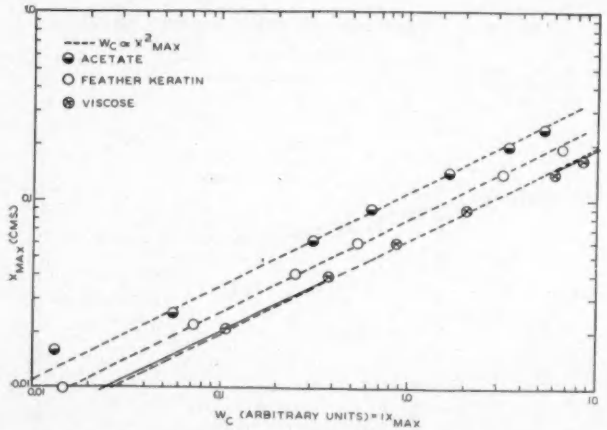


FIG. 12. *Experimental verification of equation (12) for viscose and acetate rayons and feather keratin.*

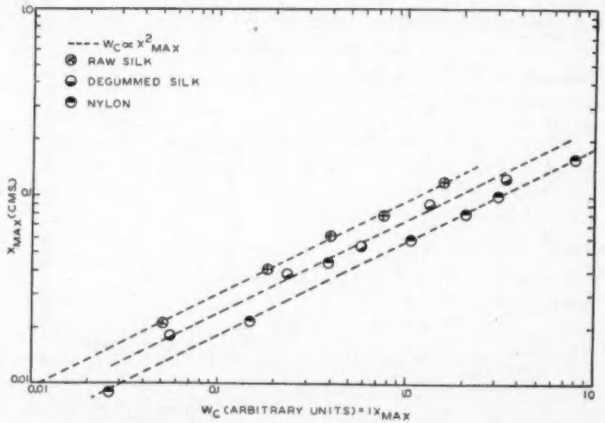


FIG. 13. *Experimental verification of equation (12) for nylon, raw silk, and degummed silk.*

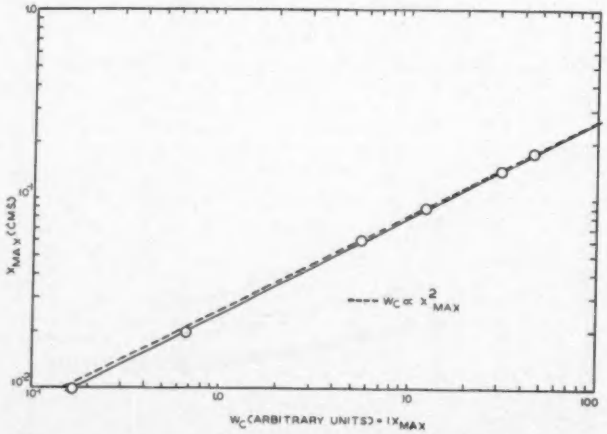


FIG. 14. *Experimental verification of equation (12) for polyethylene.*

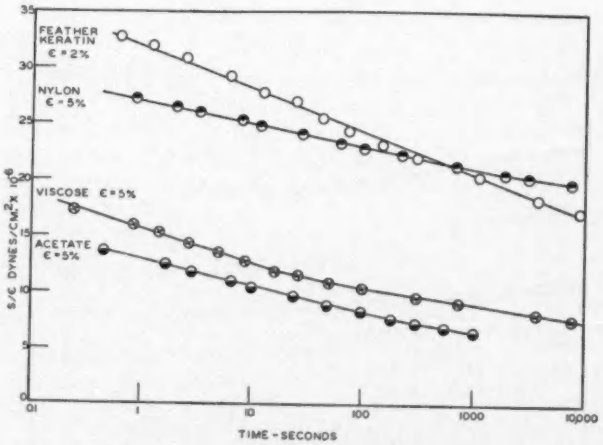


FIG. 15. *Stress relaxation for single filaments.*

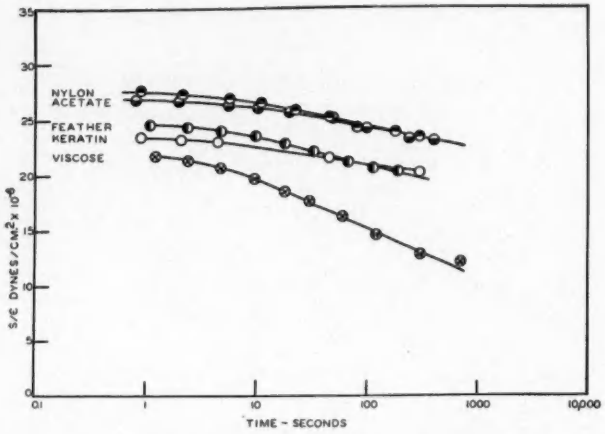


FIG. 16. *Stress relaxation for single filaments at* $\epsilon = 0.5\%$.

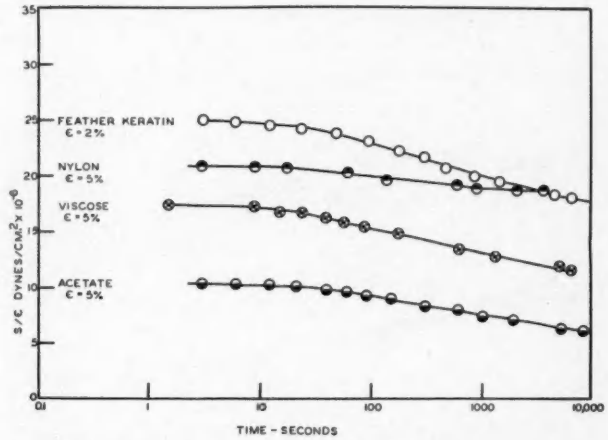


FIG. 17. *Stress relaxation for single filaments after slow elongation.*

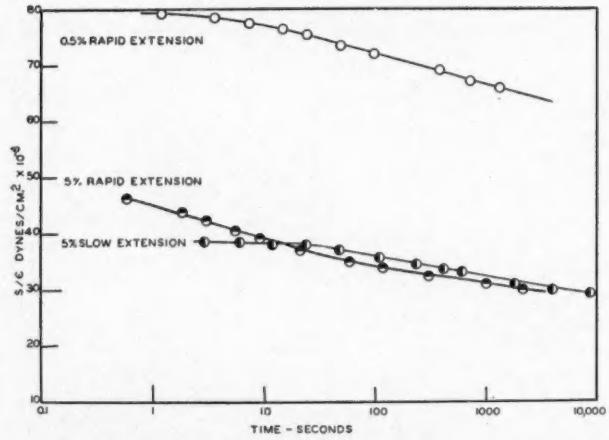


FIG. 18. *Stress relaxation for single filaments of raw silk.*

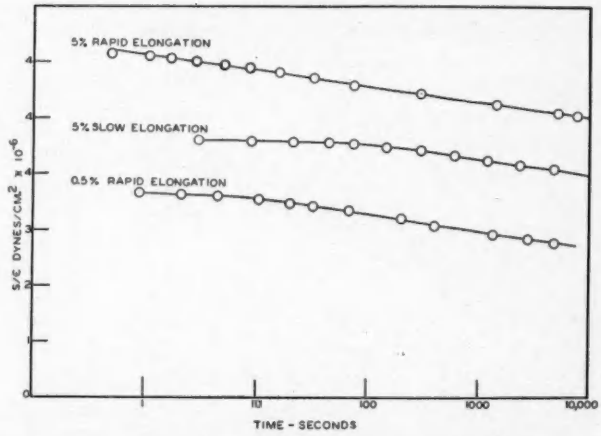


FIG. 19. *Stress relaxation for single filaments of polyethylene.*

testing machine would allow, the precreeping treatment of the vibrational experiments followed by determination of dynamic properties. Feather-keratin filaments were extended to 2% elongation since they break below 5% elongation at the rapid rate of elongation involved. All these experiments were performed at 70° F and 65% R.H.

The results of these stress relaxation experiments are plotted in Figures 15 to 19 as stress/strain against logarithmic time. The stress relaxation data used for predicting the energy-loss factor $\eta\omega$ in the paper of Tobolsky, Dunell, and Andrews [19] are those obtained from the experiments involving slow extension to 5% elongation followed by relaxation.

### Acknowledgment

The authors wish to thank Mr. W. O. Seifert for help with running some of the stress relaxation curves. Thanks are due also to the American Viscose Corporation, the Tennessee Eastman Corporation, and the Western Regional Research Laboratory of the Department of Agriculture for their kind contributions of samples which were used in this work.

One of us (B.A.D.) is grateful to Textile Research Institute for the fellowship grant which made the work possible.

Important financial support was received from The Office of Naval Research under Contract No. N7-onr-374.

### Literature Cited

1. Andrews, R. D., Hofman-Bang, N., and Tobolsky, A. V., *J. Polymer Sci.* **3**, 669 (1948).
2. Ashworth, J. N., and Ferry, J. D., *J. Am. Chem. Soc.* **71**, 662 (1949).
3. Ballou, J. W., and Smith, J. C., *J. Applied Phys.* **20**, 493 (1949).
4. Burte, H., Halsey, G., and Dillon, J. H., TEXTILE RESEARCH JOURNAL **18**, 449 (1948).
5. Dillon, J. H., and Gehman, S. D., *India Rubber World* **115**, 61, 217 (1946).
6. Dillon, J. H., Prettyman, I. B., and Hall, G. L., *J. Applied Phys.* **15**, 309 (1944).
7. Eyring, H., White, H. J., Halsey, G., Stein, R., and Reichardt, C. H., Mechanical Properties of Textiles. Parts I–XI, TEXTILE RESEARCH JOURNAL **15**, 295, 451 (1945); **16**, 13, 53, 124, 201, 329, 335, 378, 382, 635 (1946).
8. Ferry, J. D., Sawyer, W. M., and Ashworth, J. N., *J. Polymer Sci.* **2**, 593 (1947).
9. Gehman, S. D., Woodford, D. E., Stambaugh, R. B., and Jones, P. J., *Ind. Eng. Chem.* **33**, 1032 (1941); **35**, 694 (1943).
10. Hamburger, W. J., TEXTILE RESEARCH JOURNAL **18**, 102, 705 (1948).
11. Harris, M., Mizell, L. R., and Fourt, L., *J. Research Natl. Bur. Standards* **29**, 73 (1942).
12. Leaderman, H., "Elastic and Creep Properties of Filamentous Materials and Other High Polymers," Washington, D. C., Textile Foundation, 1943.
13. Lyons, W. J., TEXTILE RESEARCH JOURNAL **19**, 123 (1949).
14. Meredith, R., *J. Text. Inst.* **36**, T107 (1945).
15. Nolle, A. W., *J. Applied Phys.* **19**, 753 (1948).
16. Smith, T. L., Ferry, J. D., and Schremp, F. W., *J. Applied Phys.* **20**, 144 (1949).
17. Speakman, J. B., *J. Text. Inst.* **38**, T102 (1947).
18. Stern, M. D., and Tobolsky, A. V., *J. Chem. Phys.* **14**, 93 (1946).
19. Tobolsky, A. V., Dunell, B. A., and Andrews, R. D., TEXTILE RESEARCH JOURNAL **21**, 404 (1951) (this issue).
20. Witte, R. S., Ivey, D. G., Mrowca, B. A., and Guth, E., *J. Applied Phys.* **20**, 481, 486 (1949).

(*Manuscript received August 30, 1950.*)

# Stress Relaxation and Dynamic Properties of Polymers*

**A. V. Tobolsky,† B. A. Dunell,‡ and R. D. Andrews****

*Contribution of Princeton University and Textile Research Institute, Princeton, New Jersey*

**Abstract**

The mechanical behavior of an idealized linear polymer is discussed in terms of the Maxwell relaxation theory. When a simple rectangular distribution of relaxation times is assumed, it is shown that the dynamic properties can be related to those deduced from stress relaxation data by the equation:

$$\omega\eta_{dyn} = \frac{\pi E^o}{2 \log_e 10},$$

where $\eta_{dyn}$ is the dynamically measured internal friction or viscosity, $\omega$ the radian frequency, and $E^o$ the negative slope of the relaxation curve plotted as reduced stress vs. $\log_{10}$ time. Application of this equation to values of $\omega\eta_{dyn}$ and stress relaxation data on rubbers obtained by Dillon, Prettyman, and Hall [5] and data on textile fibers by Dunell and Dillon [6] is made. Better than order-of-magnitude agreement was obtained between dynamically measured values of $\omega\eta_{dyn}$ and those calculated by the above equation for the series of rubber stocks and fibers considered. The theory presented has interesting implications in regard to the structures of the various polymers studied, most of which would not *a priori* be considered linear in the sense of the idealized model. The relationships deduced from the "box" distribution are extended to other broad distributions of relaxation times.

## Stress Relaxation and General Elastoviscous Behavior

The simplest type of elastoviscous behavior was postulated by Maxwell to obey the equation

$$\frac{ds}{dt} = \frac{1}{E}\frac{df}{dt} + \frac{1}{\tau E} f, \qquad (1)$$

where $s$ is a component of strain (*e.g.*, simple tensile strain), $f$ is a component of stress (*e.g.*, tensile stress), $E$ is the elastic modulus, and $\tau$ is the so-called relaxation time of the system.

A mechanical model which behaves in the manner defined by equation (1) is a spring and dashpot connected in series, if the elastic constant of the spring is taken as $E$ and the damping constant or viscosity of the dashpot is taken as $\tau E$. This mechanical system is known as the Maxwell model. If a substance which obeys equation (1) is rapidly extended to a fixed strain $s_o$ and maintained at that strain, the stress will decay according to the law

$$\frac{f}{s_o} = Ee^{-t/\tau}. \qquad (2)$$

Certain substances exist whose relaxation behavior approximates equation (2)—*e.g.*, Hevea gum vulcanizate [16] and polysulfide rubbers [12] at high temperatures, where the elastoviscous behavior is controlled by chemical reactions. In relaxation curves obeying this equation, the decay of stress occurs almost completely within two cycles of logarithmic time. When this relaxation function is plotted against logarithmic time as abscissa, a change in the value of the relaxation time, $\tau$, merely shifts the relaxation curve horizontally along the logarithmic time axis.

The decay of stress in polyisobutylenes maintained at constant extension and temperature does

* This article is based on a thesis submitted by Basil A. Dunell in partial fulfillment of the requirements for the degree of Doctor of Philosophy at Princeton University.

† Department of Chemistry, Princeton University, and staff member of Textile Research Institute. Present address: Polytechnic Institute of Brooklyn.

‡ Research Fellow of Textile Research Institute. Present address: University of British Columbia, Vancouver, Canada.

** Platics Laboratory, Princeton University.

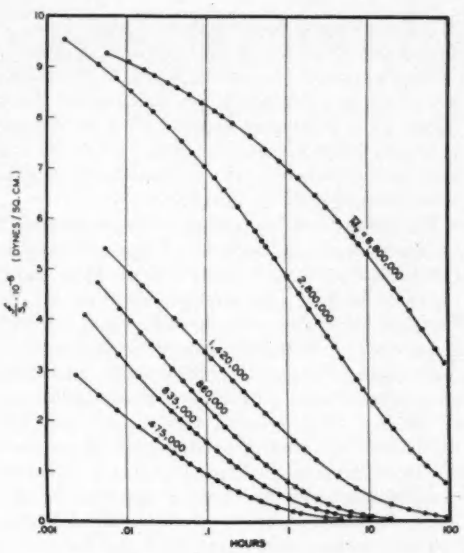


FIG. 1. *Stress relaxation of polyisobutylenes with varying viscosity average molecular weights, $\bar{M}_V$.*

not obey equation (2) [1, 2, 4]. Rather, the stress decay extends over many cycles of logarithmic time. This may be seen from relaxation curves for polymers of different viscosity average molecular weights at the same temperature (30° C), plotted in terms of $\frac{f}{s_o}$ in Figure 1 (limiting Hooke's-law modulus for small strains) against logarithmic time. In the case of vulcanized rubbers in an intermediate temperature range (which for most rubbers is around room temperature) the relaxation curve is also fairly linear when plotted against logarithmic time. At higher temperatures the initial portion of the relaxation curve plotted against logarithmic time is still linear, but the long-time end of the curve approaches the form of a Maxwell decay curve. This is shown in Figure 2 for the case of a GR-S tread stock.

To describe relaxation curves which are spread out over several cycles of logarithmic time, an extension of the Maxwell theory is required, involving the consideration of a distribution of relaxation times. The mechanical model corresponding to this generalized Maxwell theory consists of a series of Maxwell elements connected in parallel, as shown

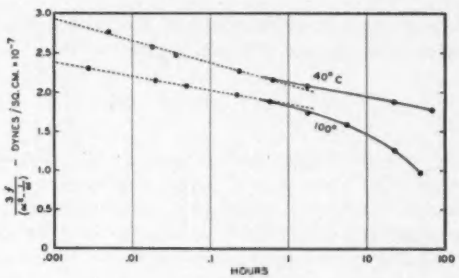


FIG. 2. *Stress relaxation of GR-S tread stock (ordinates expressed as "reduced stress"—stress at any instant divided by initial stress calculated from kinetic theory of elasticity).*

in Figure 3. The mathematical formulation of this theory is

$$\frac{ds}{dt} = \frac{1}{E(\tau)}\frac{df(\tau)}{dt} + \frac{1}{\tau E(\tau)} f(\tau), \qquad (3)$$

$$f = \int_0^\infty f(\tau)\, d\tau; \quad E = \int_0^\infty E(\tau)\, d\tau.$$

This symbolizes a continuous set of differential equations each of which describes the behavior of the component Maxwell element having a particular relaxation time, $\tau$. The function $E(\tau)$ is a distribution function, usually called the "distribution of relaxation times." $E(\tau)\, d\tau$ specifies the contribution to the total "instantaneous" tensile modulus, $E$, of the system from Maxwell elements having relaxation times between $\tau$ and $\tau + d\tau$. $E$ is the modulus of the system as a whole for an "instantaneous" deformation (where no relaxation takes place), and is equal to the sum of the moduli of the individual springs of the component Maxwell elements. The function $f(\tau)$ represents the amount of the total applied stress, $f$, which is acting on the element with relaxation time $\tau$, and $s$ is the observed deformation of the system. The solution of equation (3) depends on the knowledge of the distribution function $E(\tau)$. If a substance obeying equation (3) is rapidly extended to a fixed strain $s_o$, and main-

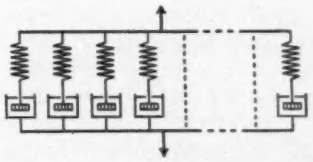

FIG. 3. *Generalized Maxwell model.*

tained at that constant strain, the decay of the stress, $f$, with time will be given by

$$f(t) = s_o \int_0^\infty E(\tau) e^{-t/\tau} d\tau. \qquad (4)$$

If we are dealing with a system whose largest relaxation time, $\tau_m$, is finite, the stress in a sample maintained at constant extension will approach zero asymptotically as time increases beyond the value of the largest relaxation time. Similarly, if there exists a minimum relaxation time, $\tau_l$, the stress at constant strain $s_o$ will approach the value $Es_o$ for values of time less than $\tau_l$. If such a system is subjected to a constant stress $f_o$, there will be an instantaneous elastic deformation $f_o/E$, followed by a progressive increase in deformation which eventually slows down to a constant rate. The final steady-state rate of tensile strain which is attained will be

$$\left(\frac{ds}{dt}\right)_\infty = f_o \Big/ \int_{\tau_l}^{\tau_m} \tau E(\tau) d\tau. \qquad (5a)$$

For the case of a shearing strain, this relation would be

$$\left(\frac{ds}{dt}\right)_\infty = f_o \Big/ \int_{\tau_l}^{\tau_m} \tau \frac{E(\tau)}{3} d\tau, \qquad (5b)$$

where the modulus distribution function, $E(\tau)$, is divided by 3 to convert from tensile to shear modulus.* According to these equations, the steady-state rate of deformation, or flow, is proportional to the applied stress, as is the case for a so-called "Newtonian fluid"; and by comparison with Newton's equation for viscosity,

$$f = \eta \frac{ds}{dt}, \qquad (6)$$

it is seen that the observed tensile flow viscosity, $\bar{\eta}_t$, of this generalized Maxwell system having a maximum relaxation time will be

$$\bar{\eta}_t = \int_{\tau_l}^{\tau_m} \tau E(\tau) d\tau, \qquad (7a)$$

and the observed shear viscosity, $\bar{\eta}$, will be

$$\bar{\eta} = \int_{\tau_l}^{\tau_m} \tau \frac{E(\tau)}{3} d\tau = \tfrac{1}{3}\bar{\eta}_t. \qquad (7b)$$

* This assumes the substance to be isotropic and to have a Poisson's ratio of 0.5—*i.e.*, there is no change in volume on stretching.

The steady-state flow viscosity is, therefore, the sum of the viscosities of the individual dashpots of all the component Maxwell elements. This relation has also been derived by Kuhn, Künzle, and Preissmann [8]. The general expression for the viscosity in terms of the relaxation function itself rather than the associated distribution of relaxation times has been given recently by Sips [11].

The generalized Maxwell equations expressed by equation (3) and a knowledge of $E(\tau)$ are sufficient to describe the most general type of *linear* elastoviscous behavior (see references [8, 10, 11] for complete definition). With these equations it is theoretically possible to describe the results of all mechanical experiments such as creep under constant stress, forced and free vibration studies, etc. [8, 10, 11]. The function $E(\tau)$ may, in principle, be determined from relaxation-of-stress measurements by an inversion of the integral in equation (4).

As an alternative to relaxation experiments, elastoviscous behavior may be characterized by means of creep measurements, in which the increase of deformation with time is observed for a sample under constant stress. However, although the steady-state flow and the instantaneous elastic deformation of the creep curve are given directly by the generalized Maxwell model which describes the relaxation of stress behavior, the "retarded elastic" portion of the creep curve can be described in terms of this model only with difficulty. It is most conveniently described in terms of a generalized Voigt model, consisting of a set of Voigt elements (a spring and dashpot in parallel) connected in series. This model is characterized by a distribution function for elastic compliance $J(\tau')$, where $\tau'$ is the retardation time of a component Voigt element. The distribution functions $J(\tau')$ and $E(\tau)$ are formally equivalent methods for specifying elastoviscous behavior, but the mathematical transformations necessary to convert one into the other are very complex. Even when the distribution function $E(\tau)$ is known, an exact calculation of the entire creep curve is often precluded because of mathematical difficulties.

The results of vibration experiments, on the other hand, can be conveniently described in terms of the distribution function $E(\tau)$ by a simple quadrature. The results of such experiments [5] may be expressed in terms of a dynamic modulus, $E_{dyn}$, and a dynamic viscosity, $\eta_{dyn}$, both of which are func-

tions of the radian frequency, $\omega$. The values of these quantities in terms of $E(\tau)$ are given by the following expressions [15]:

$$E_{dyn}(\omega) = \int \frac{\omega^2\tau^2 E(\tau)}{1+\omega^2\tau^2}\, d\tau, \qquad (8)$$

$$\omega\eta_{dyn}(\omega) = \int \frac{\omega\tau E(\tau)}{1+\omega^2\tau^2}\, d\tau. \qquad (9)$$

The distribution of relaxation times, $E(\tau)$, may be calculated from vibration data by use of equation (8) or equation (9). In this way the form of $E(\tau)$ may be determined in the range of very short times (small values of $\tau$) where measurements of relaxation of stress cannot easily be made. The prediction of dynamic modulus and dynamic viscosity from relaxation data, by use of the distribution function $E(\tau)$ which is described in the following section, has been discussed elsewhere by Dunell and Tobolsky [7]. A similar treatment of the relation between creep and dynamic properties has been given by Kuhn *et al.* [8, 10].

It has been suggested [1] in connection with earlier relaxation studies that relaxation curves for polyisobutylenes (at least, the latter part of the relaxation curves) may be approximated by a "box distribution" of relaxation times—that is, a distribution which has the form of a rectangle when plotted against logarithmic time. This distribution function was previously used by Becker [3] to describe the time relaxation of magnetization, and an essentially identical function was used by Kuhn, Künzle, and Preissmann [8] in relating creep and dynamic properties. Denoting the upper and lower limits of the distribution as $\tau_m$ and $\tau_l$, the distribution function $E'(\log\tau)$ will be

$$\begin{aligned} E'(\log\tau) &= 2.303E_o, \quad (\tau_l < \tau < \tau_m) \\ E'(\log\tau) &= 0, \quad (\tau < \tau_l, \tau > \tau_m) \end{aligned} \qquad (10)$$

where $E_o$ is a constant. (Throughout this paper log denotes logarithms to the base 10, and ln, the natural logarithms.) Expressing the distribution function in terms of $\tau$ itself,

$$\begin{aligned} E(\tau) &= \frac{E_o}{\tau}, \quad (\tau_l < \tau < \tau_m) \\ E(\tau) &= 0, \quad (\tau < \tau_l, \tau > \tau_m). \end{aligned} \qquad (11)$$

The relaxation of stress function corresponding to this distribution function is

$$\frac{f}{s_o} = E_o[Ei(-t/\tau_l) - Ei(-t/\tau_m)], \qquad (12)$$

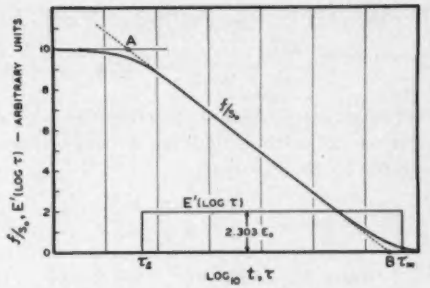


FIG. 4. *Stress relaxation and distribution function for a high polymer, with logarithmic time scale.*

where $-Ei(-x)$ is a tabulated exponential integral function [13]. In equation (12) the relaxation function is expressed in units of limiting Hooke's-law modulus for small strains ($f$ is stress in dynes/sq. cm., $s$ is fractional elongation $= (l - l_o)/l_o$, where $l$ and $l_o$ are the stretched and unstretched lengths of the sample, and the subscript zero on $s$ indicates that the strain of the sample is maintained constant throughout the experiment). If $\log\tau_l$ and $\log\tau_m$ differ by a number of cycles of logarithmic time, the central portion of the relaxation curve will be a straight line when stress or modulus is plotted on a linear ordinate scale against logarithmic time as abscissa. Figure 4 shows a relaxation curve of this type, where the distribution of relaxation times extends over five cycles of logarithmic time. The straight line defined by the central region of the relaxation curve is extrapolated by dashed lines in the figure. The slope $E^\circ$ of this straight-line section is $-2.303E_o$, which is numerically equal to the height of the rectangular "box" representing the distribution function $E'(\log\tau)$. This relation can easily be seen from the series expansion of the exponential integral function [13]. The three constants, $\tau_l$, $\tau_m$, and $E_o$, which completely specify the distribution of relaxation times, and therefore the associated relaxation curve, may be directly and conveniently evaluated from this characteristic straight line. The negative slope divided by 2.303 is $E_o$, and $\tau_l$ and $\tau_m$ are proportional, by a factor 1.781, to the time values at the intersection points of this line with the maximum stress and zero stress axes, respectively. If the time values corresponding to these two intercept points (which are indicated as $A$ and $B$ in the figure) are designated as $(t_{int})_l$

and $(t_{int})_m$, respectively, this may be written as

$$\frac{\tau_l}{(t_{int})_l} = \frac{\tau_m}{(t_{int})_m} = 1.781. \quad (13)$$

If the box distribution of relaxation times is valid, the dynamic modulus and the dynamic viscosity are given by the equations

$$E_{dyn} = \frac{E_o}{2} \ln \frac{1 + \omega^2\tau_m^2}{1 + \omega^2\tau_l^2}, \quad (14)$$

$$\omega\eta_{dyn} = E_o[\tan^{-1}\omega\tau_m - \tan^{-1}\omega\tau_l]. \quad (15)$$

It should be noted that if we have an additional spring $E_a$ in parallel with the box distribution of Maxwell units, equation (14) is modified by the addition of $E_a$, but equation (15) is unaffected. This is of importance in extending the theoretical results discussed below from systems such as polyisobutylene which relax to zero stress to cross-linked or crystalline systems which relax to a finite stress value.

Plots of $E_{dyn}$ and $\omega\eta_{dyn}$ *vs.* log $(1/\omega)$ are shown in Figure 5. If $\tau_m \gg \tau_l$, the plot of $E_{dyn}$ *vs.* log $(1/\omega)$ has a portion lying between $\omega$ values of $1/\tau_m$ and $1/\tau_l$ which approximates a straight line. The slope of this straight line is $-2.303\,E_o$, as is the slope of the relaxation curve plotted against log $t$ in the same region. The straight-line region of the dynamic modulus curve when extrapolated (as shown in Figure 4 for the stress relaxation curve) intercepts the maximum and minimum modulus axes at $\tau_l$ and $\tau_m$, respectively.

The plot of $\omega\eta_{dyn}$ *vs.* log $(1/\omega)$ assumes a nearly constant value between $\omega$ values of $1/\tau_m$ and $1/\tau_l$. The value of this constant is $(\pi/2)E_o$.

On the basis of the properties of the box distribution, we may deduce certain general relations between relaxation, dynamic modulus, and dynamic viscosity which should apply in an approximate way even for systems which do not correspond exactly to a box distribution of relaxation times, or which approximate a box distribution of relaxation times only over a limited time region. These are as follows:

1. If the stress relaxation curve plotted in the form $\frac{f}{s_o}$ *vs.* log $t$ is approximately linear over a wide range of logarithmic time, the height of the distribution function $E'(\log \tau)$ at any time value in this range is equal to the negative slope of the relaxation curve.

2. If the dynamic modulus plotted in the form of $E_{dyn}$ *vs.* log $(1/\omega)$ is approximately linear over a wide range of logarithmic frequency, the height of the distribution function $E'(\log \tau)$, at any value of $\tau$ corresponding to a value of $1/\omega$ in this range, is equal to the negative slope of the dynamic modulus curve.

3. If the value of $\omega\eta_{dyn}$ is nearly constant over a wide range of angular frequency, the height of the distribution function $E'$ (log $\tau$) at a value of $\tau$ corresponding to a value of $1/\omega$ in this range is equal to $(4.606/\pi)$ $(\omega\eta_{dyn})$.

4. If the slope of the relaxation curve plotted against log $t$, or the slope of the dynamic modulus plotted against log $(1/\omega)$, is approximately constant over a wide range of logarithmic time (or $1/\omega$), the value of $\omega\eta_{dyn}$ should be related to the negative slope of the relaxation or dynamic modulus curves by the equation

$$\omega\eta_{dyn} = \frac{\pi}{4.606} \text{ (negative slope)}. \quad (16)$$

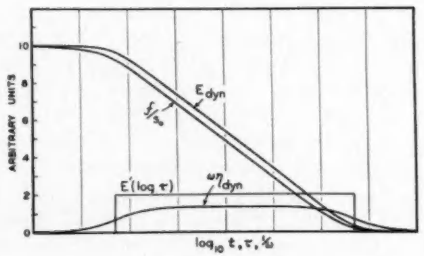


FIG. 5. *Stress relaxation, distribution function, dynamic modulus, and internal friction on logarithmic time scale.*

### Application to Experimental Data

Kuhn, Künzle, and Preissmann [8] have already shown the application of the box distribution function in relating creep and dynamic properties of polymers. Their computations are necessarily complicated because it is difficult to calculate creep in terms of the generalized Maxwell model. Nevertheless, these authors were able to show that if a creep curve for a given polymer were given by the equation

$$\frac{s}{f_o} = \frac{a + \ln t}{b}, \quad (17)$$

TABLE I. COMPARISON OF OBSERVED VALUES OF $\omega\eta$ AND VALUES PREDICTED FROM STRESS RELAXATION DATA FOR SOME RUBBERS

| Stock | Temp. (° C) | $E^e$ (dynes/cm.²) | Calculated $\omega\eta = \frac{E^e}{3}\frac{\pi}{4.606}$ (dynes/cm.²) | Observed $\omega\eta$ (dynes/cm.²) | $\frac{\omega\eta_{obs}}{\omega\eta_{calc}}$ |
|---|---|---|---|---|---|
| Hevea gum | 40 | $0.11 \times 10^6$ | $0.026 \times 10^6$ | $0.24 \times 10^6$ | 9.2 |
| | 100 | 0.20 | 0.045 | 0.13 | 2.9 |
| Hevea tread | 40 | 2.1 | 0.48 | 2.5 | 5.0 |
| | 100 | 2.5 | 0.55 | 1.1 | 2.0 |
| GR-S gum | 40 | 0.47 | 0.11 | 0.82 | 7.7 |
| | 100 | 0.47 | 0.11 | 0.42 | 3.8 |
| GR-S tread | 40 | 5.0 | 1.1 | 7.8 | 7.1 |
| | 100 | 1.8 | 0.40 | 3.0 | 7.5 |
| Butaprene NM gum | 40 | 0.75 | 0.17 | 1.7 | 10.0 |
| | 100 | 1.10 | 0.25 | 0.70 | 2.8 |
| Butaprene NM tread | 40 | 1.8 | 0.42 | 4.1 | 9.8 |
| | 100 | 1.7 | 0.40 | 1.5 | 3.7 |
| Neoprene GN gum | 40 | 1.5 | 0.33 | 0.85 | 2.6 |
| | 100 | 1.5 | 0.33 | 0.68 | 2.1 |
| Neoprene GN tread | 40 | 3.6 | 0.82 | 3.9 | 4.7 |
| | 100 | 3.8 | 0.86 | 2.0 | 2.3 |

TABLE II. COMPARISON OF OBSERVED VALUES OF $\omega\eta$ AND VALUES PREDICTED FROM STRESS RELAXATION DATA FOR SOME FIBROUS MATERIALS

| Material exp't. | $-\text{Slope}\ E^e$ (dynes/cm.²) | Calculated $\omega\eta = \frac{\pi}{4.606}E^e$ (dynes/cm.²) | Observed $\omega\eta$ (dynes/cm.²) | $\frac{\omega\eta_{obs}}{\omega\eta_{calc}}$ |
|---|---|---|---|---|
| Nylon: 5% rapid* | $1.96 \times 10^9$ | $1.3 \times 10^9$ | $3.8 \times 10^9$ | 2.9 |
| 0.5% rapid | 2.1 | 1.4 | | 2.7 |
| 5% slow† | 1.1 | 0.76 | | 5.0 |
| Acetate: 5% rapid | 2.2 | 1.5 | 1.5 | 1.0 |
| 0.5% rapid | 2.2 | 1.5 | | 1.0 |
| 5% slow | 1.65 | 1.13 | | 1.3 |
| Viscose: 5% rapid | 2.8 | 1.9 | 4.8 | 2.5 |
| 0.5% rapid | 4.5 | 3.1 | | 1.6 |
| 5% slow | 2.1 | 1.4 | | 3.3 |
| Raw silk: 5% rapid | 4.7 | 3.0 | 3.8 | 1.3 |
| 0.5% rapid | 5.1 | 3.5 | | 1.1 |
| 5% slow | 3.4 | 2.3 | | 1.6 |
| Keratin: 2% rapid | 3.7 | 2.5 | 1.5 | 0.6 |
| 0.5% rapid | 2.0 | 1.3 | | 1.1 |
| 2% slow | 1.0 | 0.70 | | 2.1 |
| Polyethylene: 5% rapid | 0.27 | 0.18 | 0.82 | 4.5 |
| 0.5% rapid | 0.30 | 0.20 | | 4.1 |
| 5% slow | 0.26 | 0.18 | | 4.5 |

* 15 sec. required to extend.
† 25 min. required to extend.

then the value of $\omega\eta_{dyn}$ is

$$\omega\eta_{dyn} = \frac{\pi b}{2a^2}. \qquad (18)$$

Dunell and Tobolsky [7] applied equation (16) to relate stress relaxation data and data on the dynamic properties of polymers.

Experimental values for $\omega\eta_{dyn}$ for natural rubber and various synthetic rubbers are available in the literature [5, 9]. The values of $\omega\eta_{dyn}$ were very nearly constant in the range of frequencies over which they could be measured—namely, 20–200 cycles per sec. Stress relaxation measurements were also made on these same rubbers, in a time range extending from 10 sec. to several hrs. [16]. The initial regions of the stress relaxation curves plotted against $\log t$ were generally nearly linear. The initial slopes of the stress relaxation curves were measured and a theoretical value of $\omega\eta_{dyn}$ calculated by use of equation (16). An example of the method used in calculating slopes is shown in Figure 2 where the slopes from which dynamic viscosity was calculated are indicated by dashed lines. The data obtained in this way for several rubbers are shown in Table I. Similar results for several fibrous materials studied by Dunell and Dillon [6] are given in Table II. In general, the values of $\omega\eta_{dyn}$ calculated from the stress relaxation data by means of equation (16) are lower than the observed values, although an order-of-magnitude agreement is obtained. It should be emphasized that the time scales of the dynamic data and stress relaxation data do not overlap. Better agreement between calculated and observed values would be anticipated if the relaxation data could be extended back for two cycles of logarithmic time and the slope of the relaxation curve could be measured in the same time region where the vibration measurements are made. Finally, in order to convert the data on stress relaxation of the vulcanized rubbers which were obtained at high deformations to units of stress per unit strain, the kinetic theory of elasticity had to be used, which also represents an approximation.

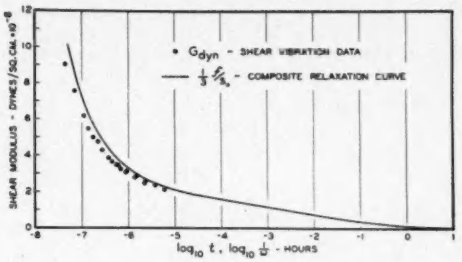


FIG. 6. *Relation between dynamic modulus and stress relaxation for polyisobutylene.*

To illustrate how stress relaxation and dynamic data may be combined to give a broad picture of the viscoelastic spectrum of polymers, stress relaxation data on polyisobutylene of Andrews, Holmes, and Tobolsky [2] and dynamic measurements of Marvin, Fitzgerald, and Ferry [9] are shown in Figure 6. The stress relaxation data at 30° C have been extended back for several decades of log time by superposition of data obtained at lower temperatures [14]. On the same graph are plotted the dynamic modulus data obtained at 30° C. The agreement between extrapolated stress relaxation data and dynamic modulus data is rather good.

Finally, in Table III is shown a comparison of $\omega\eta_{dyn}$ predicted from creep data [17] on several rubbers by use of equation (18) with the observed experimental value of $\omega\eta$. In these cases, too, the observed values are of the same order of magnitude, but are larger than the experimental values.

TABLE III. COMPARISON OF OBSERVED VALUES OF $\omega\eta$ AND VALUES PREDICTED BY KUHN'S THEORY FOR SOME RUBBERS

| Stock | $a$ | $b$ | Calculated $\omega\eta = \pi b/2a^2$ (dynes/cm.²) | Observed $\omega\eta$ (dynes/cm.²) | $\frac{\omega\eta_{obs}}{\omega\eta_{calc}}$ |
|---|---|---|---|---|---|
| Hevea gum | 148 | $4.93 \times 10^8$ | $0.35 \times 10^6$ | $1.8 \times 10^6$ | 5.1 |
| Hevea tread | 20.2 | 2.38 | 9.2 | 18 | 2.0 |
| GR-S gum | 33.4 | 1.24 | 1.75 | 6.3 | 3.6 |
| GR-S tread | 12.0 | 1.15 | 12.5 | 47 | 3.8 |
| Neoprene GN gum | 8.34 | 0.326 | 7.4 | 7.7 | 1.04 |
| Neoprene GN tread | 11.1 | 1.49 | 19 | 29 | 1.5 |

**Acknowledgments**

The authors wish to acknowledge the helpful suggestions of Dr. J. H. Wakelin in developing and applying the theory given in this paper.

One of us (B. A. D.) is particularly grateful to Textile Research Institute for the fellowship grant which has made the work possible.

It is a pleasure to acknowledge the important financial support of the work, received from The Office of Naval Research under Contract No. N7-onr-374.

**Literature Cited**

1. Andrews, R. D., Hofman-Bang, N., and Tobolsky, A. V., *J. Polymer Sci.* **3**, 669 (1948).
2. Andrews, R. D., Holmes, F. H., and Tobolsky, A. V., Paper presented at the meeting of the American Physical Society, New York City, Feb. 2, 1950.
3. Becker, R., "Probleme der technischen Magnetisierungskurve," Berlin, Springer, 1938, p. 103. Becker, R., and Doring, W., "Ferromagnetismus," Berlin, Springer, 1939, p. 254.
4. Brown, G. M., and Tobolsky, A. V., *J. Polymer Sci.* **6**, 165 (1951).
5. Dillon, J. H., Prettyman, I. B., and Hall, G. L., *J. Applied Phys.* **15**, 309 (1944); *Rubber Chem. and Technol.* **17**, 597 (1944).
6. Dunell, B. A., and Dillon, J. H., TEXTILE RESEARCH JOURNAL **21**, 393 (1951) (this issue).
7. Dunell, B. A., and Tobolsky, A. V., *J. Chem. Phys.* **17**, 1001 (1949). Dunell, B. A., "Dynamic Properties of Textile Fibres," Ph.D. Thesis, Princeton University, 1949. *Cf.* [9].
8. Kuhn, W., Künzle, O., and Preissmann, A., *Helv. Chim. Acta* **30**, 307, 464, 839 (1947).
9. Marvin, R. S., Fitzgerald, E. R., and Ferry, J. D., *J. Applied Phys.* **21**, 197 (1950).
10. Simha, R., *J. Applied Phys.* **13**, 201 (1942). Leaderman, H., "Elastic and Creep Properties of Filamentous Materials and Other High Polymers," Washington, D. C., The Textile Foundation, 1943. Alfrey, T., and Doty, P., *J. Applied Phys.* **16**, 700 (1945). Gross, B., *J. Applied Phys.* **18**, 212 (1947). Alfrey, T., "Mechanical Behavior of High Polymers," New York, Interscience, 1948.
11. Sips, R., *J. Polymer Sci.* **5**, 69 (1950).
12. Stern, M. D., and Tobolsky, A. V., *J. Chem. Phys.* **14**, 93 (1946); *Rubber Chem. and Technol.* **19**, 1178 (1946). Mochulsky, M., and Tobolsky, A. V., *Ind. Eng. Chem.* **40**, 2155 (1948); *Rubber Chem. and Technol.* **22**, 712 (1949).
13. "Tables of Sine, Cosine, and Exponential Integrals" (2 vols.), New York, WPA Tables, 1940.
14. Tobolsky, A. V., and Andrews, R. D., *J. Chem. Phys.* **13**, 3 (1945).
15. Tobolsky, A. V., and Eyring, H., *J. Chem. Phys.* **11**, 125 (1943).
16. Tobolsky, A. V., Prettyman, I. B., and Dillon, J. H., *J. Applied Phys.* **15**, 380 (1944); *Rubber Chem. and Technol.* **17**, 551 (1944). Tobolsky, A. V., and Andrews, R. D., *J. Chem. Phys.* **13**, 3 (1945); *Rubber Chem. and Technol.* **18**, 731 (1945).
17. Tobolsky, A. V., Prettyman, I. B., and Dillon, J. H., unpublished data.

(*Manuscript received January 29, 1951.*)

# Contradictory Data on Spiral Structures in the Secondary Cell Wall of Fibers of Flax, Hemp, and Ramie

**P. A. Roelofsen**

*Laboratory for Technical Botany, Technical University, Delft, Holland*

**Abstract**

Althought the microscopy of the well-known textile fibers flax, hemp, and ramie is familiar to many people and the spiral structure of their cell-wall layers is mentioned in many textbooks, the study of the original literature on this point disclosed many contradictory data. However, there cannot exist essential differences between the samples studied by the different authors, since there are no conflicting data on the direction of twist shown by the fibers on wetting or drying, nor on the optical behavior when studied with a polarization microscope.

A reinvestigation revealed that in flax there are not two, but three, layers with different spiral structure. Since usually either the outer or the inner one is very difficult to discern, previous authors described two of them, either the two outer or the two inner ones. In ramie and in hemp fibers the spiral structure of two outer layers is identical with those of flax, although the slope of the spirals and the thickness of the layers, of course, differ. If here, too, a third, innermost layer with different spiral structure could be found, the conflicting data in the literature would be understandable.

## Introduction

Striations in bast fibers were seen first by Mirbel in 1835. Naegeli described in 1886 the existence of two spiral directions in these striations in the same cell wall. Mostly, the two sets of striations were located in different layers, but sometimes they were found in one layer. Dippel in 1879, and later many others (Correns [2]), denied the occurrence of two sets of striations in one layer—they are always located in different layers.

According to Sonntag [12] the outermost layer of the secondary wall of flax and hemp fibers has an S-spiral fibrillar structure, and the inner layer a Z-spiralled one.* Later, however [13], he described an outer Z-spiral and an inner S-spiral in hemp fibers, although the reverse was said to occur sometimes.

Reimers [10] described an outer S-spiral and an inner Z-spiral in flax and ramie fibers (see rectification on p. 420 of his publication). In hemp an outer Z-spiral and an inner S-spiral was found. Later [11], ramie was mentioned to have an S-spiral both in the outer and the inner layers.

Nodder [9] found an outer S-spiral and an inner Z-spiral in flax, whereas in ramie only an S-spiral was seen, and in hemp only a Z-spiral.

Herzog [5] described an easily visible S-spiral in flax and a hardly visible, inner Z-spiral. Thick fibers from the stem base were the most suitable ones to show this. In hemp an outer Z-spiral and an inner S-spiral was seen. He stated that judging from the optical behavior between crossed Nicol prisms with a "1st-order red" compensator plate inserted below the object, the outer layers were optically predominant in both fibers. In a position parallel to the vibration plane of the polarizer, flax showed addition colors, and hemp subtraction colors.

Anderson [1] succeeded in isolating several lamellas of the secondary wall of flax, and stated that the spiral direction alternated in consecutive layers.

* Throughout this paper the terminology is used which has become the accepted practice in American textile technology. A spiral is designated as an S-spiral if the part nearest to the observer spirals upward to the left, parallel to the middle part of the letter S. Its mirror image is a Z-spiral.

Kundu and Preston [7] studied swollen and unswollen fibers of hemp. In unswollen fibers steep spiral striations were seen, mostly in Z-spirals, but also in S-spirals. They emphasized the well-known influence of swelling and compression on the slope of the spirals, and doubted the validity of observations on spiral structures done with swollen fibers. A photomicrograph of transverse sections of hemp seen between crossed Nicols was published. Double refraction is shown by the outer and occasionally by the inner layer, but the thick, midle part of the wall is isotropic.

Hock [6] could not confirm the alternating spiral structures in flax, as described by Anderson, but found in flax and ramie a thin, outer layer with Z-spiral structure, and an S-spiral structure in the rest of the wall. In hemp fibers he saw a similar outer layer with Z-spiral structure and an axial structure underneath. A good photomicrograph was given of both spirals in a swollen flax fiber. He stated erroneously that this confirmed the observations of Reimers [10]. Probably, he did not notice Reimers' rectification.

The following table summarizes the observations of the authors mentioned:

| Author | Flax | | Ramie | | Hemp | |
|---|---|---|---|---|---|---|
| | Outer | Inner | Outer | Inner | Outer | Inner |
| Sonntag [12] | S | Z | S | Z | S | Z |
| Sonntag [13] | S | Z | S | Z | Z | S |
| Reimers [10] | S | Z | S | Z | S | Z |
| Reimers [11] | S | Z | S | S | S | Z |
| Nodder [9] | S | Z | S | | Z | |
| Herzog [5] | S | Z | | | Z | S |
| Anderson [1] | Alternating | | | | | |
| Hock [6] | Z | S | Z | S | Z | Axial |

It is possible that these conflicting observations are due to the fact that the structures of different samples were really different. This, however, seems improbable, because there are no conflicting data of different authors on the direction of torsion shown by these fibers on wetting or drying. The same conclusion may be deduced from the fact that the optical behavior in orthogonal positions, as described by Herzog [5], is mentioned in literature as a means of distinguishing between flax and hemp.

We therefore decided to reinvestigate optically and microscopically the spiral structure of flax, hemp, and ramie fibers, hoping to find an explanation for the contradictory data.

## Results

### *Optical Behavior*

Several samples of flax, hemp, and ramie fibers were studied between crossed Nicol prisms with a "1st-order red" compensator plate inserted above the object and with the fibers parallel to the vibration plane of the polarizer. In case the fibers alone exhibit polarization colors of the first order, those of flax and ramie will always show subtraction colors under the conditions and in the position mentioned, whereas hemp fibers will always show addition colors. Taking into consideration that Herzog [5] inserted the compensator below the object,* our findings are in agreement with his. So there cannot exist essential differences in the spiral structures of the fibers in his samples and in ours.

As stated before, Herzog came to the conclusion that in flax fibers the S-spiralled layer in the wall is the one which predominates optically, whereas in hemp this must be a Z-spiralled one. This may be concluded from the results obtained by Naegeli and Schwendener ([8], p. 332 *et seq.*) when they studied the phenomena shown in analogous conditions by a pair of superposed birefringent plates that were orientated in such a way that the vibration axes in the two plates enclosed a small angle. We repeated and confirmed their observations, using two strips of anisotropic cellophane instead of two crystal plates. One assumption had to be made in arriving at conclusions about the predominating spiral structure in fibers—*viz.*, that the upper and the lower wall each act as one plate or cellophane strip. In case the different layers in the wall are thin, this assumption is permitted (Frey-Wyssling [3]).

However, we observed that not all fibers act as a pair of birefringent objects. As Naegeli and Schwendener showed, a pair of plates superposed, for instance, in S-fashion,† will show a subtraction color in a position parallel to the vibration plane of the polarizer provided that the polarization color of the pair is of the first order and provided the compensator plate is located above the pair. But if its polarization color is of the second order, the subtraction color will be seen perpendicular to the described position. On the other hand, thick fibers with a polarization

* This is not stated explicitly in Herzog's publication, but in that of Heermann and Herzog ([4], p. 94 and 153).

† Vibration axis in lower plate from left bottom to right top and in upper plate from right bottom to left top.

color of the second order as a rule will show subtraction or addition colors in the same position as thinner fibers of the same kind having a polarization color of the first order. There are exceptions to this rule in flax, ramie, and in hemp fibers as well, which therefore do act like a pair of plates.

We cannot explain these facts. With thick fibers the assumption that one cell wall acts as one plate probably is not true, the layers constituting the cell wall perhaps being so thick that one wall should be considered as representing two or more plates.

*Microscopical Studies on Swollen Fibers*

We used retted fibers of flax, hemp, and ramie obtained either from commercial samples or by retting stems at 35°C in a cylindrical vessel for several days. We also used ramie fibers in the degummed condition and as present in China grass. We tried most swelling media used by the aforementioned authors—*viz.*, 10% NaOH, 62% $H_2SO_4$ (s.g. 1.52), 82% $H_3PO_4$ (s.g. 1.654), IKI followed by 50%–60% $H_2SO_4$, saturated $CaCl_2$ with iodine, saturated $ZnCl_2$, boiling acetic acid, and diluted cuprammonium. We preferred using cuprammonium that was diluted with concentrated ammonia to such an extent that the fibers did not dissolve, but swelled 3–8 times their original diameter. The refractive indexes of the other media except acetic acid are too high, and they reduce the contrast of the faint striations to be studied. The slope of the spiral structures we saw is disregarded. Due to contraction of the fibers, they will always be flattened considerably.

*Flax.*—In nearly all fibers from two commercial samples of retted flax and from bleached flax, a conspicuous S-spiral structure could be seen. In favorable cases, moreover, a faint Z-spiral structure could be noted in the outermost thin layer. Figure 1 is a photomicrograph of the upper wall of a fiber in which the outer Z-spiral could be seen exceptionally well. This layer is always so thin that the S-spiral structure underneath appears to be in focus at the same time. The presence of the outer Z-spiral structure is also demonstrated by the direction of the balloonlike thickenings which occasionally can be found and which are very well known in swollen cotton fibers. These balloonlike thickenings appear to be directed in a Z-spiral fashion because they are due to the Z-spiral constrictions from the outermost layer. Whether this outer layer represents the primary cell wall or the outer layer of the secondary cell wall cannot be decided yet.* Of course, transverse markings usually were present, being remnants of dislocations.

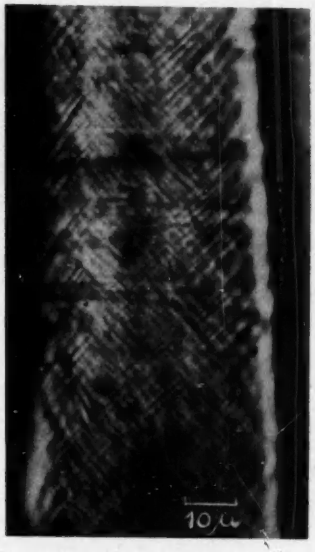


FIG. 1. *Flax fiber, showing a thin outer layer with Z-spiral structure and S-spiral structure underneath.*

We did not succeed in obtaining separate lamellas of the wall, as described by Anderson [1].

Thus far our observations fully corroborated those of Hock [6], although we noticed that inside the S-spiralled layer there still was a part of the cell wall the structure of which remained obscure.

However, when we repeated the observations, using fibers from stems that had been retted in our laboratory, we very clearly saw in nearly all fibers a conspicuous Z-spiral structure inside the S-spiralled one seen in the other samples. Figure 2 depicts this. This confirms the descriptions of all the other authors except Hock.

With difficulty and rarely the outermost Z-spiralled thin layer seen in the other samples could be found now. Figure 3 shows on the left such a faint Z-spiralled striation with the common S-spiral under-

* If this layer represents the primary cell wall, it might be composed of two differently oriented submicroscopical layers, as was discovered recently by the author in an electron microscopical study of growing cell walls in staminal hairs of *Tradescantia*, in fungal hyphae, and in young cotton hairs (see, respectively, *Protoplasma*, **40**, No. 1 (1951); *Biochim. Biophys. Acta* **6**, 357 (1951); and *ibid.* **7**, 43 (1951).

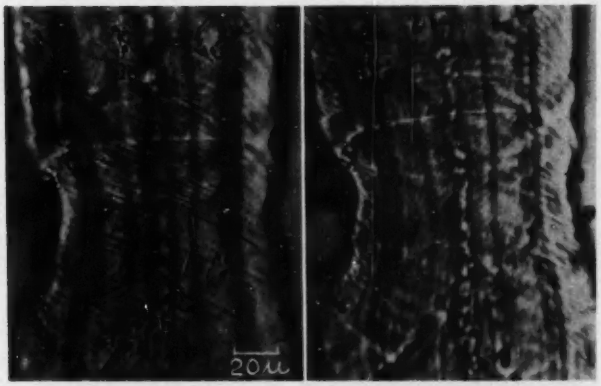


FIG. 2. *Flax fiber photographed while focussing on the surface (left) and below the surface (right). A Z-spiral structure is visible beneath the conspicuous S-spirals.*

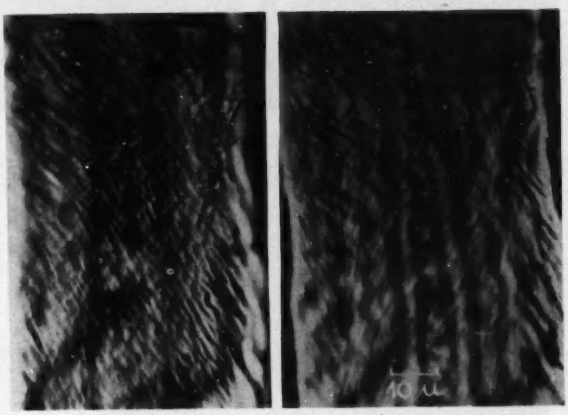


FIG. 3. *Flax fiber photographed while focussing on the surface (left) and below the surface (right). Three layers are visible with, respectively, Z-, S- and Z-spiral structures.*

neath, and on the right the inner Z-spiral on the same spot.

Thus, the contradictory observations of previous authors can now be understood. There are three layers differing in spiral structure: an outer, thin, Z-spiralled layer; then a thick S-spiralled layer; and an inner layer of considerable thickness with Z-spiral structure. There seem to exist two kinds of samples: those in which only the two outer layers can be discerned practically and those in which only the two inner ones can be seen easily. The alternative assumption is that there exist three kinds of flax with real differences in structure. This is very unlikely.

Apparently, the middle layer determines the optical properties and also the direction of twist when the fibers are moistened.

*Ramie.*—In fibers from a degummed sample and also from China grass and from stems retted in the laboratory, we always found an S-spiral structure extending from the surface to a considerable depth. Only in exceptional cases, occurring in the laboratory-retted fibers, could we discern a faint, outer, Z-spiralled striation. This is demonstrated in Figure 4. Figure 5 shows that in heavily swollen fibers the outer layer is usually split and crumpled up into bands. Apparently, these are weak and do not constrict the swollen fibers, as in hemp.

Thus, our observations confirm those of Hock, and, in a way, also those of Nodder [9] and Reimers [11]. However, our experience with flax has taught us not to deny the possibility that in special samples an in-

FIG. 4. *Ramie fiber photographed while focussing on the surface (left) and below the surface (right). There is a faint Z-spiral striation on top of the conspicuous, steep, S-spiral structure.*

FIG. 5. *Heavily swollen ramie fiber, showing the crumpling up of the outer Z-spiralled layer into bands.*

FIG. 6. *Hemp fiber, showing an outer Z-spiral structure only.*

nermost Z-spiral structure might be found, as described by Sonntag [12] and Reimers [10].

Obviously, it is the S-spiralled thick layer which determines the optical properties and the direction of twist on wetting or drying.

*Hemp.*—In retted, unbleached fibers from a commercial sample we only saw Z-spiral striations occurring in the outermost layer, which seemed to be thicker than the corresponding Z-spiralled outer layer in flax and ramie. This is depicted in Figure 6. Beneath this layer the direction of the fibrils, as a rule, was invisible, but in some cases it decidedly was S-spiralled. In fibers from stems retted in our laboratory, we always found a very conspicuous S-spiralled structure lying beneath the Z-spiralled outer one. The latter frequently split into bands, giving rise to the same spiralled balloonlike thickenings which were also found, although rarely, in flax. Figures 7 and 8 show these striations.

Inside this S-spiralled layer there remained a considerable part of the wall in which we could not see

FIG. 7. *Hemp fiber, showing an S-spiral structure in a layer the swelling of which is constricted in a Z-spiral fashion by bands formed in the outer (Z-spiralled) layer.*

FIG. 8. *Similar to Figure 7.*

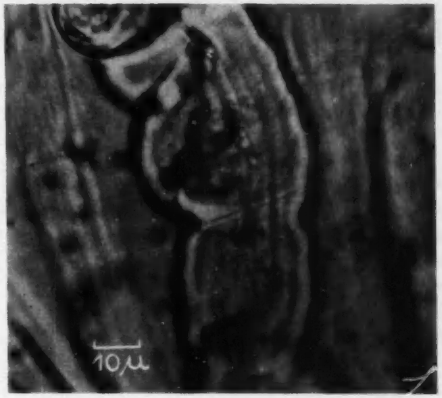


FIG. 9. *Portion of a heavily swollen hemp fiber with a narrow central part in which Z-spiral striation is visible.*

any striations. Probably, this part has an axial structure as described by Hock, but the observations of Reimers [10] and Sonntag [12] point to the possibility that in special samples an inner Z-structure may be found. Only twice did we see a Z-spiralled narrow tube around the cell lumen; this is depicted in Figure 9. The occurrence of a central layer showing birefringence in transverse sections, as depicted by Kundu and Preston [7], is also not to be neglected.

Thus, our observations confirm those of Herzog [5] and Sonntag [13], but we want to emphasize the possibility that the inner parts of the wall might be Z-spiralled, as mentioned by Reimers and seen twice by us.

The optical properties seem to be determined by the outer (and perhaps inner) Z-spirals. As is well known, the twist on wetting or drying hemp fibers is small and rather variable.

### Danger of Spirals Arising from Twisting

We have considered the possibility that a spiralled layer in a fiber may originate during swelling from an axial structure, due to a twist enforced upon the fiber by an originally spiralled layer—for instance, the outermost Z-spiralled layer. This possibility is demonstrated by the following model experiment described by Steenberg [14]. If a string is wound

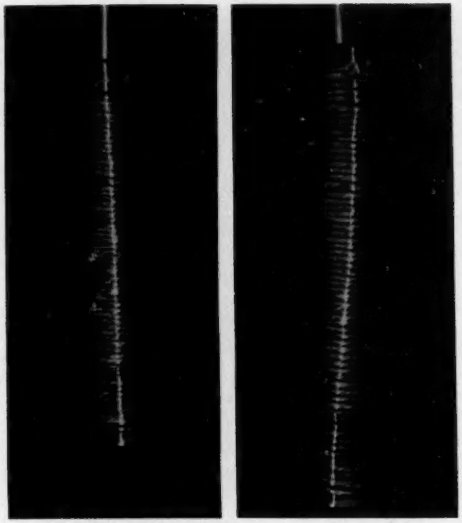

FIG. 10. *Model experiment with the inner tube of a bicycle tire with a string wound around it in S-fashion. When air is pressed into tube, it twists in Z-spiral direction (right).*

in a flat S-spiral direction around the iner tube of a bicycle tire and subsequently air is blown into the tube, the tube will twist and acquire a Z-spiral structure. Figure 10 demonstrates this. We are aware of the fact that this model is not wholly comparable with a swelling fiber, but in a mechanical sense the situation is analogous.

Of course, the originally present spiralled layer need not be the outer one. For instance, it may be the middle S-spiralled layer of flax fibers which enforces a Z-spiral structure on the outer and on the inner layer, which supposedly had axial structures originally. Or, on the contrary, the two Z-spiralled layers might have created the S-spiralled one.

Obviously, such a twist can only occur in pieces of fiber which are not in contact with other pieces and therefore are free to move under the cover glass. It may also occur in free ends of fibers. Thus, in these cases one may get a false impression. However, our observations (described above) refer to parts of fibers which obviously were not free to twist, being fixed by other fibers. They could only contract, together with the other fibers. Moreover, especially hemp fibers which are free to move do not

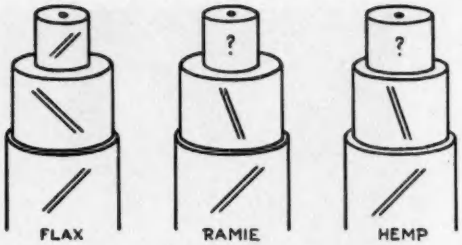


FIG. 11. *Schematic representation of the spiral structures in different layers of flax, ramie, and hemp.*

twist very much while contracting in cuprammonium, and, in fact, no difference in spiral structures could be seen between such fibers and fixed ones.

## Summary

The data given in the literature on the spiral structures in fibers of flax, hemp, and ramie do not agree. Therefore, these fibers were reinvestigated microscopically after swelling in cuprammonium. The results are depicted in Figure 11. The demonstration of the presence in flax of three layers with different spiral structure, one of which is usually not visible, explains the contradicting results of previous authors.

## Literature Cited

1. Anderson, D. B., *Am. J. Bot.* **14**, 187 (1927).
2. Correns, C., *Jahrb. f. wiss. Bot.* **23**, 254 (1892).
3. Frey-Wyssling, A., *Protoplasma* **35**, 527 (1941).
4. Heermann, P., and Herzog, A., "Mikroskopische und mechanisch-technische Textiluntersuchungen," Berlin, Springer, 1931.
5. Herzog, A., "Die Unterscheidung der Flachs- und Hanffaser," Berlin, Springer, 1926.
6. Hock, C. W., *J. Research Natl. Bur. Standards* **29**, 41 (1942).
7. Kundu, B. C., and Preston, R. D., *Proc. Roy. Soc. London, Ser. B 851*, **128**, 214 (1940).
8. Naegeli, C., and Schwendener, S., "Das Mikroskop," Leipzig, Engelmann, 1877.
9. Nodder, C. R., *J. Text. Inst.* **13**, 161 (1922).
10. Reimers, H., *Textilber.* **2**, 367, 381, 420 (1921).
11. Reimers, H., Mitteill. Deutsches Forsch. Inst. Textilstoffe, Karlsruhe, 1922. Cited by Steinbrinck, *Naturwissenschaften* **50**, 978 (1927).
12. Sonntag, P., *Flora* **99**, 203 (1909).
13. Sonntag, P., *Jahresber. Ver. Angew. Botanik* **9**, 140 (1911).
14. Steenberg, B., Svenska Träforskningsinstitutet, Meddelanda No. 20, Stockholm, 1947.

(*Manuscript received November 6, 1950.*)

# Pore-Size Distribution in a Selected Series of Closely Woven Fabrics

**Edith Honold and Evald L. Skau**

*Southern Regional Research Laboratory,* New Orleans, Louisiana*

IN a previous publication [1], the mercury-intrusion method was presented as a means of determining the pore-size distribution in textile fabrics for the range of 20 to 0.2 $\mu$ radius (approximately 5 to 500 p.s.i.a.†). In the present study, the use of an additional apparatus, with a starting pressure of $\frac{1}{2}$ p.s.i.a., has extended the radius range to 200 $\mu$. Results are here reported on a series of closely woven fabrics that were selected to eliminate a number of variables so that direct comparison could be made to show the effect of fiber maturity, of weave closeness, and of fabric state on the total void volume and its distribution.

The principles upon which the mercury-intrusion method is based, the derivation of the distribution-function equation, the general method of procedure, and the sources of error have been discussed in the literature [1, 2, 3]. The relationship between the radius, $r$, of a circular pore and the pressure, $p$, necessary to just force the mercury into the pore is expressed [4] by the equation

$$p \cdot r = -2\sigma \cos \theta, \qquad (1)$$

$\sigma$ being the surface tension of mercury and $\theta$ the contact angle. Since the pores in the fabric are not all circular in cross section, the $r$ values obtained by the use of equation (1) may be considered to be "effective" radii. In other words, at any given pressure, the pores being filled, regardless of the configuration of their pore entrances, are expressed as the hypothetical circular pore which would admit mercury at the same pressure.

The pressuring curve that is characteristic of the material shows the cumulative volume, $\Delta V$, of mercury penetrating the sample as the pressure is increased. The derived equation for the determination of $D(r)$, the distribution function, which gives the frequency of occurrence of the different-sized pores, is

$$D(r) = \frac{p}{r} \cdot \frac{d(\Delta V)}{dp}. \qquad (2)$$

In this equation $r$ is the effective radius of the pores in equilibrium at pressure $p$, and $\frac{d(\Delta V)}{dp}$ is the slope of the pressuring curve at pressure $p$, which slope is determined by graphical differentiation.

### Sources of Error

The value of the contact angle has been assumed to be 140° [1, 2]. If a higher value is assigned to the contact angle, the calculated effective radii will be higher and will cover a greater radius range, and vice versa. It is not likely that the contact angle will vary much within a series of fabrics in the same state—*i.e.*, gray, scoured, or finished. This source of error could be significantly effective only in the comparison of fabrics in different states.

The compression factor introduced by the non-rigidity of the fabric system may be neglected, for practical purposes, in the interfiber regions. However, in the lowest-pressure range, which apparently involves the filling of the surface depressions formed by the fabric weave, the compression factor may become significant; the network of slack fibers within these depressions may be compressed slightly before being penetrated by the mercury.

### Apparatus and Experimental Procedure

Determinations were made on each fabric in three separate apparatuses which cover overlapping portions of the pressure range from $\frac{1}{2}$ to 600 p.s.i.a. The high-pressure apparatus (from atmospheric pressure to 600 p.s.i.a.) is the platinum-resistance-wire dilatometer of Ritter and Drake [2] with little modification [1]. The middle-range apparatus (from 6 to 65 p.s.i.a.) is the brass- and steel-protected dilatom-

* One of the laboratories of the Bureau of Agricultural and Industrial Chemistry, Agricultural Research Administration, U. S. Department of Agriculture.

† p.s.i.a. = lbs. per sq. in. absolute.

eter previously described in detail [1]. The low-pressure apparatus (from ½ p.s.i.a. to atmospheric pressure) is an all-glass dilatometer (Figure 1); it is essentially a U-shaped tube the upper right arm of which is expanded into a chamber fitted with a flat-ground plug and the left arm of which is a calibrated capillary tube connected to the vacuum system. Three wide-mesh stainless steel screens fit into the right chamber and hold two circular samples of the fabric in a flat, horizontal position. The whole system is evacuated with a diffusion pump for several hours. The mercury, introduced through a small stopcock at the bottom of the U-tube, rises in both arms of the tube and raises the screens and interposed samples until the upper screen rests against the flat bottom of the chamber plug. The mercury finally surrounds and immerses the sample.

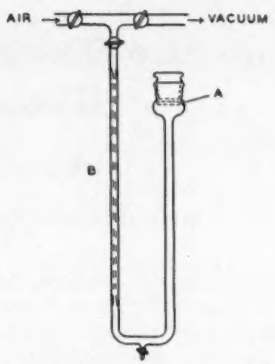


FIG. 1. *Schematic diagram of low-pressure dilatometric apparatus.* A—*Position of screens and sample circles during run.* B—*Calibrated capillary tube.*

The mercury-intrusion method permits the measurement of the void volume filled with mercury for each increment increase in pressure, regardless of the pressure at which the run is started. The pressure is increased stepwise; simultaneous readings are made of the pressure and of the change in height of the mercury column, and the latter is converted to volume of mercury entering within the boundaries of the sample. This drop in mercury height is determined in the high-pressure equipment by the resistance changes as additional length of the dilatometer wire is exposed, and in the other apparatuses by visual means using a cathetometer. In the low-pres-

TABLE I. SOME PHYSICAL PROPERTIES OF THE FABRICS

| Fabric Number | State | Thread count (warp × filling) | Weight* (oz./sq. yd.) | Thickness (mm.) | Void space† (cc./g.) (dry) |
|---|---|---|---|---|---|
| | | *Cotton of 85% maturity count* | | | |
| 114-G | Gray | 124 × 56 | 9.26 | 0.467 | 1.592 |
| 114-S | Scoured | 128 × 56 | 9.02 | 0.437 | 1.529 |
| 114-F | Finished | 128 × 56 | 9.37 | 0.434 | 1.462 |
| 116-G | Gray | 124 × 64 | 9.72 | 0.439 | 1.425 |
| 116-S | Scoured | 128 × 64 | 9.52 | 0.432 | 1.432 |
| 116-F | Finished | 128 × 64 | 9.83 | 0.432 | 1.387 |
| 118-G | Gray | 124 × 72 | 10.16 | 0.434 | 1.348 |
| 118-S | Scoured | 129 × 72 | 10.24 | 0.417 | 1.285 |
| 118-F | Finished | 130 × 70 | 10.20 | 0.417 | 1.290 |
| | | *Cotton of 30% maturity count* | | | |
| 119-G | Gray | 124 × 56 | 8.76 | 0.434 | 1.563 |
| 119-S | Scoured | 129 × 56 | 8.39 | 0.396 | 1.490 |
| 119-F | Finished | 130 × 56 | 8.49 | 0.394 | 1.465 |
| 121-G | Gray | 124 × 64 | 9.29 | 0.455 | 1.546 |
| 121-S | Scoured | 130 × 63 | 8.95 | 0.409 | 1.442 |
| 121-F | Finished | 130 × 63 | 9.00 | 0.396 | 1.389 |
| 123-G | Gray | 125 × 73 | 9.79 | 0.422 | 1.360 |
| 123-S | Scoured | 130 × 74 | 9.41 | 0.389 | 1.305 |
| 123-F | Finished | 130 × 71 | 9.52 | 0.386 | 1.280 |

* Standard conditions.

† Calculated from two previous columns, assuming 7% moisture regain at standard conditions.

sure runs, the readings are corrected from data established by blank runs with only the 3 screens in position. Since the pressure ranges in the three apparatuses have considerable overlap, the results from the three separate procedures can be combined into a smooth, continuous pressuring curve.

Various secondary plots were made from these pressuring data to depict graphically the relationships between the fabrics.

## Description of Samples

In connection with the Laboratory project on self-sealing, water-resistant cloth, several Oxford-weave cotton fabrics had been prepared in order to study their various physical properties. From this group, 18 fabrics were selected as being particularly suitable for the study of porosity with a limited number of variables. All 18 fabrics were woven from 30/2 yarns with the same number of twists per inch. Nine were composed of cotton of 85% maturity count and nine of cotton of 30% maturity count. All the fabrics were woven with 124 warp threads to the inch but with three different pickages (56, 64, and 72 filling threads per in. as woven). The series can also be grouped according to the different fabric states: gray or untreated (G), alkali-scoured (S), and finished (F), which involved an additional treatment of vat dyeing followed by a Zelan treatment. Any conclusions which may be drawn from these experiments as to the effect of scouring and Zelanizing must be considered to be specific for these particular fabrics as processed, since any change in the pore-size distribution due to processing will depend to a certain extent upon the various details of the processing method and procedure used. Some of the physical properties of these 18 fabrics are summarized in Table I.

TABLE II. PERCENTAGE OF TOTAL THEORETICAL VOID FILLED WITHIN THE EXPERIMENTAL RANGE

| Fabric number-state | Theoretical total void (average) (cc./g.) | Experimental total void filled with mercury (from 200 to 0.2$\mu$ pore radius) (cc./g.) | Theoretical void filled experimentally (%) |
|---|---|---|---|
| | *Cotton of 85% maturity count* | | |
| 114-G | 0.933 | 0.919 ± 0.020 | 99 ± 2 |
| 114-S | 0.840 | 0.788 ± 0.028 | 94 ± 3 |
| 114-F | 0.777 | 0.743 ± 0.025 | 96 ± 3 |
| 116-G | 0.758 | 0.760 ± 0.017 | 100 ± 2 |
| 116-S | 0.748 | 0.692 ± 0.011 | 93 ± 1 |
| 116-F | 0.702 | 0.649 ± 0.018 | 92 ± 3 |
| 118-G | 0.689 | 0.630 ± 0.013 | 91 ± 2 |
| 118-S | 0.617 | 0.610 ± 0.021 | 99 ± 3 |
| 118-F | 0.599 | 0.574 ± 0.015 | 96 ± 3 |
| | *Cotton of 30% maturity count* | | |
| 119-G | 0.879 | 0.900 ± 0.013 | 102 ± 1 |
| 119-S | 0.817 | 0.776 ± 0.014 | 95 ± 2 |
| 119-F | 0.797 | 0.762 ± 0.008 | 96 ± 1 |
| 121-G | 0.870 | 0.767 ± 0.027 | 88 ± 3 |
| 121-S | 0.771 | 0.682 ± 0.014 | 88 ± 2 |
| 121-F | 0.713 | 0.731 ± 0.013 | 103 ± 2 |
| 123-G | 0.686 | 0.662 ± 0.009 | 97 ± 1 |
| 123-S | 0.587 | 0.563 ± 0.028 | 96 ± 5 |
| 123-F | 0.601 | 0.603 ± 0.010 | 100 ± 2 |

## Results and Discussion

### *Total Void Volume*

The comparisons made between the void space filled with mercury within the experimental range and the total theoretical void volume available within the sample boundaries are shown in Table II. Each total void volume was calculated from sample weight and dimensions, using the average thickness as determined by the A.S.T.M. procedure D39–49. Column 3 gives the average void volume filled with mercury within the range from 200 to 0.2 $\mu$ radius (from $\frac{1}{2}$ to 528 p.s.i.a.). An over-all average of 96 ± 2% (column 4) of the theoretical total void volume is filled with mercury within the experimental range. In the previous series [1] the experimental range from 20 to 0.2 $\mu$ radius (from 5 to 528 p.s.i.a.) accounted only for approximately 60% of the total void. Thus, the addition of the low-pressure-range apparatus brings into consideration practically all of the remaining 40% of the available void space within these fabric samples.

### *Pressuring Curves*

Two modifications of the previous method of plotting pressuring curves have been introduced to facilitate the comparison of the data for the different fabrics over the whole range from $\frac{1}{2}$ to 528 p.s.i.a. First, a logarithmic scale is used for the abscissa, which may represent either pressure or pore radius by using reversed scales on the same diagram. Second, the assumption is made that the void volume of each sample is completely filled by 528 p.s.i.a. (0.2 $\mu$ radius) and the $\Delta V$ changes are plotted backward from this point. The typical curves, as presented in

Figure 2, have more or less leveled off at 0.2 $\mu$ radius, indicating a small residual void volume within the pores of radius less than 0.2 $\mu$. The sharper rise of the immature-cotton curves (represented by 119) suggests a greater volume unfilled in the immature-cotton fabrics than in the mature at a pressure of 528 p.s.i.a.

At the starting pressure of $\frac{1}{2}$ p.s.i.a. (200 $\mu$ radius), the mercury has already penetrated the boundaries of the various samples to different degrees, if the surface boundaries are considered to be parallel planes touching the outermost portions of the warp threads. Since the surface depressions of the mature-cotton fabrics are freer of slack fibers than are those of the immature, more mercury probably would have entered the depressions of the mature-cotton fabrics.

Therefore, the small percentage of available void volume not included in the experimental range seems to occur in different regions for the two types of fibers. In the mature-cotton fabrics, the greater portion of this residual volume appears to be filled at pressures below $\frac{1}{2}$ p.s.i.a.; in the immature, it apparently is divided between the region below $\frac{1}{2}$ p.s.i.a. and that above 528 p.s.i.a.

Some of the features of these pressuring curves are brought out by the representative curves shown in Figure 2. Each mature-cotton fabric (*e.g.*, 114) has two "mounds" of varying height which are separated by an intervening "valley" somewhere in the region of 4–8 $\mu$ radius. The immature-cotton fabrics do not have a consistent pattern; the mounds, when present, are shallower (*e.g.*, 119-G), and the intervening valley is at a lower pore-size radius position. Each immature-cotton fabric curve lies considerably below its corresponding mature-cotton fabric curve except in the region from 3–9 $\mu$ radius, which is the valley section of the mature-cotton fabrics; in this region, the pairs tend to approach each other.

As the mercury penetrates a cotton fabric, the filling would be expected to follow the general order of surface depressions, interyarn spaces, interfiber spaces, lumens. Actually, the different portions overlap and tend to blend into each other. From the effective pore-radius dimensions the deduction can be made that the mound in the low-pressure range of these pressuring curves pertains to the filling of the surface depressions, and, as has been shown [1], the pore-size range of the second mound corresponds predominantly to the filling of the interfiber spaces. If the valley represents the transition from the filling

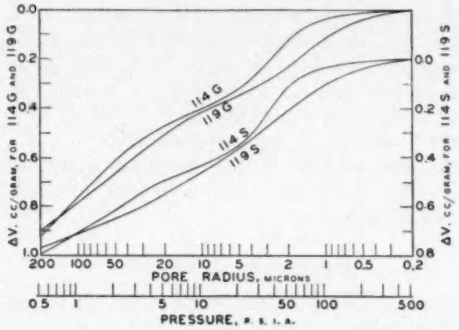


FIG. 2. *Semilogarithmic plot of pressuring curves for fabrics 114–G, 114–S, 119–G, and 119–S.*

of the surface depressions to the filling of the interfiber spaces, all the mature-cotton fabrics present a rather distinct separation between the two regions. For the immature-cotton fabrics, the separation between the two regions in the gray and finished states is considerably less pronounced, and, in the scoured, is nonexistent (*e.g.*, 119-S). In the scoured immature-cotton fabrics, the change in $\Delta V$ tends to progress more or less smoothly to the final leveling off at the highest ranges; consequently, there is no apparent separation between surface depression and interfiber filling, but, rather, a decided overlapping of all the regions. The continued rise of all the immature-cotton fabric curves at pressures above 100 p.s.i.a., the approximate range in which the mature-cotton fabric curves are leveling off, may be explained as the combined effect of the more numerous smaller-sized interfiber spaces plus the penetration of lumen channels, since it has been shown microscopically that the lumens of the immature fibers have a greater tendency to be penetrated by mercury than those of the mature fibers.

### *Distribution Curves*

Of the various methods of plotting the data, the pore-size distribution curves probably afford the best means of comparison. These curves depict the volume change per gram of cotton per micron increase in pore-radius throughout the range studied, so that the area under any part of the curve equals the total volume of the pores having radii between the selected limits.

Each fabric studied has a characteristic pore-size

distribution curve. These are best compared by considering the upper and lower portions of the range separately, since the significant differences of the low-pressure volume changes are obscured if the same scale for the $D(r)$ axis is used throughout the whole pressure range.

*Low-Pressure Range.*—For the low-pressure range, large plots were made of the distribution function, $D(r)$, against effective radius for all 18 fabrics. The most consistent feature was the relationship between the corresponding mature- and immature-cotton fabrics. The mature-cotton fabrics have a larger volume of pores of radii between 200 and 26 $\mu$ and a smaller volume of pores of radii between 26 and 5 $\mu$ than the corresponding immature-fiber fabrics. A comparison of the relative magnitude of this effect can best be made by considering the areas under the distribution curves—that is, the volume of void filled within these selected limits. Figure 3 shows these volumes, in cc./g., for the effective pore-radius range from 200 to 26 $\mu$, which range may be assumed to be related to the surface-depression filling, as has been pointed out.

A survey of these bar graphs leads to three general conclusions as to the effect of (1) fiber maturity, (2) fabric state, and (3) weave closeness.

(1) The void volume filled within this pore-size range for each mature-cotton fabric is greater than that of the corresponding immature. This is consistent with the differences in appearance, as noted on microscopic examination, which showed the surface depressions of the mature-cotton fabrics to be larger and more free from slack fibers than the immature.

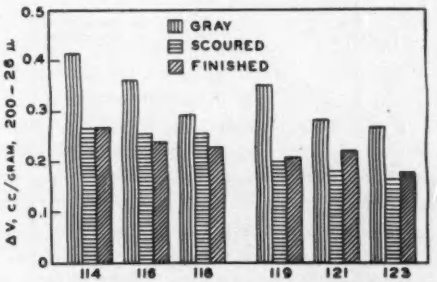


FIG. 3. *Void volumes within the large pore-size range. 114 and 119—Loosest weave. 116 and 121—Intermediate weave. 118 and 123—Closest weave.*

(2) Processing, as performed on these particular fabrics, decreased the void volume in this pore-size range, and, in this respect, seemed to affect the immature-cotton fabrics to a greater degree than the mature, with the result that in the scoured and finished states all the mature-cotton fabrics showed greater void volumes filled than did any of the immature. It is also apparent that the loss of void volume in this range tends to be more marked for the more loosely woven than for the more tightly woven fabrics. The differences between the scoured and finished states are not significant.

(3) The void volume filled within this pore-size range tends to decrease with increased pickage for both the mature- and immature-cotton fabrics in each of the three states. However, the decrease is very evident in the gray fabrics and is less marked in the processed fabrics—that is, processing seems to level-off the effect of pickage in this region.

Similar volume comparisons for the 26–5 $\mu$ radius range show that the immature-cotton fabrics have a greater void volume filled than the corresponding mature. In the majority of the fabrics, neither scouring nor finishing has a great effect on the void volume filled in this range and usually either one decreases it slightly, with the marked exception that scouring causes a consistent increase in the immature fabrics.

*High-Pressure Range.*—Unlike the low-pressure distribution curves which show a more or less gradual rise in $D(r)$ value as the pore-radius decreases, the high-pressure distribution curves rise with different degrees of sharpness to a peak and then fall. This peak represents that pore-radius at which the frequency of occurrence of pores is the greatest and represents predominantly the filling of interfiber pore spaces [1]. The distribution curves for all 18 fabrics are shown in Figure 4, and the pore radii of the peaks of the distribution curves are listed in Table III. These results are compared from three points of view: (1) maturity of fiber, (2) thread count, and (3) fabric state.

(1) The peak of the distribution curve for each immature-cotton fabric always occurs in a lower pore-size range than that of the corresponding mature. Since a greater number of immature fibers (2.4 $\mu$g./in.) are necessary to furnish the same weight as a given number of mature fibers (4.2 $\mu$g./in.) and since the yarn numbers of both yarns are approximately the same, there are approximately twice as many fibers in a cross-sectional area of the immature-

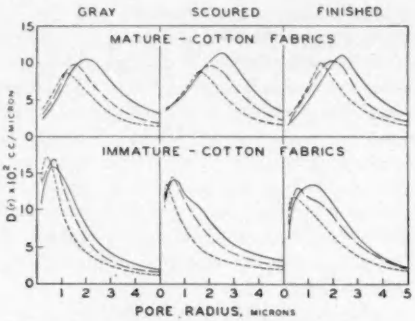


FIG. 4. *Distribution curves for all 18 fabrics.* ——— *Loosest weave.* — — — *Intermediate weave.* - - - - - *Closest weave.*

cotton yarn as in the mature. Consequently, if the gages of the yarns are the same, the average spaces between the immature fibers are considerably smaller than those between the mature fibers.

(2) As the thread count is increased, the mature-cotton fabrics in each state show a progression of peak toward a lower pore-size range. This effect is further emphasized by a comparison with the mature-cotton samples (nos. 1, 2, 3, 5, 6) of the previous publication [1]. All of those fabrics were of looser weave and had distribution peaks in a higher pore-size range, 2.6–4.4 $\mu$. As the pickage is increased, the filling threads are pressed more closely together, resulting in interfiber spaces of smaller dimensions. In the immature-cotton fabrics, a similar peak-position relationship is indicated, but the progression of peak-position is not as precise as in the mature. This lack of precision is due to the fact that the peak-position range of the immature cotton fabrics corresponds to that section of the pressuring curves in which it is difficult to obtain the accuracy of slope necessary for the precise placing of the peaks. Again, the distribution peaks of the looser-woven immature-cotton fabric (4-S and 4-F) of the previous series [1] were at a higher pore-radius position, 2.0 $\mu$, than any of the immature-cotton fabrics of the present series.

(3) Two relationships are shown between fabric states by a comparison of the distribution curves as calculated—that is, by using the same contact angle for all states. The peak of each gray mature-cotton fabric has a lower pore-size position than that of either the scoured or the finished, while the peaks of the scoured and finished are at approximately the same radius position in each case. In the immature-cotton fabrics, the scoured fabric always has the lowest peak radius position but there seems to be no further consistency in the relationship of the various fabric states.

TABLE III. RADII POSITIONS ($\mu$) OF PEAKS OF DISTRIBUTION CURVES

| Fabric number | Fabric state Gray | Scoured | Finished |
|---|---|---|---|
| | *Mature-cotton fabrics* | | |
| 114 | 2.0 | 2.5 | 2.4 |
| 116 | 1.6 | 2.0 | 2.0 |
| 118 | 1.2 | 1.6 | 1.5 |
| | *Immature-cotton fabrics* | | |
| 119 | 0.7 | 0.6 | 1.2 |
| 121 | 0.7 | 0.5 | 0.6 |
| 123 | 0.4 | 0.3 | 0.4 |

*Yarn-Fabric Comparisons*

The conclusions that the peak of the distribution curve for the fabric pertains to the interfiber (intra-yarn) spaces and that the peak moves to a smaller pore-size position with increased closeness of weave because of increased compression of the yarn are corroborated by a comparison of the distribution curves of the loosest-woven gray fabrics with those of the constituent mature- and immature-cotton yarns (Figure 5). The data for the yarns were obtained only with the middle-range apparatus (7 to 62 p.s.i.a.), which covered the pertinent range. The peaks for the yarns come at about 5 to 7 $\mu$ effective radius for the immature and mature cotton, respectively; these

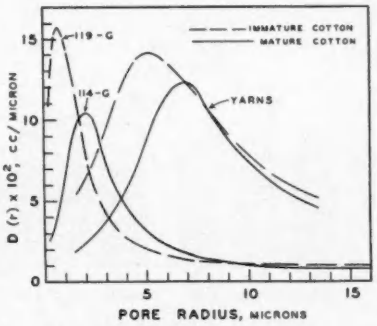


FIG. 5. *Distribution curves for the two loosest-woven fabrics and the constituent yarns.*

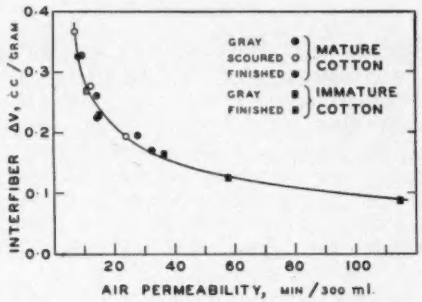


FIG. 6. *Air permeability* vs. *interfiber void volume.*

are much larger than the values for any of the fabrics studied (Table III).

The void volume filled with mercury (the area under the curve) in the pore-radius range of the peak is greater for the immature cotton than for the mature cotton in the yarn, just as it is in the fabric. Preliminary experiments indicate that this relationship holds for the fiber state as well.

*Air Permeability*

Air permeability is obviously determined by the size, length, and number of channels through a fabric. In loosely woven cloths, the interyarn pathways are the dominant factor since they are comparatively large and practically direct. The more closely woven the fabric, the smaller become the dimensions of the interyarn pathways until they approach the magnitude of interfiber spaces. In the very compact fabrics of this series, the interfiber pathways are the dominant factor in determining air permeability. Therefore, an approximate correlation might be expected between air permeability and the void volume contained within the interfiber spaces. Unfortunately, 4 of the immature-cotton fabrics (the 3 scoured and the most closely woven finished fabric) had to be excluded from this comparison, as became obvious when they were examined by transmitted light. The processing treatment had caused the formation of numerous pin-point holes in these particular fabrics.

The radius limits of the pertinent range can be estimated roughly from a survey of the pressuring curves (as represented in Figure 2) of the 14 fabrics considered. The upper pore-size limit was selected toward the end of the first mound, where the increase in slope indicates that the completion of the filling of the surface depressions has been overshadowed by the entry of mercury into the interfiber spaces. For the mature-cotton cloths this point of inflection is about 10 $\mu$ and for the immature about 5 $\mu$ radius. The lower limit of pore size cannot be deduced from the pressuring curves since it is impossible to differentiate between the filling of the lumen spaces and of the smaller interfiber spaces. The value of 1.5 $\mu$ was chosen for two reasons: (*a*) This is the order of magnitude of the effective radius of lumens of mature fibers as calculated from approximate lumen dimensions; (*b*) Microscopically it has been shown that mercury has entered the lumens of a few of the immature fibers by 65 p.s.i.a. (1.6 $\mu$). Pores with radii of less than 1.5 $\mu$ may reasonably be considered insignificant in their contribution to air permeability.

A smooth curve is obtained (Figure 6) when the void volumes within these selected pore-radius limits are plotted against the air permeability values as determined by the densometer. The plotted data of the 4 excluded samples would fall below the curve, showing a greater permeability than the void volume would warrant. In these fabrics, the air can flow more freely through the short, direct pathways instead of following the more circuitous route through the interfiber channels. Even if the void volume of the selected range should include the volume contained within these transverse pathways, the directness of the channels introduces a new factor which gives a greater air permeability.

*Effect of Processing*

*Total Void Volume.*—Processing increases the over-all density of these fabrics, resulting in a loss of total volume within the fabric boundaries. The effect of scouring is greater for the immature-cotton fabrics than for the mature, as is shown by a comparison of the figures in column 2 of Table II; the average loss in available void per gram of fabric is 7% in the mature-cotton samples, and 11% in the immature. With the exception of one case, finishing effected an additional loss of void volume per gram of fabric, the average additional loss being 5½% and 2% in the mature- and immature-cotton fabrics, respectively. Thus, the direct comparison of the finished with the gray shows approximately the same percentage loss in both the mature- and immature-cotton fabrics.

*Void Volume Distribution.*—The loss in void vol-

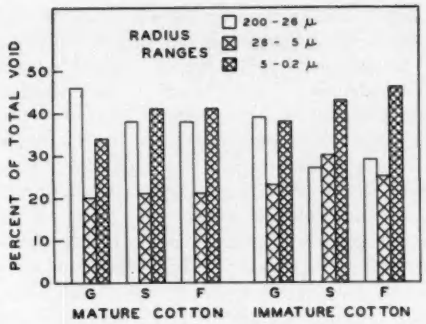


FIG. 7. *Distribution percentwise of the total experimental void volume. Averages for each of the gray, scoured, and finished fabrics, mature and immature.*

ume on scouring is not apportioned throughout the whole experimental range, but is concentrated in the largest-pore-size region. In order to show these relationships graphically, the average volumes of three ranges were calculated as percentages of the total void filled within the whole experimental range, and were plotted as a bar graph (Figure 7). The 200–26 $\mu$ radius region pertains to the filling of the surface depressions, and the 5–0.2 $\mu$ radius region to the interfiber and lumen spaces. The 26–5 $\mu$ radius region may be considered to be the transition from the filling of the surface depressions to that of the interfiber spaces.

From Figure 7 it is apparent that scouring produced a decrease in the proportion of the pores of largest sizes and an increase in the smallest. The transition region was practically unaffected in the mature-cotton fabrics, but showed a considerable percentage increase in the immature. Subsequent finishing produced no change in the percentages in the 3 regions of the mature-cotton fabrics—that is, the loss in volume was spread throughout the whole experimental range. In the immature-cotton fabrics, the finishing treatment resulted in a slight increase over the scoured in the percentage of the void volume within the largest- and smallest-sized pores at the expense of the volume percentage in the transition region.

While these conclusions apply only to this specific fabric series, they indicate that data of this nature can be used effectively to study and compare changes in the amount and distribution of the void volume caused by controlled processing procedures.

## Summary

The mercury-intrusion method for the determination of pore-size distribution was applied to 18 closely woven cotton fabrics, chosen to show the effect of maturity count, pickage, and processing (scouring and Zelan finishing). The addition of a low-pressure apparatus resulted in data which included a considerable portion of the volume of the surface depressions of the fabrics, thus permitting a survey of practically the whole (96%) of the available void enclosed by the sample instead of only 60%.

The pressuring curves of the mature-cotton fabrics disclosed a rather distinct separation between the filling of the surface depressions and of the interfiber regions; in the immature, the curves indicated a greater overlapping and blending of all regions.

When woven to a given weight and thread count the mature cotton, as compared to the immature cotton, gave fabrics having a much larger proportion of their total void volume in the surface depressions, and a much smaller proportion in the interfiber pore spaces. The peak of the distribution curve in the interfiber region was at a larger pore size for all the mature-cotton fabrics (1.9 $\mu$ average) than for the immature (0.5 $\mu$ average). The over-all average pore-size radius for the immature fabrics is definitely smaller than that of the mature. A shift of the distribution-curve peak to smaller pores was also observed as the pickage was increased; this trend was further emphasized by a comparison of the fabric data with that obtained for the corresponding yarns.

Scouring resulted in a loss of total void volume included within the sample. The proportion of void volume within the interfiber pore sizes was increased at the expense of the volume within the surface depressions. Subsequent finishing with a water-repellent treatment effected an additional loss of total void volume; however, it did not appreciably affect the pore-space distribution.

A correlation was shown between air permeability and the void volume of the interfiber region, indicating that the interfiber pathways were the dominant factor in determining air permeability in these closely woven fabrics.

## Acknowledgment

The authors are grateful to other divisions of this Laboratory for their cooperation in this work, to individual members for their assistance, and especially

to Edward G. Burleigh and Rene Durr for their help in the collection of the data. The various fabrics were made by the Cotton Mechanical Processing Division as part of the project on swelling-type, water-resistant fabrics, which project centered in the Cotton Chemical Processing Division. The Textile Testing Section supplied the data on the fabric construction and properties in Table I, the maturity counts, and also the air-permeability data used for Figure 6.

### Literature Cited

1. Burleigh, E. G., Jr., Wakeham, H., Honold, E., and Skau, E. L., TEXTILE RESEARCH JOURNAL **19**, 547–55 (1949).
2. Ritter, H. L., and Drake, L. C., *Ind. Eng. Chem., Anal. Ed.* **17**, 782–6 (1945).
3. Wakeham, H., and Spicer, N., TEXTILE RESEARCH JOURNAL **19**, 703–10 (1949).
4. Washburn, E. W., *Proc. Natl. Acad. Sci. U. S.* **7**, 115–16 (1921).

(*Manuscript received January 18, 1951.*)

# The Sorption of Synthetic Surface-Active Compounds by Carbon Black

**G. R. F. Rose, A. S. Weatherburn, and C. H. Bayley**

*Division of Applied Chemistry, National Research Laboratories, Ottawa, Canada*

### Abstract

The sorption on carbon black of a number of types of anionic, cationic, and nonionic surface-active compounds from aqueous solutions has been measured. It is shown that the sorption of these compounds does not conform to the Freundlich adsorption isotherm over the whole of the concentration range studied (0.01%–0.2% by weight). In the majority of cases an abrupt change in slope of the curve occurred at concentrations which appear to correspond, at least approximately, to the critical micelle concentrations of the various compounds. At concentrations above this critical point the plot of log $X$ *vs.* log $C$ appeared to be linear, but below the critical point considerable deviation from lineality was observed in some cases. The sorption of sodium alkyl sulfates increased with increasing chain length of the alkyl group at constant temperature, and decreased with increasing temperature at constant chain length. A series of compounds differing widely in chemical constitution, and including both anionic and cationic agents, were shown to be remarkably similar with respect to the general level of adsorption. Two typical nonionic compounds were found to be sorbed somewhat more strongly, particularly at higher concentrations, than any of the other compounds investigated. The addition of sodium sulfate to solutions of anionic compounds resulted in an increase in the sorption of the latter in every case.

THE SORPTION of surface-active compounds by the soil and by fibers is believed to be an important factor in the complex mechanism of textile detergency [1, 8, 13, 14]. It is therefore of interest to obtain data relating to the sorption of a wide variety of detergent compounds, and in this connection measurements have been made of the sorption of various pure soaps from aqueous solutions by carbon black [9, 11] and by textile fibers [12]. The present paper presents similar data for the sorption by carbon black

of a series of purified sodium alkyl sulfates and also a number of compounds extracted from commercially available surface-active agents of various types.

## Materials

Sodium alkyl sulfates having alkyl chains with from 12 to 18 carbon atoms were prepared from Eastman lauryl, myristyl, cetyl, and stearyl alcohols by the method of Lottermoser and Stoll [6]. The crude products were recrystallized repeatedly from absolute alcohol and were finally dried to constant weight *in vacuo* at 56°C. The melting points (uncorrected) and molecular weights * of the purified compounds are given in Table I.

TABLE I. PROPERTIES OF SODIUM ALKYL SULFATES USED

| Compound | Melting point (°C) | Molecular weight Found | Molecular weight Theoretical |
|---|---|---|---|
| Sodium lauryl sulfate | 179 | 289 | 288 |
| Sodium myristyl sulfate | 182 | 318 | 316 |
| Sodium cetyl sulfate | 184 | 349 | 344 |
| Sodium stearyl sulfate | 170 | 368 | 372 |

Four additional anionic compounds (A-1, A-2, A-3, and A-4) were prepared by extracting the active ingredient from various commercial preparations as follows: the commercial product was refluxed for 1 hr. with absolute alcohol, and the alcohol-insoluble matter (largely sodium sulfate) was filtered off. The filtrate was allowed to cool, and the crystals obtained were recrystallized once from fresh alcohol and dried to constant weight *in vacuo* at 56°C. Two other anionic compounds (A-5 and A-6), which would not crystallize from alcohol, were used as received after drying to constant weight. These compounds were stated by the manufacturer to contain 100% active ingredient. Three cationic agents (C-1, C-2, and C-3) and two nonionic compounds (N-1 and N-2) were also used as received. These compounds are listed in Table II.

The carbon black used throughout these experiments was uncompressed Standard Micronex,† a channel black having a mean particle diameter of about 28 mμ.

Carbon dioxide-free distilled water was used in the preparation of all solutions.

## Methods

### *Determination of Sorption*

A 0.600-g. portion of carbon black was weighed into a previously warmed 200-ml. vacuum bottle, and was agitated for 10 min.‡ with 150 ml. of detergent solution having the desired temperature and initial concentration, using a mechanical shaking device. After shaking, the suspension was weighed, and filtered under suction through a Whatman No. 42 filter paper supported in a covered, electrically heated Büchner funnel. The filter cake and filtrate were each weighed, and any loss in weight (due to evaporation of water during filtration) was made up by the addition of distilled water to the filtrate.

*Anionic Compounds.*—For the anionic compounds, the concentration of the initial (reference) solution and the filtrate (equilibrium solution) were determined by the method of Epton [4], employing the modification suggested by Weatherburn [10]. The sorption of the surface-active compound is given by the formula $X = 0.25\ (C_o - C)$, where $X$ is the quantity sorbed in millimoles per gram of carbon, and $C_o$ and $C$ are the concentrations of the reference and equilibrium solutions, respectively, in millimoles per liter ($M \times 10^{-3}$). The molecular weights of the sodium alkyl sulfates (Table I) were calculated from the known concentrations of the solutions in grams per liter and the corresponding values of $C_o$.

*Cationic Compounds.*—The concentrations of the cationic solutions were determined by adding a measured excess of 0.1% sodium lauryl sulfate solution to the aliquot of cationic solution, and back-titrating the residual anionic compound by the above method.

*Nonionic Compounds.*—The concentrations of solutions of nonionic compounds were determined by the method of Oliver and Preston [7]. Since this is a gravimetric method, and since the molecular weights of the nonionic compounds are not known, it was necessary to express the results in terms of weights of the compounds as received. Both nonionic compounds used were stated by the manufacturer to contain 100% active ingredient.

### *Determination of Critical Micelle Concentration*

The critical micelle concentrations of the various compounds were first determined by the method of Corrin and Harkins [3]. However, since it was de-

* The molecular weights were determined by the method described later in this paper.

† Obtained from Binney & Smith Co., New York.

‡ Preliminary experiments indicated that equilibrium was established in less than 10 min., shaking times up to 1 hr. producing no increase in adsorption.

TABLE II. COMMERCIAL SURFACE-ACTIVE COMPOUNDS USED

| Reference No. | Formula or type of principal ingredient | Preliminary treatment |
|---|---|---|
| Anionic compounds | | |
| A-1 | $R—OSO_3Na$ (R=alkyl) | Extracted, recrystallized, dried |
| A-2 | $C_{11}H_{23}COOCH_2CH(OH)CH_2OSO_3Na$ | Extracted, recrystallized, dried |
| A-3 | $C_{17}H_{33}CON(CH_3)\ C_2H_4SO_3Na$ | Extracted, recrystallized, dried |
| A-4 | $C_{17}H_{33}COOCH_2CH_2SO_3Na$ | Extracted, recrystallized, dried |
| A-5 | Sodium alkyl aryl sulfonate | Dried |
| A-6 | $H_2C—COOC_8H_{17}$ \| $HC—COOC_8H_{17}$ \| $SO_3Na$ | Dried |
| Cationic compounds | | |
| C-1 | $C_{16}H_{33}(C_5H_5N)Br$ | Used as received |
| C-2 | $R—(CH_3)_2(C_6H_5CH_2)NCl$ | Used as received |
| C-3 | $C_{16}H_{33}(CH_3)_3NBr$ | Used as received |
| Nonionic compounds | | |
| N-1 | Alkyl aryl polyethylene glycol ether | Used as received |
| N-2 | Polyoxyethylene ester of mixed fatty and rosin acids | Used as received |

sired to apply these data to equilibrium solutions containing sodium sulfate in addition to the surface-active compound, and since the extent of sorption of the sodium sulfate was not known, this method was considered unsatisfactory. Accordingly, the method was modified as follows: To 10 ml. of each of the various equilibrium solutions was added 0.05 ml. (1 drop) of a $2 \times 10^{-3}$ $M$ solution of pinacyanol chloride. The solutions were maintained at 50°C for about 10 min., after which the color of each solution was observed. A blue color indicated that the concentration of the solution was above the critical micelle concentration, and a red color indicated that it was below. With some solutions a purple color was obtained, and in these cases the concentration of the solution was taken as the approximate critical micelle concentration. In other cases there was a sharp change from red to blue with increasing concentration, and the critical micelle concentration was taken as falling between the highest concentration which gave a red color and the lowest concentration which gave a blue color. In this way it was possible to obtain an approximate value for the critical micelle concentration under the identical conditions employed during the sorption experiments.

The sorption of each of the compounds listed in Tables I and II was determined over an initial concentration range of 0.01% to 0.2%. All of the measurements, with three exceptions, were made at 50°C. The sorption of sodium stearyl sulfate was determined at 70°C, and that of the two nonionic compounds at 30°C, since clear solutions of these compounds were not obtained at 50°C. (The solubility of nonionic compounds in general decreases with increasing temperature [2].) The results are given in Figures 1–4 (solid curves in Figures 1 and 2).

A similar series of experiments, on the anionic compounds only, was carried out in which the initial solutions contained anhydrous sodium sulfate in an amount equal to 1.5 times the weight of surface-active compound present, the concentrations of the latter and the temperatures being the same as in the first series. The ratio of sodium sulfate to surface-active compound was chosen to correspond to a detergent formulation containing, on a dry basis, 40% of surface-active compound and 60% of inorganic salt, a proportion that is commonly encountered in commercial detergent preparations. The results of this series are given by the dotted curves in Figures 1 and 2.

In order to determine the effect of variations in temperature on the sorption, a limited series of experiments was carried out at 30° and 70°C with three of the compounds listed in Table I. These results are given in Figure 5.

## Discussion

All of the compounds studied show the same general type of sorption curve. According to the Freundlich adsorption isotherm ($X = kC^n$, where $X$ is the quantity adsorbed, $C$ is the equilibrium concentration,

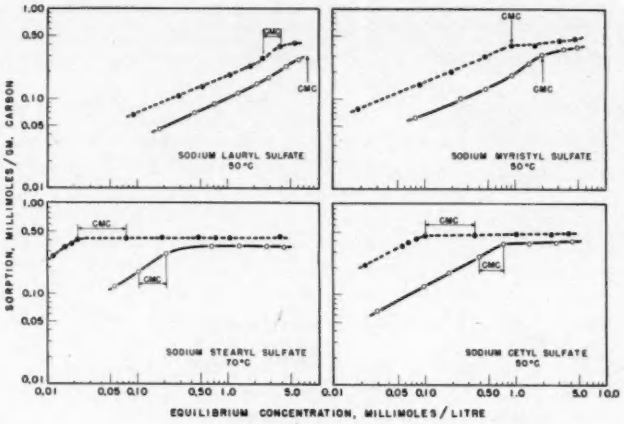


FIG. 1. *Sorption of sodium alkyl sulfates by carbon black. Sodium alkyl sulfate,* ———. *Sodium alkyl sulfate plus sodium sulfate,* – – –.

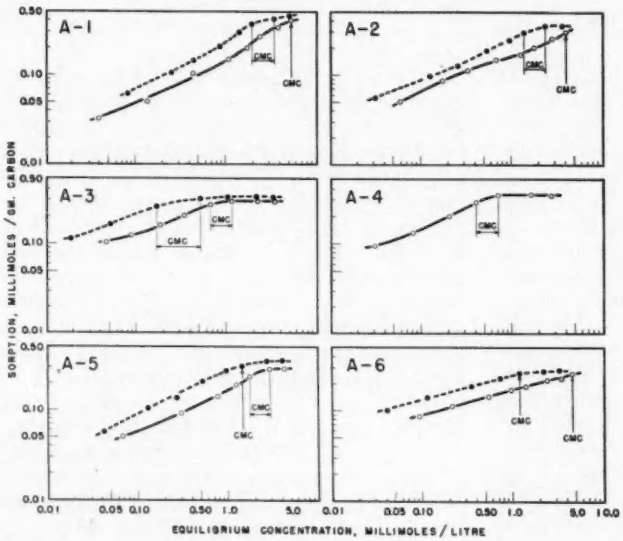


FIG. 2. *Sorption by carbon black of anionic surface-active compounds extracted from commercial preparations. Anionic compound,* ———. *Anionic compound plus sodium sulfate,* – – –. *Temperature, 50°C.*

and $k$ and $n$ are constants) a plot of log $X$ *vs.* log $C$ should give a straight line. It is apparent from the data of Figures 1–4 that none of the compounds studied, with the possible exception of compound A-6, are sorbed in conformity with the equation over the entire concentration range covered. Most of the curves exhibit a more or less abrupt change in slope at concentrations which appear to correspond, at least approximately, to the critical micelle concentrations of the compounds. Of the compounds which do not show this change in slope (sodium lauryl sulfate, compounds A-2, A-6, and possibly A-1), all of the sodium lauryl sulfate equilibrium solutions were found to be below the critical micelle concentration for this compound, while only the highest concentration of each of the other compounds was equal to the critical micelle concentration. It is probable that these compounds would also have given curves of similar form if they had been taken to higher concentrations, particularly since in the presence of added sodium sul-

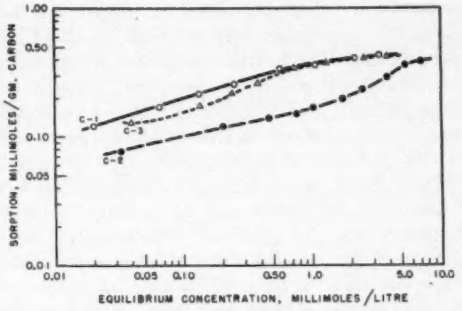


FIG. 3. *Sorption of cationic surface-active compounds by carbon black. Temperature, 50°C.*

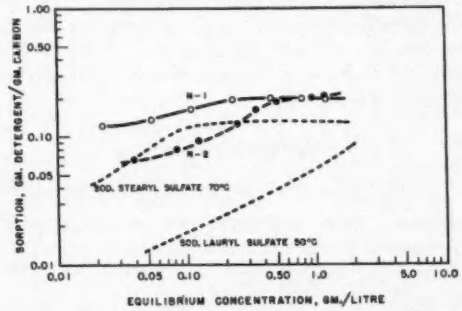


FIG. 4. *Sorption of nonionic surface-active compounds by carbon black. Temperature, 30°C.*

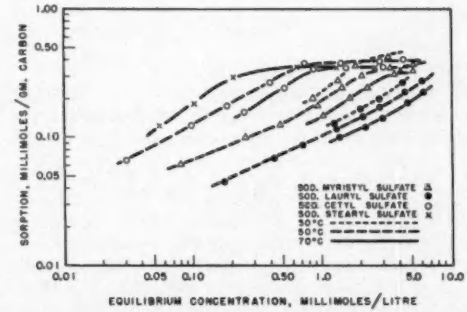


FIG. 5. *Effect of temperature on the sorption of sodium alkyl sulfates by carbon black.*

fate all of the compounds exhibited the characteristic break in the sorption curves at concentrations corresponding to the critical micelle concentrations of the respective compounds under these conditions.

In order to eliminate the possibility that the change in slope of the curves might be related to some property of the particular carbon employed rather than to the concentration of surface-active compound, sorption curves were obtained for three of the compounds using two carbons other than the Micronex. These carbons were Statex B,* having a mean particle diameter of 34 mμ, and Neo Spectra II,* having a mean diameter of 12.7 mμ. While the magnitude of the sorption of any one surface-active compound varied with the different carbons, the finer carbon giving higher sorption, the breaks in the curves occurred at virtually the same equilibrium concentration, and this concentration was again found to correspond to the critical micelle concentration as measured by the above method. It is felt that this is conclusive evidence that a change occurs in the sorption characteristics of these surface-active compounds at or near the critical micelle concentration.

The portions of the sorption curves above the critical micelle concentration appear to be linear, in conformity with the Freundlich equation, but below this concentartion the curves for some of the compounds exhibit considerable deviation from lineality.

It is interesting to note that linear sorption curves were obtained for sodium laurate and sodium stearate over an initial concentration range of 0.01%–0.2% [11]. In the case of sodium laurate the concentrations of the equilibrium solutions varied from 0.25 to 8.0 $M \times 10^{-3}$, all of which were below the critical micelle concentration for this soap. In the case of sodium stearate the equilibrium concentrations varied from 0.06 to 3.2 $M \times 10^{-3}$, which includes the critical micelle concentration for this soap. However, the sorption of soap is complicated by selective sorption of the fatty-acid constituent, resulting in accentuated hydrolysis. It is impossible to predict the effect of these factors on the critical micelle concentration, and, unfortunately, no measurements of the latter were made on the equilibrium solutions at the time.

The data of Figures 1 and 5 indicate that at constant temperature there is a regular increase in sorption of the sodium alkyl sulfates with increasing chain length of the alkyl group at concentrations below the critical micelle concentration. At higher concentrations the curves for the $C_{14}$, $C_{16}$, and $C_{18}$ compounds appear to level off at about the same degree of sorption. It is possible that the curve for the $C_{12}$ com-

* Obtained from Binney & Smith Co., New York.

pound might also have reached this level if it had been carried to sufficiently high concentrations.

Figure 5 also shows the effect of temperature on the sorption of the sodium alkyl sulfates. It may be seen that the curves for each compound are essentially parallel at temperatures varying from 30°C to 70°C, and that the degree of sorption decreases with increasing temperature over this range. The concentrations at which the change in slope of the curves occurs are increased slightly with increasing temperature, this being in agreement with the effect of temperature on the critical micelle concentration [5].

The anionic and cationic compounds listed in Table II, although differing widely in chemical constitution, are remarkably similar with respect to sorption characteristics (Figures 2 and 3). The two nonionic compounds also gave curves of similar form (Figure 4). As has been pointed out previously, it was not possible to express the sorption of these compounds in the usual molar units. However, for the sake of comparison, the data for sodium lauryl sulfate at 50°C and sodium stearyl sulfate at 70°C have been recalculated in terms of weight units and are included in Figure 4. It may be seen that the nonionic compounds show higher sorption than the anionics at concentrations above the change in slope of the curves. Attempts were made to obtain critical micelle concentration data for the cationic and nonionic compounds by the method described above, but since no marked color changes were obtained over the whole range of concentrations, it was concluded that the method is not applicable to these compounds. It can only be concluded by inference, therefore, that the breaks in these curves correspond to the critical micelle concentrations.

In every case the addition of sodium sulfate to solutions of the anionic compounds caused an increase in the sorption of the latter, this effect being most pronounced at concentrations below the critical micelle concentration. The presence of sodium sulfate also resulted in the critical micelle concentrations, and hence the change in slope of the sorption curves, occurring at lower concentrations, this being in accord with the known effect of electrolytes on the critical micelle concentration.

The filtering characteristics of the suspensions of carbon in the various solutions are of some interest. Suspensions prepared from solutions of all of the compounds at concentrations below the critical micelle concentration filtered rapidly and gave filtrates which were perfectly clear and free of carbon. At higher concentrations, however, the filtration was much slower, and many of the compounds gave dark-colored filtrates during the early stages of filtration. It was found that once a filter cake of carbon had been formed on the filter paper, the filtrate came through clear, and that when the first small quantity of filtrate was refiltered through this cake, all of the carbon was eliminated from the filtrate. It is concluded that the surface characteristics of the filter paper and/or the carbon particles are modified by the sorption of micelles of the surface-active compounds, and under these conditions the finer carbon particles are enabled to pass through the filter paper. Single, nonaggregated molecules of the compounds apparently do not have this effect.

## Literature Cited


1. Adam, N. K., *J. Soc. Dyers and Colourists* **53**, 121–8 (1937).
2. Barker, G. E., *Soap and Sanit. Chemicals* **24**, No. 6, 46–8, 65 (1948).
3. Corrin, M. L., and Harkins, W. D., *J. Am. Chem. Soc.* **69**, 679–83 (1947).
4. Epton, S. R., *Trans. Faraday Soc.* **44**, 226–30 (1948).
5. Klevens, H. B., *J. Colloid Sci.* **2**, 301–3 (1947).
6. Lottermoser, A., and Stoll, F., *Kolloid-Z.* **63**, 49–61 (1933).
7. Oliver, J., and Preston, C., *Nature* **164**, 242–3 (1949).
8. Preston, C., *Dyer* **101**, 144 (1949).
9. Reade, M. A., Weatherburn, A. S., and Bayley, C. H., *Can. J. Research* **F27**, 426–8 (1949).
10. Weatherburn, A. S., *J. Am. Oil Chemists' Soc.* (in press).
11. Weatherburn, A. S., Rose, G. R. F., and Bayley, C. H., *Can. J. Research* **F27**, 179–93 (1949).
12. Weatherburn, A. S., Rose, G. R. F., and Bayley, C. H., *Can. J. Research* **F28**, 51–61 (1950).
13. Weatherburn, A. S., Rose, G. R. F., and Bayley, C. H., *Can. J. Research* **F28**, 213–25 (1950).
14. Weatherburn, A. S., Rose, G. R. F., and Bayley, C. H., *Can. J. Research* **F28**, 363–75 (1950).


*(Manuscript received December 26, 1950.)*

# Letters to the Editor

Short communications in the form of Letters to the Editor are intended to provide prompt publication of significant new research results and to permit an exchange of views on papers previously published in the JOURNAL. These communications are not submitted to formal review as are research papers, and the editors do not assume any share of the author's responsibility for the information given or the opinions expressed. When work previously published in the JOURNAL is the subject of critical comment, the authors of the original paper are given an opportunity to submit a reply, which will be published concurrently when possible.

## A Cold-Solvent Extractor

SOUTHERN REGIONAL RESEARCH LABORATORY *
New Orleans, Louisiana
March 1, 1951

To the Editor
TEXTILE RESEARCH JOURNAL

*Dear Sir:*

I believe that readers of TEXTILE REASEARCH JOURNAL will be interested in a compact, leakproof modification of the Soxhlet extractor developed at this Laboratory. We have found this apparatus useful for the extraction of textiles in amounts larger than commonly used in samples for analysis.

Innumerable modifications of the Soxhlet extractor have been published. Yet for the laboratory-scale extraction of a material with a solvent at substantially room temperature or somewhat below, there seems to be no adequate, compact apparatus. Most makeshift assemblies from stock glass-jointed apparatus leak or fail to perform without frequent attention, and are of great complexity—for example, that described in [1].

A modification of a standard Soxhlet extraction apparatus has been devised which is entirely satisfactory for the purpose mentioned. Three views of the modified apparatus are given in Figure 1. The change consists of an added jacketed U-connector between the distillate-collection funnel and the extraction chamber. The modified apparatus is stable, requires no additional clamping, and occupies the same table space as the original extractor. Its use in the conventional manner (with the solvent somewhat warm or even heated by lamps) is in no way hindered.

The original apparatus is the assembly identified as #3885–EGYUA in catalog LP–28 of the Corning Glass Works, Corning, New York.† The modification can be made in less than an hour. The cooling attachment is blown from lengths of tubing which may be determined from the scale of the drawing. None of the dimensions are critical because the U-connector remains full of liquid at all times. If desired, the cooling condenser may be used with ice-water mixtures instead of tap-water; in this way temperatures somewhat below room temperature are obtainable. The extraction chamber is preferably insulated for this use. In no case should the cover plate fit air-tight; this is essential to the proper operation of the siphon.

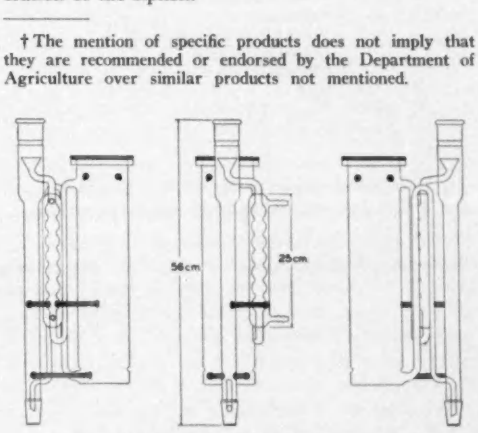

FIG. 1. *Modified Soxhlet extraction apparatus.*

* One of the laboratories of the Bureau of Agricultural and Industrial Chemistry, Agricultural Research Administration, U. S. Department of Agriculture.

† The mention of specific products does not imply that they are recommended or endorsed by the Department of Agriculture over similar products not mentioned.

The writer wishes to acknowledge the contribution of Mr. Louis Dufrene and Miss Leah Katz who put their skill into the construction and depiction, respectively, of the apparatus described.

**Literature Cited**

1. Mysels, K. J., Pomeroy, H. H., and Smith, G. H., *Anal. Chem.* **20**, 878–9 (1948).

EDMUND M. BURAS, JR.

# Principles of Textile Research

## Summer Session at M.I.T., July 2–27, 1951

THE M.I.T. SUMMER COURSE in Principles of Textile Research is intended to review recent developments in textile technology and to familiarize the student with methods and apparatus which will be of great importance in future laboratory work. The course will include a survey of the precise and sensitive equipment—much of it developed in the M.I.T. Textile Division—now available, and will review the more powerful and efficient means for the analysis and interpretation of research findings.

The summer program in Principles of Textile Research will combine lectures, demonstrations, and seminar sessions covering the following subjects:

Planning of experiments
Recording and presentation of data
Analysis of variance
Significance testing
Polarized light and its applications
Tensile testing
Heat transmission
Abrasion
Sound velocity techniques
Applications of servos
Photomicrography
Sampling techniques
Precision of measurements
Correlation analysis
Improved sectioning
Air permeability
Resilience
Flexibility
Creep and relaxation
Impact
Applications of electronics
Stereographs

Emphasis will be placed upon the functioning of a textile research laboratory in connection with quality control programs, new product development, instrumentation, processing, and in the field of education at college level.

The course will be under the direction of Professor Edward R. Schwarz, in charge of the Textile Division in the M.I.T. Department of Mechanical Engineering.

Requests for further information and letters of application should be sent to Professor Walter H. Gale, Director of Summer Session, Room 3-107, Massachusetts Institute of Technology, Cambridge 39, Mass.

# INDUSTRIAL SECTION

## The Measurement of Stiffness in Textile Fabrics*

**N. J. Abbott†**

*Ontario Research Foundation, Toronto, Canada*

**Abstract**

In Part I the subjective evaluation of stiffness is used as a standard with which to compare the results obtained from five laboratory methods of measuring stiffness. Measurements were made on a range of nineteen fabrics of varying fiber content, weave, and weight. The results indicated significant correlation in four of the five methods. The test was repeated with a new range of of eleven fabrics, with approximately the same results. The Peirce cantilever test was selected as being the most convenient to carry out in the laboratory, and at the same time giving good correlation with the subjective estimate. Part II describes a more detailed examination of certain aspects of the cantilever test, and a specific technique is recommended which combines simplicity of equipment with ease of measurement.

## Part I: A Comparison of Five Methods of Laboratory Evaluation

### Introduction

Stiffness is one of the characteristics of a fabric which goes into making up that important quality known as "hand." Other physical properties which have been suggested as contributing to the hand of a fabric are compressibility, extensibility, resilience, density, surface contour, surface friction, and thermal character [1]. All of these properties may not be equally important, and others—thickness, for example—may contribute substantially to the sensation one gets when feeling a fabric. An attempt to evaluate the hand of a fabric in the laboratory is made difficult by the fact that no specific definition of hand exists, nor, indeed, does a specific definition exist of many of its components, such as stiffness, compressibility, resilience, and so on. This, then, is the problem confronting any attempt to measure any of these properties in such a way that the results will mean something to the man who is accustomed to handling fabric, and who uses these terms presumably to signify some specific subjective reaction upon feeling the fabric.

When a person who is accustomed to handling textiles feels a fabric, he is able to form a definite opinion as to whether he considers it stiff or soft. It might be possible, then, to use this subjective evaluation as a reference standard of stiffness with which to compare the evaluation resulting from a laboratory test. This could only be done, however, provided the subjective estimate is a sensitive one—that is, it can distinguish between two fabrics of nearly the same stiffness—and provided a number of such evaluations, made by different people, agree. Clearly, this is a case simply of ranking fabrics in a given order, without regard to the absolute value of the difference between them. Therefore, if a group of persons can rank a range of fabrics in essentially the same order, and any given laboratory test ranks them in the same order, this may be considered to be evidence of the fact that a definite relationship exists between what the test measures and what is commonly known as

* Presented in part by the author before sub-committee B-1 of committee D-13 on Textiles, American Society for Testing Materials, New York, Mar. 15, 1951.

† Research Fellow, Textile Department.

stiffness. Moreover, if the test gives a quantitative measure, a scale of stiffness has been obtained, so that absolute differences may be obtained.

A comparison of different methods of measuring stiffness has been made previously by Winn and Schwarz [12], but these were only compared with one another, not with a subjective evaluation. This method of approach has, however, been adopted by Dreby [5, 6] in his work on the measurement of hand. In this case the range of fabrics selected was limited to 80 × 80 cotton percales, and the results indicate that even with this rather narrow restriction on fabric construction, there were two fabrics in the group which could not be ranked in the same order by laboratory and subjective evaluation. When these two were discarded, good correlation resulted. This is not a very satisfactory situation, for it would indicate that it is not possible to know in advance whether the laboratory method is reliable, even though the range of constructions under examination is very limited.

In the present investigation the only restriction placed upon the fabrics chosen was that they could be ranked in a fairly well-defined order by subjective evaluation. A range of fiber type and fabric construction was chosen, so as to present what would appear to be the worst conditions for comparison on a basis of laboratory evaluation.

### Materials Used

A range of nineteen fabrics was selected, of various constructions, weights, and fiber contents. They were identified by code letters, as shown in Table I.

TABLE I

| Code letter | Fabric | Weight (oz./sq. yd.) |
|---|---|---|
| A | Acetate taffeta | 3.1 |
| B | Viscose rayon taffeta | 3.2 |
| C | Acetate-viscose satin | 3.1 |
| D | Viscose rayon crepe | 3.0 |
| E | Spun viscose rayon plain weave | 3.2 |
| F | Cotton broadcloth | 4.3 |
| G | Cotton broadcloth | 2.0 |
| H | Cotton broadcloth | 5.1 |
| I | Nylon plain weave | 1.7 |
| J | Nylon twill | 2.0 |
| K | Nylon broken twill | 2.0 |
| L | Nylon matte | 1.8 |
| M | Nylon plain weave | 2.2 |
| N | Nylon satin | 2.3 |
| O | Nylon matte | 3.2 |
| P | Nylon matte | 2.5 |
| Q | Nylon-cotton broken twill | 1.9 |
| R | Silk fabric | 1.6 |
| S | Wool flannel | 10.0 |

### Subjective Evaluation

Swatches of these fabrics were cut about 1 ft. square, and they were ranked in order of stiffness by seventeen persons, not all of whom were equally used to handling fabrics. Accordingly, a weight, varying from one to four, depending upon the individual's familiarity with fabrics, was assigned to each ranking, and a weighted average rank obtained for each fabric. In order to make sure that each estimate was a reasonable one, duplicate swatches of two of the fabrics were included. Invariably, these pairs were placed very close together, if not adjacent. The results of the subjective evaluations are given in Table II. In order to avoid confusion, mention of the duplicate swatches is omitted from the table. Each column in the table under the heading "rank" indicates one individual's estimate of the stiffness, in the order from soft (1) to stiff (19).

It will be seen that except in a few instances remarkably good agreement was obtained, even though in many cases there was very little apparent difference in stiffness between a fabric and its neighbor. Thus, the weighted average can be considered to be a reasonably reliable estimate of the rank of the fabric, and a standard rank number can then be assigned to each fabric. This is indicated at the bottom of Table II.

### Test Methods

Measurements on each of these fabrics were carried out at 65% R.H., 70°F, using five methods which had been proposed for measuring stiffness. These were as follows.

*Cantilever Test*

This test was proposed by Peirce [7], and consists simply of allowing a 1-in.-wide strip of fabric to project as a cantilever from a horizontal platform and measuring the angle between the horizontal and the chord from the edge of the platform to the tip of the fabric. Peirce then defines two quantities which can be calculated from this angle, $\theta$: the bending length, $c = l \cdot f(\theta)$, where $l$ = length of fabric overhanging the platform, and $f(\theta) = \left(\frac{\cos 0.5\,\theta}{8 \tan \theta}\right)^{\frac{1}{3}}$; and the flexural rigidity, $G = wc^3$, where $w$ = weight per unit area of fabric.

TABLE II. SUBJECTIVE EVALUATION OF STIFFNESS

| Fabric | Rank | | | | | | | | | | | | | | | | | Weighted average |
|---|---|---|---|---|---|---|---|---|---|---|---|---|---|---|---|---|---|---|
| A | 17 | 19 | 17 | 18 | 19 | 18 | 15 | 17 | 15 | 19 | 19 | 15 | 16 | 16 | 17 | 19 | 17 | 17.5 |
| B | 16 | 16 | 15 | 15 | 13 | 15 | 12 | 14 | 19 | 16 | 16 | 12 | 12 | 17 | 14 | 8 | 15 | 14.4 |
| C | 13 | 10 | 9 | 10 | 14 | 11 | 16 | 7 | 13 | 16 | 12 | 16 | 13 | 14 | 15 | 11 | 12 | 12.3 |
| D | 1 | 1 | 1 | 1 | 2 | 3 | 3 | 1 | 2 | 1 | 4 | 4 | 1 | 1 | 2 | 3 | 1 | 1.73 |
| E | 12 | 3 | 3 | 3 | 4 | 5 | 8 | 3 | 8 | 3 | 3 | 13 | 4 | 4 | 4 | 4 | 3 | 4.3 |
| F | 18 | 15 | 16 | 13 | 16 | 18 | 18 | 17 | 16 | 10 | 10 | 17 | 19 | 18 | 18 | 17 | 18 | 16.0 |
| G | 14 | 5 | 5 | 7 | 5 | 4 | 7 | 5 | 3 | 4 | 2 | 6 | 5 | 5 | 5 | 5 | 5 | 5.0 |
| H | 19 | 17 | 19 | 19 | 18 | 17 | 18 | 19 | 18 | 14 | 17 | 18 | 18 | 19 | 19 | 18 | 19 | 18.0 |
| I | 5 | 13 | 14 | 17 | 15 | 12 | 10 | 16 | 10 | 13 | 14 | 11 | 15 | 11 | 11 | 9 | 10 | 12.4 |
| J | 6 | 7 | 6 | 8 | 8 | 8 | 4 | 11 | 7 | 7 | 6 | 5 | 7 | 9 | 7 | 7 | 8 | 7.2 |
| K | 2 | 8 | 7 | 9 | 6 | 7 | 9 | 6 | 4 | 8 | 13 | 7 | 10 | 8 | 8 | 12 | 7 | 8.1 |
| L | 3 | 4 | 8 | 6 | 7 | 6 | 6 | 8 | 6 | 6 | 7 | 3 | 6 | 6 | 6 | 6 | 6 | 6.1 |
| M | 9 | 14 | 18 | 16 | 17 | 16 | 14 | 13 | 11 | 15 | 18 | 10 | 17 | 15 | 16 | 15 | 16 | 15.4 |
| N | 8 | 9 | 11 | 11 | 9 | 9 | 5 | 9 | 9 | 11 | 9 | 8 | 8 | 11 | 10 | 13 | 9 | 9.9 |
| O | 10 | 11 | 12 | 14 | 12 | 10 | 13 | 12 | 14 | 9 | 8 | 14 | 11 | 13 | 12 | 10 | 13 | 11.6 |
| P | 11 | 12 | 13 | 12 | 10 | 14 | 11 | 10 | 12 | 12 | 15 | 9 | 14 | 12 | 10 | 14 | 11 | 12.2 |
| Q | 7 | 6 | 4 | 4 | 3 | 1 | 2 | 4 | 5 | 5 | 5 | 2 | 3 | 3 | 3 | 2 | 4 | 3.6 |
| R | 4 | 2 | 2 | 2 | 1 | 2 | 1 | 2 | 1 | 2 | 1 | 1 | 2 | 2 | 1 | 1 | 2 | 1.68 |
| S | 15 | 18 | 10 | 5 | 11 | 13 | 17 | 15 | 16 | 17 | 11 | 19 | 9 | 7 | 13 | 16 | 14 | 12.6 |
| Weights | 1 | 2 | 4 | 3 | 3 | 2 | 1 | 1 | 2 | 3 | 2 | 1 | 3 | 3 | 2 | 4 | 4 | |
| Average rating (soft to stiff) | R | D | Q | E | G | L | J | K | N | O | P | C | I | S | B | M | F | A | H |
| Standard rank No. | 1 | 2 | 3 | 4 | 5 | 6 | 7 | 8 | 9 | 10 | 11 | 12 | 13 | 14 | 15 | 16 | 17 | 18 | 19 |

When $l$ is in cm., $c$ is in cm.; and when $w$ is in mg. per sq. cm., $G$ is in mg. cm. This is a reasonable unit for most fabrics.

In the present investigation the length of overhang was 4 cm. for all fabrics. Subsequent investigations showed that this was not the best basis for comparison, but at the same time the results cannot be so far removed from the truth as to be misleading.

*Heart Loop Test*

This method was also proposed by Peirce [7], and consists of bending the ends of a 1-in.-wide strip of fabric through 540°, bringing the ends together, thus forming a heart-shaped loop, and measuring the length of this loop under the force of gravity. This length, $l$, will be less for stiff fabrics than for soft ones. If the total length of the fabric strip is $L$, then, under no gravitational or other force, the length, $l_o = 0.1337L$.

Peirce shows that the bending length, $c = l_o f(\theta)$, where $\theta = 32.85° \cdot \frac{d}{l_o}$, $d = l - l_o$, and $f(\theta) = \frac{\cos \theta}{\tan \theta}$. The flexural rigidity, $G = wc^3$, where $w$ = weight per unit area of fabric.

A constant length of strip—namely, 20 cm.—was used for all fabrics. This also has been shown to be a rather unsatisfactory standard for comparison [10], but while any one fabric might not be ranked in the correct order, the results considered as a whole cannot be misleading.

*Schiefer Flexometer*

This instrument [8] measures the amount of work required to fold a pair of samples. The samples are mounted between a fixed and a moving plate in such a way as to form a couple opposing the rotation of the moving plate towards the fixed one. The force required to cause this motion is transmitted through one of a series of calibrated spring strips. Thus, the amount of work required to fold the samples to a minimum angle, determined by the thickness of the fabric, can be calculated, and this is taken as a measure of the stiffness of the material.

*Planoflex*

This method was developed by Dreby [5, 6] in connection with some work sponsored by A.S.T.M. Committee D-13. In this instrument a 3-in.-wide strip of fabric is mounted in a frame which permits lateral displacement of one end of the fabric, in the plane of the fabric. This movement distorts the fabric, and is carried on until diagonal wrinkles

TABLE III. RESULTS OF LABORATORY MEASUREMENTS

| Fabric | Cantilever | | Heart loop | | Schiefer Flexometer | Planoflex | Drapeometer |
|---|---|---|---|---|---|---|---|
| | $c$(cm.) | $G$(mg.cm.) | $c$(cm.) | $G$(mg.cm.) | (ergs) | (degrees) | (cm.) |
| A | 2.13 | 102 | 1.70 | 54 | 2.65 | 22.3 | 10.62 |
| B | 2.23 | 121 | 1.89 | 78 | 2.40 | 34.4 | 11.19 |
| C | 1.98 | 81 | 1.70 | 52 | 1.75 | 50.8 | 11.06 |
| D | 1.30 | 22 | 1.27 | 20 | 0.60 | 33.1 | 10.48 |
| E | 1.75 | 57 | 1.50 | 36 | 1.00 | 42.8 | 10.97 |
| F | 1.95 | 107 | 1.74 | 77 | 1.35 | 19.5 | 10.28 |
| G | 1.76 | 37 | 1.50 | 24 | 0.80 | 28.8 | 10.09 |
| H | 1.82 | 103 | 1.86 | 114 | 1.85 | 10.0 | 10.93 |
| I | 1.93 | 42 | 1.44 | 18 | 1.20 | 28.7 | 10.16 |
| J | 1.55 | 25 | 1.58 | 26 | 0.85 | 54.2 | 10.12 |
| K | 1.75 | 36 | 1.66 | 31 | 1.10 | 51.3 | 10.17 |
| L | 1.85 | 39 | 1.56 | 23 | 0.82 | 55.1 | 9.87 |
| M | 1.98 | 57 | 1.54 | 27 | 1.25 | 23.8 | 9.84 |
| N | 1.89 | 53 | 1.55 | 29 | 1.20 | 37.6 | 10.22 |
| O | 1.99 | 86 | 1.50 | 37 | 1.55 | 42.5 | 10.12 |
| P | 2.00 | 68 | 1.64 | 38 | 1.20 | 36.9 | 9.96 |
| Q | 1.75 | 35 | 1.46 | 20 | 0.95 | 58.5 | 10.32 |
| R | 1.76 | 29 | 1.38 | 14 | 1.05 | 50.2 | 10.93 |
| S | 2.08 | 302 | 1.65 | 151 | 2.30 | 35.4 | 11.34 |

appear. The angle through which the frame has been moved at the appearance of the wrinkles is read off a scale on the instrument. This angle is determined on each side of the center, and the sum of the two angles so obtained is taken as a measure of the stiffness of the material.

*M. I. T. Drapeometer*

This instrument [10] was designed to measure drape rather than stiffness, but in so far as the measure is based on simple bending under zero gravitational force, it was felt that it might correlate with other test methods designed specifically to measure stiffness. One end of a 4.7-in-wide strip of fabric 10 in. long is strapped to the edge of a circular disc of circumference 9.4 in., and the fabric is allowed to hang vertically. The curvature of the fabric at any given depth below the support will depend upon the stiffness of the fabric, and perhaps on other things as well. The chord length at a level 18 cm. below the support was taken as the measure required.

## Results

Measurements were made both warpwise and weftwise in each fabric by all five methods of test. The number of samples tested in each case was as follows:

| | |
|---|---|
| Cantilever | 3 samples cut each way, each sample tested both sides |
| Heart loop | 3 samples cut each way, each sample tested both sides |
| Schiefer Flexometer | 2 pairs of samples cut each way |
| Planoflex | 5 samples cut each way |
| Drapeometer | 3 samples cut each way, each sample tested both sides |

For each method a mean of all the figures for warpwise bending was taken as a measure of the stiffness of the warp, and similarly for the weft. The geometric mean of these two figures is taken as representative of the fabric as a whole [7]. This is the figure quoted in Table III, which summarizes the results obtained by laboratory measurements.

In order to compare these results with those obtained from the subjective rating, the fabrics have been ranked in order, from soft to stiff, for each method of measurement. The results are given on page 439, top. The underlined letters indicate fabrics which were rated the same stiffness in a particular test.

It can be seen that most of the tests appear to rank the fabrics approximately in the right order—that is, the high numbers at the right, the low ones at the left. It is difficult to obtain any more precise estimate of the agreement from inspection alone. Since these are rank numbers only, not absolute measures of stiffness, statistical methods of rank correlation may be used. The best measure of correlation for a small number of observations is

| | | | | | | | | | | | | | | | | | | | |
|---|---|---|---|---|---|---|---|---|---|---|---|---|---|---|---|---|---|---|---|
| Subjective rating: | R | D | Q | E | G | L | J | K | N | O | P | C | I | S | B | M | F | A | H |
| Cantilever, $c$: | D | J | *E* | *K* | *Q* | G | R | H | L | N | I | F | *C* | *M* | O | P | S | A | B |
| $G$: | D | R | Q | K | G | *J* | *L* | I | N | *E* | *M* | P | C | O | A | H | F | B | S |
| Heart loop, $c$: | D | R | I | Q | *E* | *G* | *O* | M | N | L | J | P | S | K | *C* | *A* | F | H | B |
| $G$: | R | I | *D* | *Q* | L | G | J | M | N | K | E | O | P | C | A | F | B | H | S |
| Schiefer Flexometer: | D | G | L | J | Q | E | R | K | *I* | *N* | *P* | M | F | O | C | H | S | B | A |
| Planoflex: | Q | N | J | K | C | R | E | O | N | P | S | B | D | G | I | M | A | F | H |
| Drapeometer: | M | L | P | Q | *O* | *J* | I | K | N | F | Q | D | A | *H* | *R* | E | C | B | S |

Or, assigning numerical ranks:

| | | | | | | | | | | | | | | | | | | | |
|---|---|---|---|---|---|---|---|---|---|---|---|---|---|---|---|---|---|---|---|
| Subjective rating: | 1 | 2 | 3 | 4 | 5 | 6 | 7 | 8 | 9 | 10 | 11 | 12 | 13 | 14 | 15 | 16 | 17 | 18 | 19 |
| Cantilever, $c$: | 2 | 7 | 3 | 4 | 8 | 1 | 5 | 19 | 6 | 9 | 13 | 17 | 12 | 16 | 10 | 11 | 14 | 18 | 15 |
| $G$: | 2 | 1 | 3 | 8 | 5 | 6 | 7 | 13 | 9 | 4 | 16 | 11 | 12 | 10 | 18 | 19 | 17 | 15 | 14 |
| Heart loop, $c$: | 2 | 1 | 13 | 3 | 4 | 5 | 10 | 16 | 9 | 6 | 7 | 11 | 14 | 8 | 12 | 18 | 17 | 19 | 15 |
| $G$: | 1 | 13 | 2 | 3 | 6 | 5 | 7 | 16 | 9 | 8 | 4 | 10 | 11 | 12 | 18 | 17 | 15 | 19 | 14 |
| Schiefer Flexometer: | 2 | 5 | 6 | 7 | 3 | 4 | 1 | 8 | 9 | 11 | 13 | 16 | 17 | 10 | 12 | 19 | 14 | 15 | 18 |
| Planoflex: | 3 | 6 | 7 | 8 | 12 | 1 | 4 | 10 | 9 | 11 | 14 | 15 | 2 | 5 | 13 | 16 | 18 | 17 | 19 |
| Drapeometer: | 16 | 6 | 11 | 5 | 7 | 10 | 13 | 8 | 9 | 17 | 3 | 2 | 18 | 1 | 19 | 4 | 12 | 15 | 14 |

Kendall's coefficient of rank correlation, $\tau$. Its use has been described by Schwarz and Fox [9], and also by Winn and Schwarz [11]. The values of the Kendall coefficient for each method of measurement, giving its correlation with the subjective evaluation, is given in Table IV.

An application of the $t$-test shows that all these coefficients, with the exception of that for the Drapeometer, are significantly different from zero at the 95% probability level. That is, there is a reasonably well established relation between the subjective rating and the laboratory rating, and one can reasonably expect that any of the first six quantities might be used to evaluate stiffness.

### Repetition of the Test

None of the coefficients is sufficiently higher than the others to suggest that one test is decidedly the best. This may not, however, be the result of a lack of correlation, but may only reflect inaccuracies in establishing the subjective ranking. The range of fabrics used perhaps was not selected in the best way, for it can be seen by referring to Table I that there was not complete agreement upon the rank of any fabric in the group. Therefore, another test was carried out in which the fabrics were ranked subjectively at the start, and only those were selected for laboratory measurement which were ranked without difficulty. Twenty-two fabrics were originally included, from which eleven were selected. They were as shown in Table V.

These were ranked from soft to stiff by eleven people, as shown in Table VI.

TABLE IV. RANK CORRELATION OF LABORATORY MEASUREMENTS WITH SUBJECTIVE MEASUREMENT

| Method | Kendall coefficient ($\tau$) |
|---|---|
| Cantilever, $c$ | 0.56 |
| Cantilever, $G$ | 0.78 |
| Heart loop, $c$ | 0.63 |
| Heart loop, $G$ | 0.62 |
| Schiefer Flexometer | 0.70 |
| Planoflex | 0.58 |
| Drapeometer | 0.09 |

TABLE V

| Code letter | Fabric | Weight (oz./sq. yd.) |
|---|---|---|
| A′ | Viscose rayon plain weave | 2.9 |
| B′ | Nylon sportswear | 2.8 |
| C′ | Nylon twill | 1.8 |
| D′ | Nylon sportswear | 3.1 |
| E′ | Nylon taffeta | 2.4 |
| F′ | Nylon/bemberg crepe | 2.6 |
| G′ | Nylon/viscose satin | 4.0 |
| H′ | Nylon twill | 2.0 |
| I′ | Nylon taffeta | 2.8 |
| J′ | Nylon twill | 4.8 |
| K′ | Cotton sportswear gabardine | 5.7 |

| | Code letters | | | | | | | | | | | Standard rank Nos. | | | | | | | | | | |
|---|---|---|---|---|---|---|---|---|---|---|---|---|---|---|---|---|---|---|---|---|---|---|
| Cantilever, $c$: | F′ | C′ | D′ | G′ | H′ | E′ | A′ | B′ | I′ | J′ | K′ | 3, | 1, | 6, | 5, | 4, | 7, | 2, | 9, | 8, | 11, | 10 |
| $G$: | C′ | F′ | A′ | H′ | E′ | G′ | D′ | I′ | B′ | K′ | J′ | 1, | 3, | 2, | 4, | 7, | 5, | 6, | 8, | 9, | 10, | 11 |
| Heart loop, $c$: | F′ | C′ | G′ | H′ | E′ | A′ | B′ | D′ | J′ | I′ | K′ | 3, | 1, | 5, | 4, | 7, | 2, | 9, | 6, | 11, | 8, | 10 |
| $G$: | C′ | F′ | H′ | E′ | A′ | G′ | B′ | I′ | D′ | J′ | K′ | 1, | 3, | 4, | 7, | 2, | 5, | 9, | 8, | 6, | 11, | 10 |
| Schiefer Flexometer: | C′ | H′ | F′ | A′ | E′ | G′ | J′ | D′ | I′ | B′ | K′ | 1, | 4, | 3, | 2, | 7, | 5, | 11, | 6, | 8, | 9, | 10 |

Of the methods investigated in the first test, the cantilever test and Schiefer's Flexometer apparently gave the best correlations. Therefore, these two methods were selected for investigation with the second range of fabrics. The heart loop was also included, because of its essential similarity to the cantilever, and because it was felt that the comparison between them needed to be verified. The Planoflex was not included because of its apparent inability to give reliable comparison between fabrics that are different in construction [5, 6]. For example, a sample of glass fabric, which felt very stiff, was measured on the Planoflex. The angle obtained was 44°, which would indicate a rather soft fabric. Schwarz, in a private communication, has indicated a similarly high Planoflex reading for a very stiff, plastic-coated fabric. Thus, it would appear that the Planoflex reading is influenced only in part by the bending stiffness of the fabric, which appears to be what the subjective evaluation estimates. Some other factor—perhaps the tendency for one set of yarns to slide over the other—also appears to have a rather marked influence.

The values obtained by each of these methods of measurement are given in Table VII. In each case the figure quoted is an average of the value obtained in the warp and weft directions, as described previously.

Again ranking the fabrics in order from soft to stiff and assigning the rank numbers obtained from the subjective evaluation, we obtained the results given at the top of this page.

Kendall's coefficient of rank correlation can be calculated as before; the values obtained are given in Table VIII.

Again, all coefficients are significantly different from zero at the 95% probability level. With one exception—the flexural rigidity as determined by the cantilever test—the coefficients are not appreciably different from the values obtained in the previous test. However, the coefficient 0.89 is considerably higher than it was before. If the selection of a suitable test were to be based on the size of the coefficient, then one would select the flexural

TABLE VI. SUBJECTIVE RANKING

| Fabric | | | | | | | | | | | | Average rank |
|---|---|---|---|---|---|---|---|---|---|---|---|---|
| A′ | 2 | 2 | 2 | 2 | 2 | 1 | 2 | 1 | 1 | 1 | 1 | 1.5+ |
| B′ | 8 | 9 | 9 | 9 | 9 | 9 | 9 | 9 | 9 | 10 | 9 | 9.0 |
| C′ | 1 | 1 | 1 | 1 | 1 | 2 | 1 | 2 | 2 | 2 | 2 | 1.5− |
| D′ | 6 | 6 | 6 | 6 | 6 | 6 | 6 | 6 | 6 | 6 | 5 | 5.9 |
| E′ | 7 | 7 | 7 | 7 | 7 | 7 | 7 | 7 | 7 | 7 | 7 | 7.0 |
| F′ | 4 | 3 | 3 | 3 | 3 | 3 | 3 | 3 | 3 | 3 | 3 | 3.1 |
| G′ | 5 | 5 | 5 | 5 | 4 | 5 | 5 | 5 | 5 | 5 | 6 | 5.0 |
| H′ | 3 | 4 | 4 | 4 | 5 | 4 | 4 | 4 | 4 | 4 | 4 | 4.0 |
| I′ | 9 | 8 | 8 | 8 | 8 | 8 | 8 | 8 | 8 | 8 | 8 | 8.1 |
| J′ | 11 | 11 | 11 | 11 | 11 | 11 | 11 | 11 | 11 | 11 | 11 | 11.0 |
| K′ | 10 | 10 | 10 | 10 | 10 | 10 | 10 | 10 | 10 | 9 | 10 | 9.9 |

| Average rating | C′ | A′ | F′ | H′ | G′ | D′ | E′ | I′ | B′ | K′ | J′ |
|---|---|---|---|---|---|---|---|---|---|---|---|
| Standard rank No. | 1 | 2 | 3 | 4 | 5 | 6 | 7 | 8 | 9 | 10 | 11 |

TABLE VII. LABORATORY EVALUATION OF STIFFNESS

| Fabric | Cantilever | | Heart loop | | Schiefer Flexometer |
|---|---|---|---|---|---|
| | Bending length, $c$ (cm.) | Flexural rigidity, $G$ (mg.cm.) | Bending length, $c$ (cm.) | Flexural rigidity, $G$ (mg.cm.) | Work to fold (ergs) |
| A′ | 2.42 | 67 | 1.50 | 38 | 122 |
| B′ | 2.65 | 212 | 1.57 | 41 | 195 |
| C′ | 1.65 | 28 | 1.22 | 11 | 80 |
| D′ | 1.80 | 166 | 1.63 | 57 | 175 |
| E′ | 2.30 | 118 | 1.45 | 25 | 133 |
| F′ | 1.62 | 41 | 1.19 | 15 | 105 |
| G′ | 2.16 | 140 | 1.42 | 39 | 157 |
| H′ | 2.22 | 75 | 1.45 | 21 | 80 |
| I′ | 2.68 | 185 | 1.79 | 55 | 193 |
| J′ | 2.77 | 667 | 1.78 | 100 | 170 |
| K′ | 3.02 | 544 | 1.80 | 123 | 255 |

TABLE VIII. RANK CORRELATION OF LABORATORY MEASUREMENT WITH SUBJECTIVE MEASUREMENT

| Method | Kendall coefficient ($\tau$) |
|---|---|
| Cantilever, $c$ | 0.60 |
| Cantilever, $G$ | 0.89 |
| Heart loop, $c$ | 0.60 |
| Heart loop, $G$ | 0.71 |
| Schiefer Flexometer | 0.67 |

rigidity as determined by the cantilever test. However, this cannot be the sole criterion. Simplicity of apparatus required and the ease with which the test may be carried out are important considerations. On these grounds one would also select the cantilever test. Therefore, it would seem to be the test most worthy of serious consideration as a standard laboratory test for stiffness. A further investigation into the use of this test is described in Part II.


### Summary

The subjective evaluation of fabric stiffness was used to rank a range of fabrics in order as a reference standard with which to compare some laboratory measurements of stiffness. Five different laboratory methods were used, and the correlation of the results of each method with the subjective evaluation was calculated using Kendall's coefficient of rank correlation. The most promising correlations were obtained from the flexural rigidity as determined by Peirce's cantilever test and from Schiefer's Flexometer. A second range of fabrics was tested in a similar way, with approximately the same results. Due to the simplicity both of technique and of apparatus required for the Peirce cantilever test, it was therefore selected for further study, as described in Part II.


# Part II: A Study of the Peirce Cantilever Test for Stiffness of Textile Fabrics

### Introduction

The cantilever test, as described by Peirce [7], has been shown to give results which correlate well with a subjective rating of stiffness which has been adopted as a reference standard. However, the best technique to be used for carrying out the test is not definitely established. Winn and Schwarz [10] have shown that the value obtained for bending length, as measured by the heart loop, is dependent upon the length of the fabric strip tested. No such information is available giving the effect of length of overhang in the cantilever test upon the value for the bending length obtained. There is little information about the best basis of comparison for different types of fabric—whether the measurements should be made on the basis of constant length of overhang, or perhaps constant angle of bend. Peirce [7] states: "The length of overhang should be chosen to give a deflection of 20° to 30°, or more for flimsy materials, since very short lengths also mean increased errors of observation." Also, in the description of the test method in "Methods of Test for Textiles," published by the British Standards Institution [3], it is suggested that a length of overhang be used which gives an angle of 20° to 40°. No reason is given for such a statement, and no experimental evidence to support it. Therefore, it was felt that a measurement of bending length for different lengths of overhang for a range of fabrics would be valuable.

### Fabrics Used

The range of fabrics used is described in Table I. They were chosen to represent a variety of fibers and weaves, as well as a rather wide range of stiffness.

### Method of Measurement

Measurements were made at 65% R.H., 70°F, on an instrument such as is described by Peirce [7], using a strip of fabric 1 in. wide by 6 in. long. Four strips were cut with the long dimension parallel to the warp, and four with the long dimension

TABLE I

| Code letter | Fabric | Weight (oz./sq. yd.) |
|---|---|---|
| A″ | Nylon sateen | 2.2 |
| B″ | Viscose rayon plain weave | 2.8 |
| C″ | Viscose rayon crepe | 3.2 |
| D″ | Nylon plain weave (sportswear fabric) | 3.5 |
| E″ | Nylon twill (tarpaulin fabric) | 3.9 |
| F″ | Spun viscose plain weave | 4.5 |
| G″ | Cotton poplin (sportswear fabric) | 6.1 |
| H″ | Nylon oxford weave (sportswear fabric) | 6.1 |
| I″ | Acetate rayon satin (sportswear fabric) | 7.7 |
| J″ | Worsted men's suiting | 8.5 |
| K″ | Wool overcoating | 14.0 |

parallel to the weft. Four readings were taken on each fabric sample, one at each end with the face up, and the same with the back up. Thus, sixteen readings were obtained for warpwise bending and sixteen for weftwise bending. An arithmetic mean of each set of sixteen readings was taken, and also

TABLE II. BENDING LENGTH AT DIFFERENT LENGTHS OF OVERHANG

| Fabric | Length of overhang (cm.) | Mean angle of dip (degrees) | Mean bending length (cm.) Method (*a*) | Method (*b*) | Method (*c*) | Method (*d*) |
|---|---|---|---|---|---|---|
| A″ | 2 | 10.1 | 1.81 | 1.79 | 1.79 | 1.78 |
| | 3 | 30.9 | 1.74 | 1.74 | 1.74 | 1.76 |
| | 4 | 52.5 | 1.70 | 1.72 | — | 1.76 |
| | 5 | 64.6 | 1.82 | 1.76 | — | 1.84 |
| B″ | 2 | 10.7 | 1.75 | 1.73 | 1.73 | 1.71 |
| | 3 | 31.6 | 1.72 | 1.73 | 1.77 | 1.76 |
| | 4 | 52.4 | 1.71 | 1.71 | — | 1.77 |
| | 5 | 62.4 | 2.02 | 1.82 | — | 1.90 |
| C″ | 2 | 10.9 | 1.71 | 1.73 | 1.73 | 1.73 |
| | 3 | 36.8 | 1.59 | 1.60 | 1.60 | 1.62 |
| | 4 | 57.2 | 1.59 | 1.59 | — | 1.65 |
| | 5 | 68.1 | 1.75 | 1.63 | — | 1.75 |
| D″ | 3 | 7.4 | — | 3.21 | 3.21 | 3.22 |
| | 4 | 21.0 | 2.80 | 2.85 | 2.85 | 2.89 |
| | 5 | 39.8 | 2.57 | 2.59 | — | 2.63 |
| | 6 | 52.6 | 2.60 | 2.58 | — | 2.65 |
| E″ | 4 | 8.4 | 3.89 | 3.90 | 3.89 | 3.90 |
| | 5 | 15.8 | 3.80 | 3.86 | 3.86 | 3.86 |
| | 6 | 27.0 | 3.73 | 3.74 | 3.74 | 3.77 |
| | 7 | 38.0 | 3.65 | 3.69 | 3.70 | 3.74 |
| | 8 | 46.9 | 3.68 | 3.70 | — | 3.80 |
| F″ | 2 | 8.2 | 1.95 | 1.95 | 1.95 | 1.95 |
| | 3 | 26.1 | 1.87 | 1.89 | 1.89 | 1.91 |
| | 4 | 47.0 | 1.84 | 1.85 | — | 1.90 |
| | 5 | 60.3 | 1.92 | 1.89 | — | 1.97 |
| G″ | 4 | 13.4 | 3.22 | 3.30 | 3.29 | 3.29 |
| | 5 | 30.4 | 2.95 | 2.97 | 2.95 | 3.00 |
| | 6 | 46.0 | 2.80 | 2.82 | — | 2.88 |
| | 7 | 59.9 | 2.70 | 2.65 | — | 2.78 |
| H″ | 3 | 6.3 | 3.14 | 3.15 | 3.15 | 3.15 |
| | 4 | 18.5 | 2.85 | 2.86 | 2.87 | 2.87 |
| | 5 | 34.6 | 2.73 | 2.75 | 2.76 | 2.78 |
| | 6 | 47.0 | 2.75 | 2.78 | — | 2.84 |
| | 7 | 58.4 | 2.76 | 2.75 | — | 2.85 |
| I″ | 4 | 8.2 | 3.80 | 3.95 | 3.95 | 3.82 |
| | 5 | 16.3 | 3.70 | 3.76 | 3.76 | 3.76 |
| | 6 | 31.2 | 3.45 | 3.49 | 3.48 | 3.51 |
| | 7 | 44.0 | 3.40 | 3.38 | — | 3.41 |
| | 8 | 54.7 | 3.30 | 3.34 | — | 3.42 |
| J″ | 3 | 16.3 | 2.26 | 2.28 | 2.30 | 2.30 |
| | 4 | 34.5 | 2.20 | 2.21 | 2.22 | 2.24 |
| | 5 | 49.7 | 2.21 | 2.15 | — | 2.24 |
| | 6 | 61.1 | 2.28 | 2.22 | — | 2.34 |
| K″ | 3 | 7.3 | 3.05 | 3.07 | 3.07 | 3.07 |
| | 4 | 22.0 | 2.67 | 2.70 | 2.72 | 2.72 |
| | 5 | 37.5 | 2.62 | 2.64 | 2.65 | 2.68 |
| | 6 | 51.6 | 2.59 | 2.57 | — | 2.68 |
| | 7 | 62.3 | 2.63 | 2.56 | — | 2.68 |

a geometric mean of the warp and weft values in order to obtain one figure which would be representative of the fabric as a whole. A similar set of readings was made for at least four lengths of overhang for each fabric, using the same set of samples each time, thus reducing differences due to sampling to a minimum. These figures are given in Table II.

The calculation of the bending length from the observations can be made in several ways. Peirce [7] has described one method, and Bickley [2] has described several others which are based on a more rigorous solution of the differential equations involved. In order to compare these methods, the bending length was calculated in four ways:

(*a*) a graph of $c/l$ against $\theta$; (*b*) a graph of $l^3/c^3 \tan\theta$ against $\theta$; (*c*) a table, with first and second differences, giving $l^3/c^3$ in terms of $\tan\theta$; (*d*) the relationship $c = l \cdot \left(\frac{\cos 0.5\,\theta}{8 \tan\theta}\right)^{\frac{1}{3}}$ where $c$ = bending length, $l$ = length of overhang, and $\theta$ = angle of dip. The first three methods are suggested by Bickley, the fourth by Peirce.

Method (*c*) is considered by Bickley to be the most reliable of these methods of computing bending length, then (*b*), (*a*), and (*d*), in that order. Method (*d*), which is Peirce's, gives consistently high results except at the low angles. In the middle range of angles (30°–50°) there is little difference between (*a*), (*b*), and (*c*), Bickley's methods.

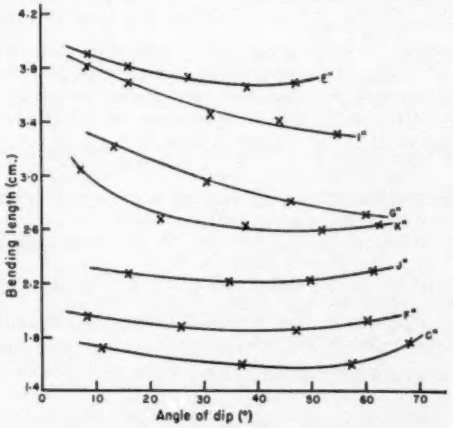


FIG. 1. *The variation of bending length with angle of dip.*

However, at low and high angles differences may show up due to the fact that in many cases the available graphs had to be extrapolated, which inevitably introduces error. It would appear, therefore, that it would be safe to accept method (*a*) as a simple, reliable method of computation. Figure 1 shows the results computed by method (*a*) for the bending length of some of these fabrics plotted against the angle of dip. It is unnecessary to confuse the graph by plotting the remainder of the results, for they are all essentially the same shape—that is, slightly concave upwards. In most cases the variation in bending length is not great. However, if one were to pick the most satisfactory range of angles over which the measurement should be made, the range 40°–50° would seem to be the best since in this range the bending length is most nearly constant for all the fabrics tested. In making the recommendation of 20°–30° as a suitable range, Peirce may have had in mind that his method of computation is more accurate up to 30° than it is at higher angles. However, it seems clear that in some cases the slope of the bending length *vs.* angle curve is rather too great in the region 20°–30° to make it a satisfactory range.

In this light of this decision, consideration should be given to the method used by Chu, Cummings, and Teixeira [4], in which the overhang corresponding to a given angle is measured, rather than the angle corresponding to a given overhang. It is obviously not feasible to select a standard length of overhang for all fabrics, but a standard angle could be chosen, provided it is in the range of 40°–50°. This happens to be a convenient range, for it is here that $c/l$ is about 0.5. Chu *et al.* took $c/l = 0.500$ at 43°, which is obtained from Peirce's data. Using Bickley's more accurate data, it is found that $c/l = 0.500$ at 41°—that is, for an angle of dip of 41° the bending length is one-half the length of overhang.

The adoption of such a method of measurement simplifies the calculation, and also the equipment required, for all that is needed is a horizontal platform, an indicator inclined at an angle of 41° below the horizontal, and a means of measuring length of overhang. A satisfactory device has been found to be a steel rule carrying a centimeter scale, with a thin sheet of rubber cemented to the back. The rule is laid on top of the fabric strip with its zero opposite the end of the fabric, and the pair slid together slowly but steadily off the edge of the

platform until the angle of dip is 41°. The reading on the rule, opposite the edge of the platform, gives the length of overhang directly. The rubber backing on the rule prevents any slippage between the rule and the fabric. It is also advisable to place a weight on top of the rule and the fabric in such a way that they are held flat against the horizontal platform right to its edge.

Measurements of bending length of all these fabrics were also made in this way. Results are given below, and for comparison the values obtained previously at the same angle (41°), as read from a plot such as Figure 1, are also given.

| Fabric | Mean bending length: Constant angle, 41° | Previous value, 41° | Ratio |
|---|---|---|---|
| A″ | 1.58 | 1.72 | 0.93 |
| B″ | 1.54 | 1.71 | 0.91 |
| C″ | 1.40 | 1.58 | 0.88 |
| D″ | 2.24 | 2.56 | 0.86 |
| E″ | 3.39 | 3.66 | 0.93 |
| F″ | 1.67 | 1.84 | 0.91 |
| G″ | 2.37 | 2.84 | 0.84 |
| H″ | 2.48 | 2.74 | 0.91 |
| I″ | 3.03 | 3.39 | 0.90 |
| J″ | 1.98 | 2.19 | 0.90 |
| K″ | 2.17 | 2.58 | 0.83 |

The fact that the values obtained by this method are somewhat lower than those obtained by the previous method could hardly have been anticipated by intuitive reasoning. However, since in the constant-angle method the bending moment is continually increasing up to the final observation, while in the constant-length-of-overhang method it is continually decreasing, one would hardly expect to get the same result for the two methods. Nevertheless, there is no reason to feel that one is a less reliable method than the other. Moreover, since the ratio of the results obtained by the two methods is sensibly constant, both will rank fabrics in essentially the same order. Since this is a comparative scale only, it would seem immaterial which method is used, provided all measurements are done the same way. In view of this, the constant-angle method is recommended as the simplest both from a standpoint of equipment required and of technique.


## Summary

A technique has been developed for the measurement of stiffness in textile fabrics using the cantilever method as suggested by Peirce. It is proposed that the best basis for comparison of fabrics is measurement made at a standard angle of dip, 41°, at which angle the bending length is one-half the length of overhang. It was shown in Part I that the best measure of stiffness is the flexural rigidity of the fabric, which is its weight per unit area multiplied by the cube of its bending length.



## Acknowledgments

The author acknowledges with pleasure the assistance of all those who participated in this work, which has been carried out intermittently over the past seven years, either by making the measurements in the laboratory, or by helping to establish the subjective ranking. He is particularly grateful for the advice and criticism offered by Dr. A. C. Goodings and by Dr. Lyman Fourt, who is chairman of a task group on the measurement of hand in A.S.T.M. Committee D-13 on Textile Materials. The work described was done under the sponsorship of Canadian Industries Limited, Nylon Division, with whose permission it has been published.


## Literature Cited


1. A.S.T.M. Standards on Textile Materials, D123–50, 1950, appendix III.
2. Bickley, W. G., *Phil. Mag.* **17**, 603 (1934).
3. British Standards Institution, "Methods of Test for Textiles," British Standard Handbook No. 11, 1949, p. 124.
4. Chu, C. C., Cummings, C. L., and Teixeira, N. A., TEXTILE RESEARCH JOURNAL **20**, 539 (1950).
5. Dreby, E. C., *Am. Dyestuff Reptr.* **30**, 651 (1941).
6. Dreby, E. C., *Am. Dyestuff Reptr.* **31**, 497 (1942).
7. Peirce, F. T., *J. Text. Inst.* **21**, T377 (1930).
8. Schiefer, H. F., *J. Research Natl. Bur. Standards* **10**, 647 (1933).
9. Schwarz, E. R., and Fox, K. R., *A.S.T.M. Bull.* No. 119, 21 (Dec. 1942).
10. Winn, L. J., and Schwarz, E. R., *Am. Dyestuff Reptr.* **28**, 688 (1939).
11. Winn, L. J., and Schwarz, E. R., *Am. Dyestuff Reptr.* **29**, 400 (1940).
12. Winn, L. J., and Schwarz, E. R., *Am. Dyestuff Reptr.* **29**, 469 (1940).


*(Manuscript received March 2, 1951.)*

# An Experimental, Gas-Fired, Infrared Textile Slasher

**Ralph A. Rusca and George J. Kyame**

*Southern Regional Research Laboratory,* New Orleans, Louisiana*

**Abstract**

An experimental, gas-fired, infrared textile slasher designed by the textile engineers of the Southern Regional Research Laboratory is described. The slasher processes warps 21 in. wide on beams with 18-in. heads, and is used in operations of pilot-plant scale. Among the features which represent departures from conventional methods of textile slashing are: a new system for the preparation and distribution of the sizing material; a new and more flexible design of size box; an improved means for drying the size-impregnated warp, which combines the best features of radiant and convection drying methods; and a sensitive drive system capable of controlling the warp tension during processing.

SEVERAL YEARS AGO the Southern Regional Research Laboratory was in need of a slasher to complete the equipment requirements of its textile processing laboratory. A slasher was desired which would process warps of pilot-plant scale—in particular, warps 21 in. wide by 300–600 yds. long. Commercially available slashers were either too small or too large. The laboratory-scale units were intended primarily for slashing small experimental lots of yarn, while the mill-size slashers were impractical for pilot-scale operations. It was necessary, therefore, for the Southern Laboratory's textile engineers to design a slasher to meet their specific needs. A semi-production-size machine was constructed the full length and about half the width of a production model; it handles warps 21 in. wide on beams with 18-in.-diameter heads. Since the slasher has several unconventional features, it was felt that a description of it would be of interest to research organizations and textile mills.

## Slashing Equipment

The efficient and satisfactory slashing of warps is one of the major problems of the textile industry. No weave room can maintain quality and production unless properly sized warps are produced by the slashers.

All slashers are essentially the same in design, differing mainly in the drying means employed [1]. The cylinder or can-type drier is the most popular in North America, although a number of hot-air driers have been installed in recent years. Hot-air driers are used quite extensively in Europe. Lately, the mills have begun to augment their slasher capacities by using infrared radiation supplied by the use of gas burners or, occasionally, by electric lamps.

Present slashing methods are fairly adequate from the standpoint of production; but the quality of the product frequently is inferior to that desired. The use of steam cylinders results in nonuniform drying and baking of the size, and drying of the size film in a flattened shape [1]. Subsequent splitting of the warp leaves the size film harsh and ragged. There are also complaints regarding the size cooking and handling equipment and the control of yarn tension during the beam windup. These factors lead to lower weaving efficiency and higher manufacturing costs.

The Laboratory's engineers have attempted to incorporate improvements over existing methods and equipment in the S.R.R.L. slasher. Ample instrumentation was provided to permit the use of the slasher in exploratory and experimental research.

* One of the laboratories of the Bureau of Agricultural and Industrial Chemistry, Agricultural Research Administration, U. S. Department of Agriculture.

The present paper describes the design and operating principles of the new machine.

### Size Preparation and Storage System

The size system of the S.R.R.L. slasher is shown schematically in Figure 1. The system diagrammed has no storage tank and is used for research applications requiring less than one tankful of size; in this instance, the makeup tank later serves as a storage tank. For production purposes a separate unit—without the size box—is employed to prepare the size, and the system illustrated is used for storage and distribution.

Conventional size formulations and preparation procedures are followed with this new system, but its operation differs somewhat from standard practice. In use, fluid is withdrawn simultaneously from the makeup tank and the size box, mixed in the pump, and then forced through the heat exchanger for heating. The discharge from the heat exchanger divides into two streams—one replenishing the size in the size box, and the other returning to the makeup tank. The returning streams are fed back into their respective tanks, at a point below the fluid level, in a manner that produces a vigorous top-to-bottom turnover of the tank contents. Agitation is more thorough than with the whirlpool-like spinning action usually encountered with paddle-type agitators. For preparing the size solution, the fluid circulation is confined, by proper valve adjustment, to the makeup tank, pump, and heat exchanger.

A system of this type minimizes the disadvantages existing in the size-preparation methods and equipment in use today. Dispersal of dry ingredients is very rapid because of their passage through the pump and the vigorous agitation of the tank contents. The pump used to circulate the size is a self-priming, positive-displacement device that employs a single-thread, helical-screw rotor within a double, internal, helical-thread stator. Such pumps are less violent than the impeller types and cause little or no starch breakdown, thereby having relatively little effect on the viscosity of the size. Starch lump formation due to the use of live steam and inadequate agitation [2] is eliminated. Heat transfer in the heat exchanger is better than in the conventional steam coils or steam-jacketed kettles because an insulating film of size is not formed in the fluid-carrying coil. This method of heating also prevents dilution of the size, as is the case with live steam.

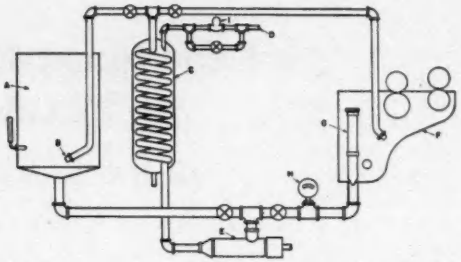

FIG. 1. *The S.R.R.L. size system.* A—*Makeup tank.* B—*Jet.* C—*Heat exchanger.* D—*Steam inlet.* E—*Pump.* F—*Size box.* G—*Float valve.* H—*Temperature controller.* I—*Solenoid valve.*

Size temperature is maintained constant through the use of a temperature controller located in the suction line at the intake of the pump. The controller activates a solenoid valve which controls the flow of steam to the heat exchanger.

An inexpensive float valve, seen in Figure 1, automatically regulates the size level in the size box by varying the area of the drain hole as the size level varies. A constant rate of size imput maintains the size level without the risk of air entrainment, which is present in the familiar, overflow-type system.

### The Size Box

Foremost among the factors that affect the attainment of an "ideally" sized warp are the amount of size applied to the yarn and the degree of penetration therein. To facilitate a study of these factors, the S.R.R.L. size box is provided with a greater than normal depth of warp immersion, and control of the immersion of the size rolls (Figure 1). The latter is accomplished by making the size rolls of unequal diameters and mounting them at different levels so that with the proper adjustment of the size level one or both rolls can be immersed in the bath.

Other features include the elimination of troublesome stuffing boxes by suspending the size rolls from specially designed hangar bearings, and contouring the size box to fit closely to the rolls so as to minimize unused space and reduce size stagnation due to lack of agitation.

The squeeze rolls are of equal diameter and are covered with the conventional wool blanket. Loading of the squeeze rolls is done by a set of calibrated steel springs, with scales at each spring to indicate the load being applied.

All parts of the size box and size preparation unit coming in contact with the size solution are of stainless steel with the exception of a synthetic-rubber pump stator.

### The Drying System

The development of an improved drying system received a great deal of attention. Preliminary research included studies of the relative efficiency and practicability as well as the possible effect on the physical properties of yarn of conduction, convection, and radiation heating methods. Heating systems investigated included high-pressure steam cylinders, high-frequency dielectric heating, radiant heating, and direct- and indirect-fired convection ovens.

The drying method adopted for the experimental slasher is based on the fact that cotton yarn will not be damaged by exposure to intense heat as long as the yarn is saturated with free water. The application of this principle led to the design of the combination radiation-convection drier depicted schematically in Figure 2 and photographically in Figures 3, 4, and 5. The drier consists of an elongated, double-walled structure formed into a modified U-shaped chamber. In a 6-ft.-high vertical section comprising one arm of the U, four gas-fired burners are mounted in staggered relationship on opposite walls; these are adjustable inwardly and outwardly. The burners emit radiant energy from aluminum-oxide refractories heated to incandescence—approximately 2,300°F—by an air-natural gas mixture, and are designed to give temperatures up to 700°F in this section of the drier, with no wet warp present. The remaining section of the drier forms the other part of the U and consists of an inclined portion 15 ft. long, which terminates at its outlet end in a short vertical run. An exhaust blower draws the hot combustion products from the burners through the inclined section to provide the convection-heating stage of the drying operation.

In passing through the burner section the warp is subjected to the combined effect of hot air and infrared radiation. This action, coupled with the well-known penetrating power of the infrared heat, quickly raises the temperature of the size to the boiling point. Since the atmosphere in the oven is made up of the combustion products of the air-gas mixture fed to the burners, the warp is heated in a nonoxidizing atmosphere of low relative humidity. At no time is the warp exposed to the deteriorative effects of oxidation and high relative humidity in the presence of high temperatures [3, 4]. If desired, however, additional air may be bled in through openings which may be uncovered around each burner and at the top of the vertical section. This feature, together with regulating the ratio of air and gas fed to the burners, permits control of the drying medium to such an extent that an oxidizing, reducing, or neutral atmosphere can be maintained within the drier.

The burner control system is interlocked electrically with the drive system so that the burners are automatically turned down when the slasher is operated at creep speed, and are cut off completely and rapidly cooled at stopping.

Control over the intensity and penetrability of the infrared radiation and over the hot-air velocity makes the drier particularly adaptable to the drying of surface coatings. Heating may be done so rapidly that surface coatings may be dried or cured without materially affecting the underlying base.

The interior walls of the inclined section fit rather closely to the warp in order to attain high air velocities without the need for large and expensive blower systems. No unequal heating effects have been experienced from side-wall radiation with this design.

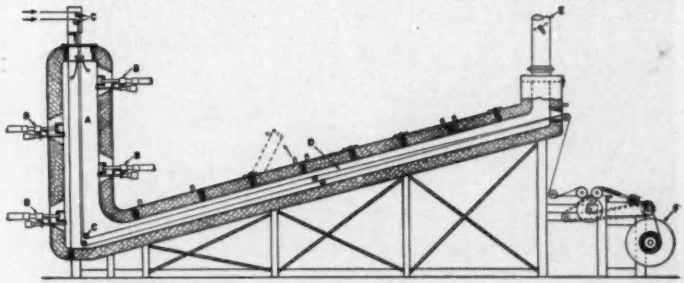

FIG. 2. *The radiation-convection drier.* A—*Radiation drying section.* B—*Burners.* C—*Wet-split rolls.* D—*Convection drying section.* E—*Exhaust duct.* F—*Beam wind-up section.*

An air-intake valve at the exhaust blower regulates the air flow through the drier. Access to the warp is provided by a large hinged door on the vertical section and six smaller doors on the inclined section and outlet end.

The warp is wet-split into two sheets prior to en-

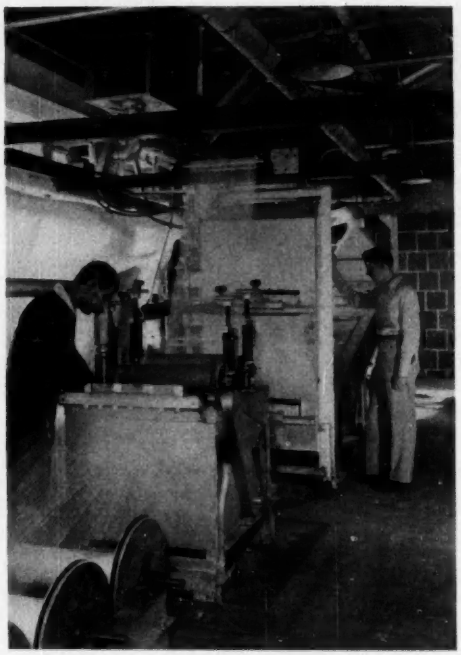

FIG. 3. *View from rear end of the slasher.*

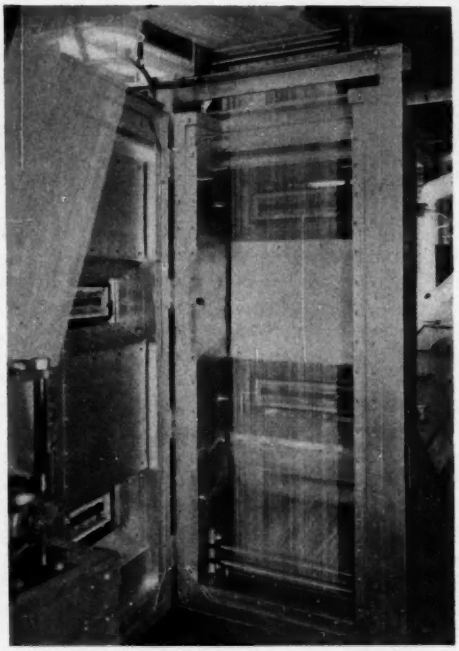

FIG. 4. *Interior of the radiant drying section.*

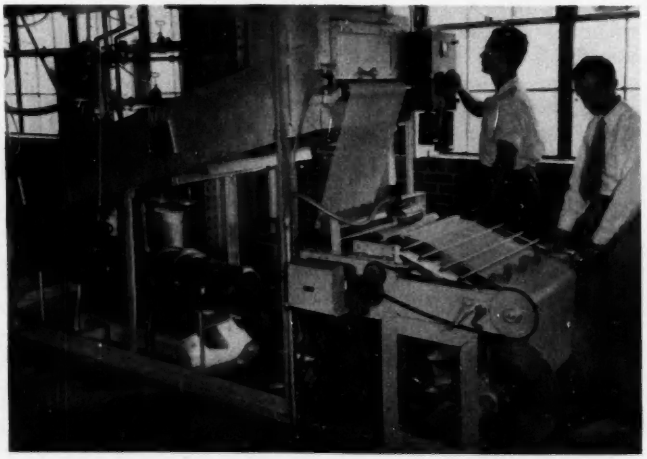

FIG. 5. *Front end of the slasher.*

tering the drier. Six conveyor rolls are mounted in pairs at three points in the drier—at the top and at the bottom of the vertical section, and in the middle of the inclined section. These rolls are staggered in both the horizontal and vertical planes, and are so positioned that the two warp sheets are centered between the burners and are spaced about $\frac{3}{16}$ in. apart in the vertical section. The sheets enter the inclined section about 2 in. apart and come together on a roll mounted outside the drier outlet. The rolls in the vertical section are water-cooled to minimize size pickup.

### The Drive System

The slasher driving system uses three variable-voltage D.C. motors to power the size rolls, the delivery roll, and the windup beam, respectively. The delivery roll and the size rolls are driven at a constant speed; a manually operated rheostat controls the speed differential between the two motors so as to maintain the warp tension desired between the size box and the delivery roll. A similar rheostat in the beam motor circuit adjusts the warp tension between the delivery roll and the windup beam. As the beam diameter increases the beam speed is automatically decreased to keep the horsepower, and hence the warp tension, constant. The over-all production speed of the slasher is regulated by means of a master control which changes the speeds of all three motors simultaneously. The master control is operable by hand or automatically by a moisture-regain controller. This system has been found to provide stable speed control over a range of 2 to 50 yds. per min., and to maintain constant the tension in the warp.

Mounted between the delivery roll and the windup beam are a series of split rods, an expansion comb, and a positively driven, eccentrically rotating guide roll. The guide roll causes the warp to traverse the dents of the comb, and distributes the wear on the wires. It should be noted that this guide roll can be used successfully only with a beam windup system that responds instantly to the changes in warp tension by the eccentric motion of the roll.

### Instrumentation

Graphic recording instruments are used to measure the variables of the slasher operation. One of these instruments is the previously mentioned moisture-regain controller, a commercially available unit which measures and records the electrical resistance of a section of the moving warp. The instrument is calibrated to read directly in percent moisture regain, and its control action operates the master rheostat governing the speed of warp movement through the drier. A change in the galvanometer of the instrument was found necessary in order to give the unit the high-speed response required for the S.R.R.L. slasher.

A four-point potentiometer records temperatures in the size box and at both ends of the convection drying section of the drier. The fourth point is reserved for a "roving" temperature-measuring element which is used to study temperature distribution within the drier as well as other thermal variables. Warp speed is indicated by an electric tachometer that is attached to the warp-driven roll mounted just outside the drier outlet. Two yardage counters show the yardage input to the drier and the yardage output. Three permanently mounted water manometers measure the gas pressure, air pressure, and air-gas-mix pressure for the infrared burners. A gas meter measures the rate and total consumption of fuel, and a recording watt-hour meter measures the electric power consumed. A side-arm thermometer mounted in the side of the makeup tank indicates the size temperature during the cooking and storage stages. Safety measures include full electrical ignition of the gas burners and an improved, automatic protective system to shut off the gas in case of flame failure.

### Conclusion

The mechanical phases in the development of the slasher were completed in Jan. 1951. In operation about two months, the slasher has been found to produce warps of good quality for use in the Southern Regional Research Laboratory pilot-plant applications. The size preparation and distribution system maintains size viscosity within close limits; the size box applies the solution to the warp with reasonable uniformity; drying in the radiant-convection oven is accomplished with 70% to 80% thermal efficiency; and the sized warps are wound on the loom beam under constant tension from start to finish. At this time (Mar. 1951) research has not been sufficient to determine the possibilities of the slasher for industrial utilization.

U. S. Patent 2,516,884 has been granted, and others are pending, on the essential features of the slashing equipment. These will be available for license from the Secretary of Agriculture on a royalty-free, nonexclusive basis. Complete engineering details of the slasher are available on request to the Southern Re-

gional Research Laboratory, 2100 Robert E. Lee Blvd., New Orleans 19, La.

### Literature Cited

1. Seydel, P. V., "Cotton Slashing," Atlanta, Ga., *Textile Industries*, 1949, p. 156.
2. Seydel, P. V., "Cotton Slashing," Atlanta, Ga., *Textile Industries*, 1949, p. 138.
3. Walker, A. C., TEXTILE RESEARCH **13**, 15 (Mar. 1943).
4. Wiegerink, J. G., TEXTILE RESEARCH **10**, 493–509 (Oct. 1940).

*(Manuscript received April 2, 1951.)*

# Book Reviews

**The Japanese Cotton Industry.** W. T. Kroese. Leiden, Holland, H. E. Stenfert Kroese's, 1950. 158 pages. Price, f. 8.50. (Available through bookstores in U. S. A.)

Cotton-industry executives will find much of value in this report by Dr. Kroese, who is an executive director of a large vertical mill. Up-to-date information is presented which will help assess the progress in recovery by the Japanese cotton industry since 1945 and its potentials as far as competition for world markets is concerned. In addition to a study of the economic factors of the industry, such as imports and exports of cotton textiles and materials, and labor practices, data on production efficiency and operating costs are presented in considerable detail.

---

**Rayon Fabric Construction.** A. T. C. Robinson. London, Thomas Skinner & Co., 1950. 180 pages. Price, 25/–.

This is intended as a text and reference book for the student and the designer. It is a somewhat revised edition of a series of articles on the subject by the head of the Textile Department, Halifax College of Technology, which have appeared in *Silk and Rayon* over the past two years.

The scope is wide, ranging from plain weaves, twills, and satins to figured weaves, figured double plains, mass crepes, and cloques to furnishing fabrics. In addition to detailed discussion of the fabrics, their design, uses, and, in many instances, methods of weaving, 274 excellent illustrations (some in color) show the finished fabrics and weaves. The readable type and good-quality paper add much to the value of the book from the reader's viewpoint.

---

**A Study of the Effects of Form Factors on the Translation of the Inherent Physical Properties of Textile Fibers into Textile Structure.** Walter J. Hamburger, Milton M. Platt, and Marcellotte W. Ross. Textile Series Report No. 59, Office of The Quartermaster General. 308 + ix pages. Price, $8.25. (Available through the Office of Technical Services, U. S. Dept. of Commerce, Washington 25, D. C.)

This is a compilation of abstracts which constitutes a review of the literature published before 1947. The

survey was prepared as part of a project sponsored by the Office of The Quartermaster General. The subject matter covered by the survey is much broader in scope than the title indicates. Not only does it review textile geometry and its influence on the physical properties of textiles, but it includes such subjects as the effect of humidity, visco-elastic behavior, and fabric finishing. The survey is divided into two parts. Part I (134 pages) includes abstracts of articles dealing with mechanical properties and behavior; viscosity deformation; adsorption; friction; and fiber, yarn, and fabric theory. Part II is divided into the following main sections: Sub-Fiber Structure; Testing; Fibers; Yarns; Fabrics; and Modification of Properties Through Finishing.

Because of the over-all treatment of a wide variety of information the usefulness of this survey to all persons engaged in textile research can hardly be overestimated.

---

**Modern Chemical Processes.** Editorial Staff of *Industrial and Engineering Chemistry*. New York, Reinhold Publishing Corp., 1950. 218 pages. Price, $4.00.

*(Reviewed by L. E. Hilbert, Carbide and Carbon Chemicals Division, Union Carbide and Carbon Corp., S. Charleston, W. Va.)*

As stated in the foreword by the editor, this book is a compilation of articles which have appeared in *Industrial and Engineering Chemistry* since 1948 describing processes of significant importance in the chemical industry. It includes not only processes among the basic heavy chemicals but it also represents a good cross section of the organic chemicals, fine chemicals, and medicinals.

The book does not, of course, include minute details of each process, but it does give a comprehensive description such as would serve the need of one who desires a good general knowledge of related industries. The treatment of the historical background leading up to the development of each process is excellent, and the reviewer considers the thoroughness with which each is relegated to its proper place of importance, economically and technologically, to be a major achievement of this book.

It will not only serve as a handy reference for men of industry in both technical and executive capacities, but it should also prove invaluable to students of chemical technology in general. Although these articles have appeared individually in the journal over a period of years, their being presented in book form for quick reference is convenient. The publication of other volumes, as the data become available, is a goal of which the editors can be very proud.

The reviewer considers the articles "Production of Iodine from Oil Well Brines," "Continuous Superphosphate Production," "Carotene and Chlorophyll Production," and the article dealing with extraction of vegetable oils to be particularly interesting because they include descriptions of certain processing techniques that are not too familiar to the reviewer. By the same token, each individual in reading this book will likewise profit from a review of techniques employed by industries both related to and far removed from his own.

---

**Colloidal Dispersions.** Earl K. Fischer. New York, John Wiley & Sons, Inc., and London, Chapman & Hall, Ltd., 1950. 387 + vii pages. Price, $7.50.

*(Reviewed by E. I. Valko, Polytechnic Institute of Brooklyn, Brooklyn, N. Y.)*

This book fills admirably a long-existent void in scientific and technical literature. Its subject is the dispersion of finely divided solids in liquids, and thus it complements the available literature on emulsions.

The first five chapters deal with particle size (including a very useful explanation of the different meanings of average diameter), wetting, stability, flocculation, and the flow properties of dispersions. These chapters occupy about half of the volume. The second half is devoted to the preparation of dispersions, explaining the role of surface-active agents and the construction, operation, and mode of action of mills. The last chapter on the flushing process represents the first adequate treatment this important method has received in the literature.

Because of the close interrelation of this field with many other branches of colloid science, inclusion or omission of specific topics were in some cases unavoidably a matter of arbitrary choice. For example, the discussion of carbon black includes particle size, optical properties, dispersion on the rubber mill, and suitable dispersing aids in the form of surface-active substances, but only brief space is given to the reinforcing effect of the pigment in rubber. The effect

of pigments in paints and printing inks is discussed rather extensively. Colloidal hydrosols possessing particles entirely in the submicroscopic region are in general not covered. The topic of aerosols admittedly lies outside the main scope of the book and it claims only a scant page. Nevertheless, in appraising the end-result, it appears that the author drew the lines of demarcation of his topic wisely, since the monograph is unusually coherent and well balanced. For its size it contains an amazing wealth of information, and the text is amply documented by well-chosen and up-to-date references to books, original papers, and patents.

Dr. Fischer uses clear and vivid language. If he feels that the prevailing theories are not adequate, he says so, and in this rather complex field he has more than one occasion to do so. However, in many other cases, the reader will share the reviewer's gratification for the successful application of fundamental knowledge to intricate industrial processes. The broad experience of the author in the field of colloidal dispersions enabled him to present his material with authority whether he deals with theory or with practical problems.

The mere assembly of available knowledge in this field would alone represent a notable achievement, but Dr. Fischer achieved more than that through his critical evaluation and integration of this knowledge.

The book will serve not only as an excellent guide for the technical man but it will also be of great value as a reliable source of information for the research man. Textile chemists will be particularly interested in what they can learn from this book on the manufacture and properties of pigment dispersions. They will also find in it inspiring information on many other fields which bear close relation to their own.

**Aminoplastics.** C. P. Vale. London, Cleaver-Hume Press, Ltd., and New York, Interscience Publishers, Inc., 1950. 250 pages. Price, $2.75.

*(Reviewed by S. D. Douglas, Carbide and Carbon Chemicals Division, Union Carbide and Carbon Corp., South Charleston, W. Va.)*

The expansion of the aminoplastics industry in recent years has been accompanied by the appearance of a wealth of literature, most of which has been in the form of magazine articles, chapters in general textbooks, and patents. Accordingly, a book which assembles and deals effectively with all of the various ramifications of this subject is particularly welcome. *Aminoplastics* covers the chemistry of these materials, their manufacture, and a survey of their applications. It should therefore be of value to those engaged in the utilization of urea and melamine resins as finishing agents, adhesives, coatings, and molding powders, as well as to the resin chemist and manufacturer. Other amino resins of more than experimental interest, including those made by reacting thiourea and guanidine, respectively, with formaldehyde, are described in a chapter appropriately entitled Miscellaneous Amino Resins.

Chemical reactions involved are discussed in sections dealing with the proposals advanced by numerous investigators to explain the formation of these three-dimensional structures. Further intensive research will be required before the exact mechanism is clearly understood. The appendix contains a comprehensive bibliography and a useful list of manufacturers in the U. S. and abroad, together with the proprietary names of their products.

In the opinion of this reviewer, this work provides a compact, well-balanced picture of an important segment of the plastics industry.

**Sinews of "Cordura" make a carpet stronger,** lighter, and more flexible. The chain warp in carpets must be strong enough to bind the surface tufts firmly in place. Because "Cordura" is much stronger than natural fibers, a smaller-gauge yarn does the job . . . and ties a smaller, tighter knot around the tufts, at no extra cost.

# More strength at no more cost with this Du Pont yarn

Small strong cords of Du Pont "Cordura"* High Tenacity Rayon can do the work of large cords of natural fibers. This means that when you use "Cordura" you can reduce the bulk of a strength section and also cut down on the amount of expensive carcass required. In many cases this not only holds down cost, but improves the product as well.

For example, "Cordura" makes conveyor belts thinner yet stronger, tires that are cooler running, V-belts smaller yet more efficient, high-pressure hoses lighter and safer.

Chances are that the extra strength of "Cordura" can help you improve a product or a process . . . without increasing cost. It may even help you bring a new product into production. We'll be glad to work with you.

*REG. U. S. PAT. OFF.

## Du Pont "Cordura" High Tenacity Rayon

**STRENGTH AT LOW COST**

DU PONT

REG. U. S. PAT. OFF.

**BETTER THINGS FOR BETTER LIVING... *THROUGH CHEMISTRY***

NYLON
VISCOSE RAYON
ACETATE RAYON
ORLON* acrylic fiber
DACRON* polyester fiber

*DU PONT TRADE MARKS

**for fibers today... for fibers to come... look to DU PONT**